Texture development in titaniferous-magnetites found in Layer 21 in the Bushveld Igneous Complex, South Africa

Tahnee Otto

10691317

MSc Geology

University of Pretoria

2017

UNIVERSITEIT VAN PRETORIA
UNIVERSITY OF PRETORIA
YUNIBESITHI YA PRETORIA
Denkleiers • Leading Minds • Dikgopolo tša Dihlalefi

Acknowledgements

I would like to thank my supervisor, Dr James Roberts, for all his support, guidance, and understanding throughout this project. I would like to thank my co-supervisor, Professor Roland Merkle, for his input throughout the writing of this dissertation. I would like to thank Dr Roger Dixon for the use of his samples and thin sections as part of my investigation. I would also like to thank Mr Carel Coetzee and the Metallurgical Department at the University of Pretoria for the use of the Scanning Electron Microscope.

Thank you to Ms Tawnee Britt and Mr Erasmus Burger for their advice throughout their writing of this paper. A big thank you to my parents for their provision and support throughout this investigation.

Declaration of Authenticity

University of Pretoria

Full names of student: **Tahnee Otto**

Declaration

1. I understand what plagiarism is and am aware of the University's policy in this regard.

2. I declare that this thesis is my own work. Where other people's work has been used (either from a printed source, Internet, or any other source), this has been properly acknowledged and referenced in accordance with departmental requirements.

3. I have not used work previously produced by another student or any other person to hand in as my own.

4. I have not allowed, and will not allow, anyone to copy my work with the intention of passing it off as his or her own work.

Signature……..

Date……..

Abstract

Very limited studies have been conducted on titaniferous-magnetite exsolution textures and the conditions needed for the formation of these textures. Published research surrounding the exsolution textures consider only a particular element of the oxide, or a specific condition. The Upper Zone of the Rustenburg Layered Suite in the Bushveld Igneous Complex boasts 25 magnetite layers. The 21st layer counted from the Main Magnetite layer is called Layer 21, which is the uppermost titaniferous-magnetite layer in the Upper Zone. Uncommon exsolution textures in the titaniferous-magnetite grains were studied in order to gain a greater understanding of the formation of oxide exsolution textures. The exsolution texture presents itself as a three-dimensional framework of ulvöspinel-rich lamellae together with magnetite prisms. This is called a cloth texture exsolution. The data collected for this investigation included Scanning Electron Microscope (SEM) images, elemental weight percentage data, and SEM line scans. Previous studies do not show exsolution textures that are exactly similar to the exsolution textures seen in Layer 21, although the same basic type of microtexture can be seen. This indicates that conditions such as temperature, pressure, and oxygen fugacity, as well as the bulk mineral chemistry, plays a large role in the formation of the exsolution texture. A rough model has been provided that considers all of the information collected in previous studies in order to start the development of a complete model. Another model has been provided explaining the physical appearance of the cloth texture exsolution. The exsolution textures need to be investigated on a three-dimensional basis in order to develop a more accurate understanding of why the titaniferous-magnetite exsolution textures are different from location to location.

Table of Contents

List of Figures

List of Tables

CHAPTER 1 INTRODUCTION

The study of specific layers found in layered intrusions have widely been used in order to gather important information regarding the surrounding layers, mineral crystallisation processes, and the geochemistry of the magma present in the area. The mineralogy, textures, and geochemistry of the minerals present in such a layer provide information on the factors that were influencing the area, as well as the processes that were present during crystallisation.

In this study, changes in the mineralogy and geochemistry of Layer 21 in the Bushveld Igneous Complex, South Africa, have been analysed in order to gain information regarding the intrusion. Special focus has been given to the exsolution textures present in titaniferous-magnetite (titanomagnetite), which is present throughout the analysed material. Data was collected using a Scanning Electron Microscope (SEM), with analysis focusing on SEM images and line scan data. This data may provide an understanding of the physical and chemical formation of the cloth texture exsolution pattern seen in titaniferous-magnetite, with emphasis placed on evaluating the conditions that would result in these microstructures forming.

A limited number of studies have been conducted on Layer 21. Layer 21 is a titaniferous-magnetite layer in the Upper Zone of the Rustenburg Layered Suite in the Bushveld Igneous Complex. It occurs approximately 1033m-1019m below the top of the intrusion, and is surrounded by anorthosite and troctolite (Reynolds, 1985). The formation of Layer 21 is a debated topic, with cyclic variations considered for the formation of the entire Upper Zone, and fractional crystallisation being suggested for the formation of Layer 21 (Reynolds, 1985).

Three boreholes were drilled through the Upper Zone of the Western Limb of the Bushveld Igneous Complex, known as the Bierkraal cores. These three boreholes (BK1, BK2, and BK3) extend from Main Zone, through the Upper Zone, into the Lebowa Granite Suite (Walraven and Wolmarans, 1979). The thin sections that were analysed in this study were made from samples collected from BK1.

The exsolution textures present in the analysed oxides have not been documented extensively, but received some focus when the textures appeared more abundant than previously thought. The existence of the two-phase intergrowth of ulvöspinel-rich and magnetite-rich oxides was first noted by Mogensen (1946), and further studies noted that titaniferous-magnetite exsolution is a common feature in rocks occurring in plutonic and hyperbassal environments. The feature used to typically describe the texture seen in titaniferous-magnetites is a three-dimensional framework of ulvöspinel-rich lamellae, otherwise known as a cloth texture exsolution. This lamella usually lies on {100}, with inter-lamellar magnetite-rich blocks (Price, 1980). The exsolution microstructure only develops on a small scale, due to the slow rate of the kinetic processes involved in unmixing at the solvus temperature.

SEM analysis provided images, elemental data, and line scans with the necessary information to investigate the exsolution textures seen in the titaniferous-magnetite of Layer 21. Previous studies focused on conditions and mechanisms in isolation, but this dissertation focuses on trying to understand the development of the microstructures on a physical and chemical level in Layer 21. Multiple models of formation will be compared to the collected data in order to develop an outline as to the formation of the microtextures.

Investigation of the exsolution features suggest that temperature, pressure, oxygen fugacity, the mechanism of exsolution, and the mineral bulk chemistry is of most importance when considering the formation of the texture. This investigation sheds light on the need for a proper understanding of the textures that formed, and why titaniferous-magnetite textures can vary so extensively between different samples, for which a model has been suggested to explain the physical formation of the exsolution textures.

CHAPTER 2 GEOLOGICAL BACKGROUND

THE BUSHVELD IGNEOUS COMPLEX

The Bushveld Igneous Complex is the world's largest layered intrusion which was emplaced ~2.06 Ga in the north-east of South Africa. The Bushveld Igneous Complex is found in the upper Transvaal basin and intruded at an unconformity between the volcano-sedimentary Pretoria Group and the Rooiberg Group (Eriksson, 1994; Hartzer, 1995; Clarke *et al*., 2009). The complex is found in approximately 20km of volcanic and sedimentary rocks of the Transvaal Sequence, being preserved in the Kanye, Transvaal and Griqualand structural basins (Eriksson and Reczko, 1995a). The complex is estimated to cover an aerial extent of approximately 65000km$_2$ (Eales and Cawthorn, 1996).

The Bushveld Igneous Complex consists of three major plutonic suites, which are characterised in terms of age and chemistry. The first major plutonic suite is the Rustenburg Layered Suite, which is the initial mafic-ultramafic component that cross-cuts the sedimentary rocks of the Pretoria Group (Eales and Cawthorn, 1996; Clarke *et al*., 2009). The second and third suites are the felsic Lebowa Granite Suite and Rashoop Granophyre Suite, both intruding at a later stage into the Rooiberg Group lavas and into the Rustenburg Layered Suite (Hunt, 2006).

The Bushveld Igneous Complex outcrops in five geologically discrete areas, which is considered the limbs of the complex. These limbs are known as the Eastern Limb, Western Limb, Far Western Limb, Northern or Potgietersrus Limb and the South-eastern Limb (Figure 1). The Eastern and Western Limb are theorised to be connected due to similarities in stratigraphic successions, whereas the other limbs show more differences than similarities (Cawthorn and Webb, 2001).

The Complex has been widely studied in the past century, mainly due to the richness of ore deposits. These commodities include palladium, rhodium, platinum, chromium and vanadium. Other economically exploitable commodities include the platinum-group elements (PGE's), sulphide, magnetite, chromite, and ilmenite (Lee, 1996).

The nature of emplacement of the Bushveld Igneous Complex is speculative, mainly due to the lack of reliable outcrops in certain areas and the complicated relationships between the various sections and layers (Britt, 2015). A number of models have been proposed to explain the formation of the complex. This includes that of Hatton and Schweitzer (1995) which suggest a mantle plume beneath the Kaapvaal Craton. Formation as a result of subduction was suggested by Hatton (1988), with the melting of detrital material forming the complex. Rhodes (1975) proposed that the formation of the Bushveld Igneous Complex was due to multiple meteorite impacts. These meteorite impacts resulted in the generation of magma and the shape of the complex.

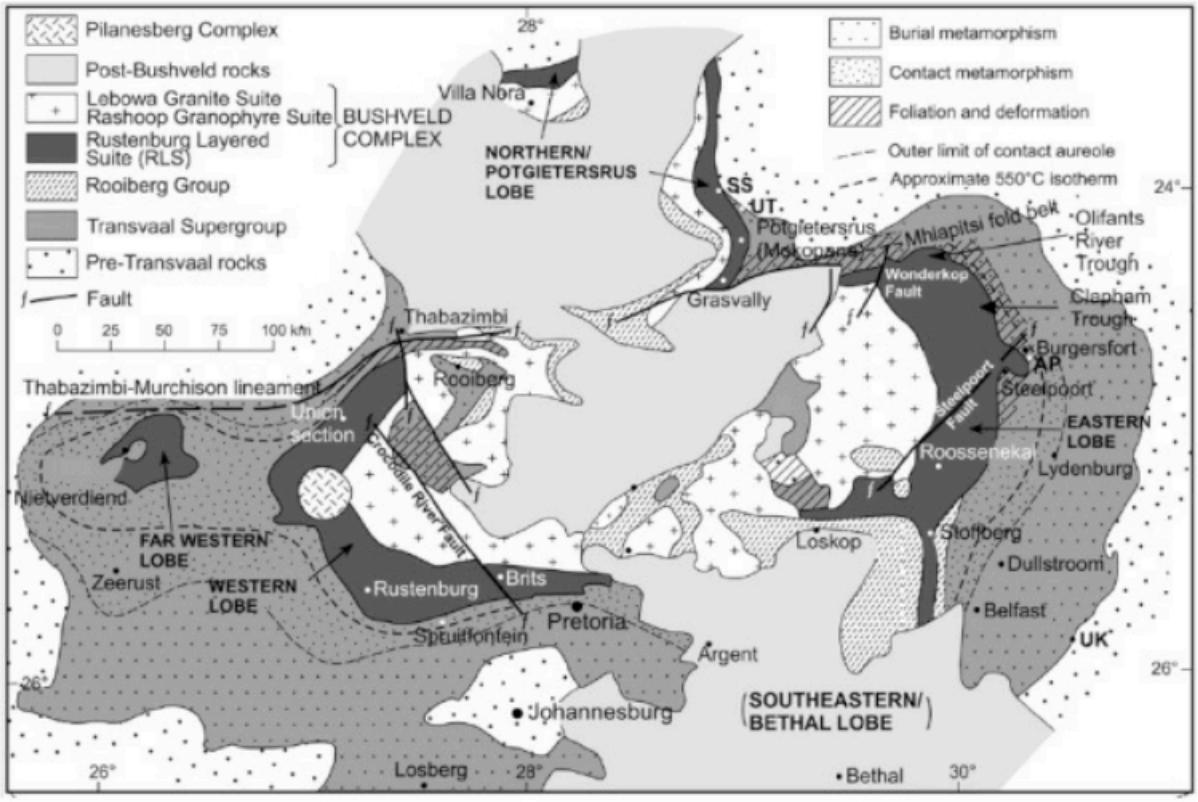

Figure 1. A simplified geological map of the Bushveld Igneous Complex. From Clarke *et al.* (2009), modified after Cawthorn *et al*. (2006).

The model most generally accepted suggests that the emplacement of the Bushveld Igneous Complex occurred as a series of magma pulses, injecting new magma in short succession of the previous pulse (Cawthorn and Walvaren, 1998). Sagging of the complex occurred due to the weight of the crystallising magma, with strata dipping slightly towards the centre of the complex (Webb *et al*., 2011). The tectonic activity that affected both the Transvaal Sequence and the Bushveld Igneous Complex after their formation is considered to be interrelated, although minimum alteration and deformation can be seen.

The Rustenburg Layered Suite, which is an important component of the Bushveld Igneous Complex, makes up a large part of the layered intrusion. The focus of this project lies within the Rustenburg Layered Suite.

THE RUSTENBURG LAYERED SUITE

The intrusion of the ultramafic to mafic Rustenburg Layered Suite led to the lifting of the Rooiberg Group lavas which is present as the roof of the Bushveld Igneous Complex in some areas (Hartzer, 1995). Recent studies using U–Pb from zircons in the suite show that the Rustenburg Layered Suite crystallised within 1.02 ± 0.63 My. Crystallisation of the Rustenburg Layered Suite resulted from greatly fractionated intercumulus melts, found at temperatures between 1200ºC and 1400 ºC (Zeh *et al*., 2015).

The Rustenburg Layered Suite is divided into various zones, distinguishable based on their chemical, mineralogical, and isotopic differences. These zones are known as the Marginal Zone, Lower Zone, Critical Zone, Main Zone, and the Upper Zone (Figure 2).

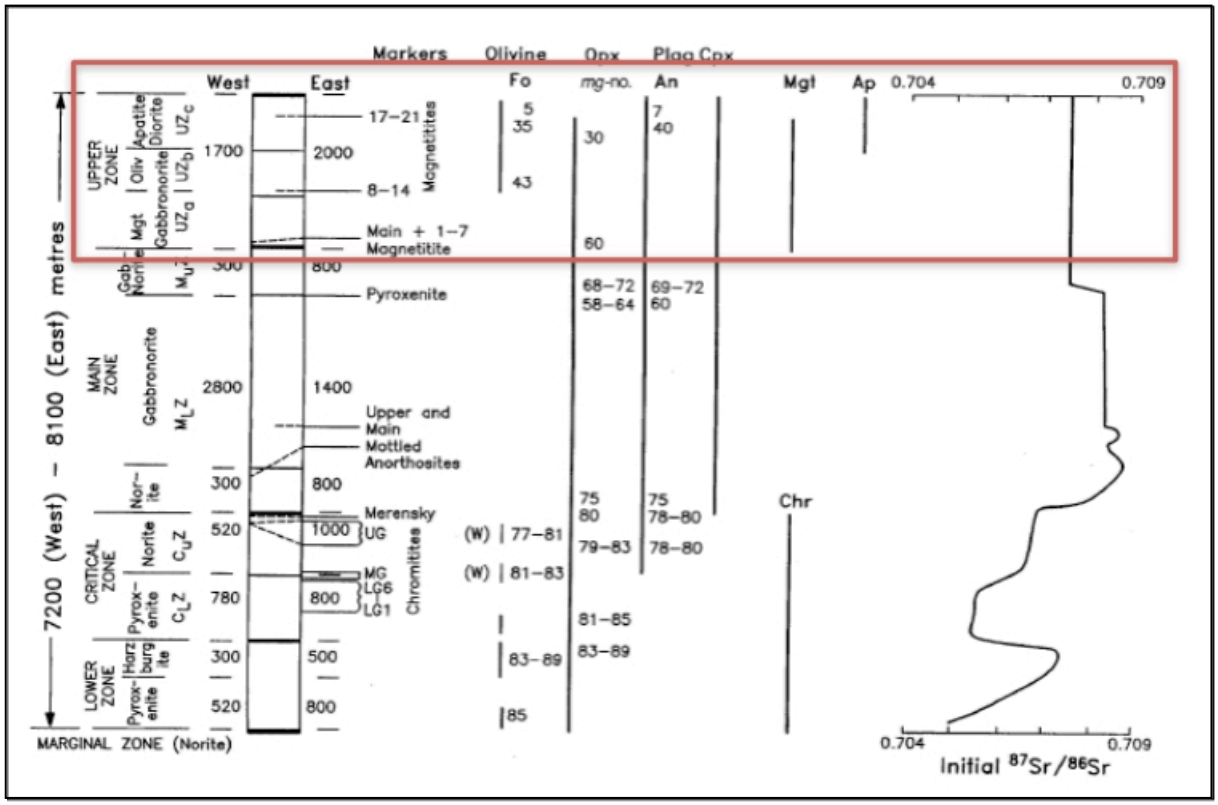

Figure 2. Stratigraphy of the Eastern and Western Limbs of the Bushveld Igneous Complex, with the subdivisions or zones of the Rustenburg Layered Suite (Cawthorn and Walraven, 1998). The red block indicates the Upper Zone.

The Marginal Zone ranges in thickness from 0m to approximately 800m, but is not present along the entire Rustenburg Layered Suite. The Marginal Zone is mostly limited to the base of the suite. Rocks found in the Marginal Zone are mainly heterogeneous, medium grained norites, with variations in mineral proportions of quartz, clinopyroxene, biotite, and horneblende (Eales and Cawthorn, 1996; Cawthorn and Walraven, 1998). The norites are not considered to be genetically related to the overlying cumulates. The proportions of minerals reflect the degrees of contamination that have been incurred by the sediments of the Pretoria Group.

The Lower Zone has developed best along the north-eastern and north-western limbs of the Bushveld Igneous Complex, and in the south of the northern limb of the complex. The thickness of the zone ranges from 0m to no more than 1300m. The floor structure of the complex has largely controlled the thickness and distribution of the Lower

Zone (Eales and Cawthorn, 1996). Facies changes in tilted areas of the sedimentary floor show that they imposed a degree of compartmentalisation during crystallisation of the suite. The rock types range from pyroxenites, to harzburgites alternating with dunites. The pyroxenite layers usually contain magnetite veins. Continuous magma influx is suggested due to the layering in addition to the oscillations in the bulk Mg content of mineral and whole rock compositions (Cawthron and Walraven,1998).

The Critical Zone, which is considered to be up to 1500m thick, is divided into upper and lower sub-zones based on mineralogy. The upper noritic to anorthositic sub-zone (520m to 1000m thick) contains pyroxenite, harzburgite, chromitite, norite, and anorthosite rocks. The lower pyroxenitic sub-zone (500m to 800m thick) is ultramafic and is made up of orthopyroxenitic cumulates, as well as numerous chromite layers (Cawthorn and Walraven, 1998; Ashwal *et al*., 2005). The Critical Zone hosts large amounts of chromite and platinum deposits which are found in different reefs. These include the Upper Group 2 Chromitites (UG2) and the Merensky Reef (Eales and Cawthorn, 1996). These reefs characterise the layering in the zone. The base of the overlying Main Zone is regarded as the top of the Giant Mottled Anorthosite, occurring 45m to 90m above the Merensky Reef (Ashwal *et al*., 2005).

The Main Zone forms a very large part of the Rustenburg Layered Suite, with a thickness of 2200m to 3000m. The Main Zone is made up of successions of gabbronorite with pyroxenite and anorthosite bands, generally lacking olivine or chromite (Mitchell, 1990). A proper boundary between the Critical Zone and Main Zone is hard to identify and is usually taken at the top of the mottled anorthosite. The Pyroxenite Marker, which is a layer made up solely of orthopyroxenite, is found approximately 2400m above the base of the Main Zone (Eales and Cawthorn, 1996). The Main Zone shows extreme layering which is associated with the influx of new magma during emplacement.

All the layers contain orthopyroxene, plagioclase, and clinopyroxene, but in varying proportions. Lighter layers would have larger amounts of plagioclase, and darker layers would have less plagioclase. This layering is a result of magma pulses during emplacement which caused the mechanical redistribution of crystals. A constant Sr value of 0,7073 shows that this magma mixed rapidly with the cumulous melt before crystallisation occurred (Kruger *et al*., 1987). This study focuses specifically the Upper Zone.

THE UPPER ZONE

The Upper Zone (Figure 2) is approximately 2270m thick (Von Gruenewaldt, 1971), and is generally characterised by the appearance of cumulous magnetite (Eales and Cawthorn, 1996). The Upper Zone represents the final crystallisation of the Rustenburg Layered Suite, and is well exposed in the Eastern Bushveld Igneous Complex. The zone is considered to have formed due to a single magma pulse as indicated by Sr/Sr values performed in a study by Tegner *et al.,* (2006) after Kruger *et al.,* (1987). Other theories suggest magma recharge from a homogenous magma chamber (Scoon and Mitchell, 2012), or multiple magma injections at the Pyroxenite Marker (Vantongeren and Mathez, 2013).

The Upper Zone in the eastern limb of the Bushveld Igneous Complex boasts 25 magnetite layers, clustered into 4 groups with 7 layers each. The Upper Zone is dominated by anorthosite with varying amounts of olivine, pyroxene, magnetite, and apatite (Eales and Cawthorn, 1996). Fractionated rocks in the upper 200m of the sequence are fayalites and/or hornblende-bearing ferrodiorites. Some of these rocks contain intercumulus quartz and/or K-feldspar (Molyneux, 1974). The top of the succession shows an increase in the proportions of ilmenite and a drop in magnetite. The base of the Upper Zone is characterised by cumulus

magnetite. Pigeonite is common at the base but lessens towards the top of the zone. Some interstitial minerals are also present such as biotite and hornblende.

Opaque minerals are common throughout the Upper Zone, with the proportions of the oxide minerals varying over short distances. This links with the layering found in the zone. Magnetite layers show sharp bases and gradational tops, and the thickest is 6m in total. Two major zones of Fe-Ti oxide enrichment show the formation of distinct ore rich layers (Reynolds,1985). The Main Magnetite layer near the base of the Upper Zone is 2m thick, and is mined for its large vanadium content found in titaniferous-magnetite.

The South African Committee for Stratigraphy (SACS) divided the Upper Zone into 3 sub-zones, namely UZ_a, UZ_b and UZ_c (Figure 2). These sub-zones are defined by rock composition. Sub-zone “a” compromises of anorthosite and magnetite ferrogabbro, and is approximately 700m thick. 130m above the base of the Upper Zone is the Main Magnetite Layer. Sub-zone “b” shows the appearance of olivine, as well as troctolite, anorthosite, and olivine. UZ_b is 580m thick. Sub-zone “c’s” base is marked with cumulus apatite, and is 1000m thick. Also found in this sub-zone is olivine dorite, anorthosite, diorite, and troctolite. (Von Gruenewaldt, 1971; Eales and Cawthorn, 1996). These subdivisions are not similar in all the limbs of the Bushveld Igneous Complex, but the sub-zones provide a good analysis of the rock changes throughout the zone.

Well-exposed areas in the eastern limb of the Bushveld Igneous Complex showed at least 30 titaniferous-magnetite layers in the Upper Zone (Molyneux, 1970). The Main Magnetite layer is considered the datum, and the most continuous titaniferous-magnetite layers were assigned numbers below and above the datum. The layers found below the Main Magnetite layer are numbered 1 to 4, and the layers above the Main Magnetite layer are numbered 1-21 as they appeared with increasing stratigraphic height (Molyneux, 1970a). Some of these numbered layers are considered to be composite, consisting of two or more ore-rich layers separated by narrow silicate rock layers. Most of the ore-rich layers are relatively thin, consisting of less than 30cm of titaniferous-magnetite. Important exceptions are the Main Magnetite layer, as well as Layer 21 (Molyneux, 1970a).

Lower contacts between ore-rich layers and silicate layers are generally sharp and often undulating.The upper contacts are usually gradational and show a decrease in the opaque oxide content of the rocks (Reynolds, 1985). The ore-rich layers composed of silicate rich areas as well as Fe-Ti rich oxides. The silicates that are present are mostly plagioclase, inverted pigeonite, and augite. Layer 21 consists of relatively thin ore-rich layers separated by narrow partings and lenses of olivine-bearings anorthosite or troctolite (Reynolds, 1985).

In 1974, the Council of Geosciences (South African Geological Survey) drilled three holes into the Rustenburg Layered Suite in the Bierkraal area, north of Rustenburg (Reynolds, 1985). The Bierkraal area is in the Western Limb of the Bushveld Igneous Complex, where the Upper Zone is badly exposed. These three boreholes gave a complete vertical section of the Upper Zone and allowed for studies regarding the stratigraphy of the Upper Zone in a poorly exposed area (Walraven and Wolmarans, 1979). BK1 is approximately 1600m deep and extends to the Lebowa Granite Suite. BK2 intersects the Pyroxenite Marker and the Main Zone, ending at the Main Magnetite layer. BK3 was used transverse the space between BK1 and BK3.

LAYER 21

Opaque oxides are found in high concentration at a depth of 1445m to a depth of 1472m in BK1, with the lowermost 14m of this interval consisting of a titaniferous-magnetite layer. The uppermost 13m of the interval contains much less oxides, showing thinner titaniferous-magnetite layers. This oxide rich horizon is considered to be Layer 21, the uppermost titaniferous-magnetite layer in the Upper Zone. Layer 21 is found from approximately 1033m-1019m below the top of the intrusion (Reynolds, 1985), and approximately 1450m-1480m along BK1 (Figure 3).

The ore-rich layers are composed almost completely of titaniferous-magnetite, with only approximately 6 volume percent present as ilmenite (Molyneux, 1970a). According to Von Gruenewaldt (1976), who conducted modal analysis of the sulphide minerals in the Upper Zone, four layers contained sulphides that totaled more than 3%, which included Layer 21. Droplike-shaped bodies of sulphides were found in titaniferous-magnetite grains, and larger concentrations can be found throughout the layer.

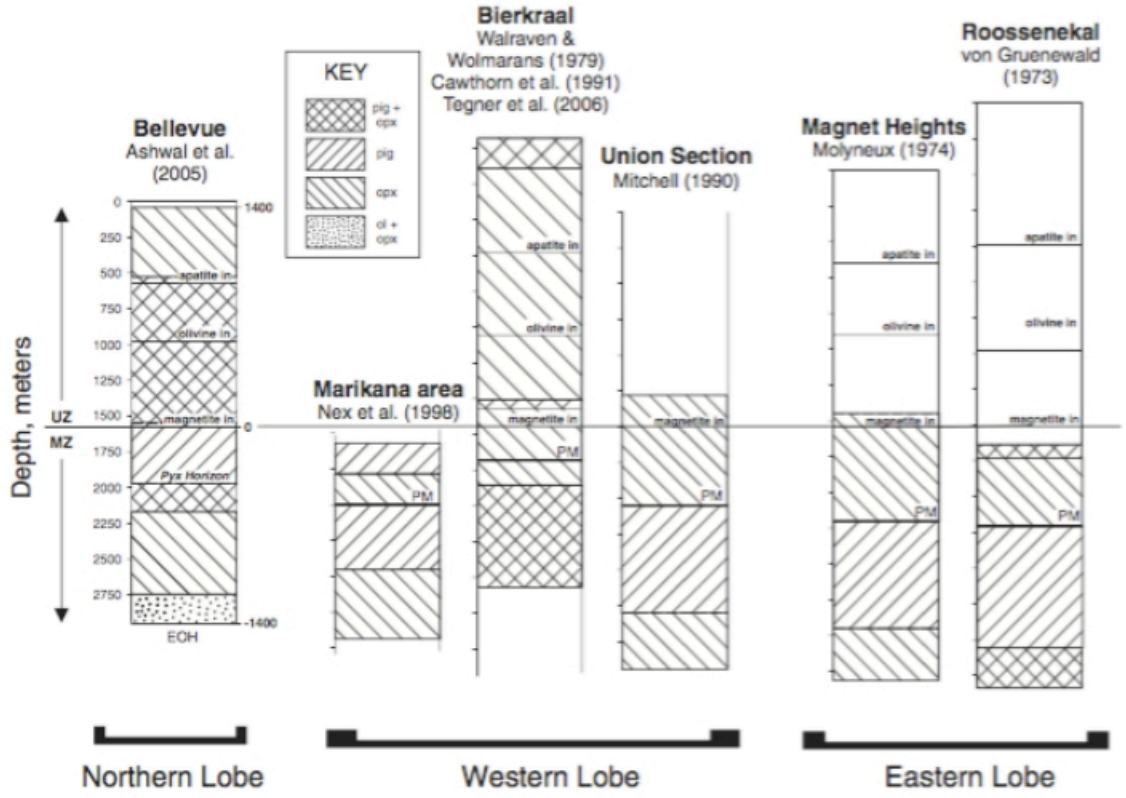

Figure 3. Vertical sections showing differences and correlations between the different lobes in the Main and Upper Zone (Cawthorn and Ashwal, 2009).

Titaniferous-magnetite grains in ore-rich layers are generally larger than 10mm in diameter, this being approximately three times larger than the grain size would be in silicate bearing portions of the same layer (Reynolds, 1985). Silicate free areas form poly-crystalline aggregates, in which titaniferous-magnetite crystals meet in well-defined triple junctions. Ilmenite crystals may be located as small polygonal crystals that are interstitial between titaniferous-magnetite grains (Reynolds, 1985).

Very few complete major and minor elemental analyses of titaniferous-magnetites in the Bushveld Igneous Complex have been published; with Reynolds (1985) reporting that virtually nothing is is known about their trace element geochemistry. TiO_2 bulk content

increases with increasing stratigraphic height (Reynolds, 1985). The base of the Upper Zone has approximately 12 percent TiO_2 and the top of the sequence has approximately 20 percent TiO_2 (Reynolds, 1985). The distribution of Mg and Mn is largely controlled by preferential partitioning into ilmenite rather than titaniferous-magnetite during crystallisation. Re-equilibration with coexisting olivine and pyroxene complicates the Mg and Mn distribution pattern (Reynolds, 1985).

A systematic study by Von Gruenewaldt *et al*., (1985) of the exsolution textures in the titaniferous-magnetite grains found in the massive magnetite layers of the Upper Zone suggest differences that point to a change in magma oxidation state during cooling and crystallisation. Composite lamellar intergrowths of ilmenite and magnetite found in Layer 21 and other of the uppermost magnetite layers in the Upper Zone suggest subsolvus oxidation of ulvöspinel in ulvöspinel-rich magnetite.

TITANIFEROUS-MAGNETITE (TITANOMAGNETITE) FORMATION

Titaniferous-magnetite ($Fe_{3-x}Ti_xO_4$, where x is the ulvöspinel content in the magnetite-ulvöspinel solid solution) is used to describe oxide minerals with more than 2 percent titanium (Singewald, 1913). Titaniferous-magnetite is a major rock-forming mineral with a spinel-structure, commonly associated with mafic igneous rocks that occur in layers or in complex intrusive bodies (Petrochilos, 2010). Titaniferous-magnetites also contain approximately 0.2 percent to 1 percent of vanadium, present in the magnetite (Fischer, 1975). Large deposits of titaniferous-magnetite occur in various parts of the world, such as Russia, Australia, New Zealand, India and China (Samanta *et al*., 2014). Titaniferous-magnetite ore can occur in large masses of rock in disseminated pieces, segregated in layers, or as plugs or dykes injected into the already crystallised magma.

The Upper Zone hosts a number of magnetite-rich layers, and many of these layers are considered to be titaniferous-magnetite layers. The occurrence of these titaniferous-magnetite layers are a well-documented feature due to economic interest surrounding the production of steel, iron, and high-titanium materials (Reynolds, 1985). Various descriptions of the Fe-Ti mineralogy in the Upper Zone can be found, but many of these reports have been based on data obtained in the better exposed eastern limb of the Bushveld Igneous Complex. Titaniferous-magnetites found in the BK1 borehole below 825m are considered to be titanium-rich (Reynolds, 1985). The oxide-rich layers show geological relationships and distributions indicating that they are components that form part of the layered sequence and its genesis.

Earlier genetic models acknowledged that titaniferous-magnetite layers in the Bushveld Igneous Complex represented “magmatic segregation deposits” (Singewald, 1912). These models proposed links between Fe-Ti oxide ores and their host rocks, suggesting mechanisms that involved the separation and accumulation of titaniferous-magnetite to form layers. Other models postulated the crystallisation of ores from of Fe-Ti oxide liquids, which were injected into partially consolidated host rocks late during crystallisation (Du Toit, 1918). Later genetic models include mechanisms where increases in oxygen fugacity (otherwise known as *fo2)* triggers titaniferous-magnetite crystallisation, resulting in Fe-Ti rich layers. These theories followed experimental studies that indicated the importance of *fo2* in the formation of magnetite, as well as other iron bearing oxide phases (Reynolds, 1985). Various other models were proposed, with Molyneux (1970a) suggesting that titaniferous-magnetite crystallisation took place near the base of the magma chamber as the melt responds to *fo2.* Irvine (1975) suggested that episodic oxidation events resulted in the formation of titaniferous-magnetite layers. These oxidation events were a result of contamination of the parent magma by granitic fluid. Klemm *et al.,* (1982) speculated that titaniferous-magnetite layer formation may have resulted from higher *fo2,* caused by the

presence of volatiles that were derived from floor rocks undergoing thermal metamorphism below the intrusion.

Reynolds (1985) identified the problem faced by the majority of *fo2* triggered hypotheses. The occurrence of oxidation would have to be more or less simultaneous over the entire width of the magma chamber to allow the lateral continuity and uniform thickness shown by titaniferous-magnetite layers. This rules out mechanisms involving a localized process, such as contamination. Widespread processes such as pressure changes caused by fracturing through to the surface would be more important (Ulmer, 1969). This suggests that magma mixing models also cannot effectively account for the common presence of numerous titaniferous-magnetite layers within small vertical intervals, and variations in silicate mineral content within individual layers (Reynolds, 1985).

The restriction of titaniferous-magnetite layers to later crystallising sections of the Bushveld Igneous Complex indicate that extensive periods of Fe-Ti enrichment had to have occurred before Ti would precipitate. Tholeiitic rocks are considered to have a marked degree of late-stage Fe enrichment that would be needed for the precipitation of titaniferous-magnetite. A primary chemical control is indicated by the gross chemical composition of the fractionating magma. Titaniferous-magnetite precipitation in tholeiitic rocks usually occur during long periods of silicate fractionation, where primary spinel is not formed (Reynolds, 1985). Reynolds (1985) suggests that the precipitation of titaniferous-magnetite at the base of the Upper Zone may be due to a decrease in temperature of the overall melt. The increase in bulk TiO_2 content in titaniferous-magnetites with increasing stratigraphic height could be due to progressive fractional crystallisation. The high temperature member of the magnetite-ulvöspinel solid solution series is represented by magnetite, resulting in the expectation that the ulvöspinel content would increase with progressive fractional crystallisation. The relationship between the minerals remain complicated, because the ulvöspinel content of magnetite that precipitates at the same time as ilmenite is controlled by both *fo2* and temperature.

The relative abundance of titaniferous-magnetite in the Upper Zone silicate rocks, which is typically 5-10 volume percent (Molyneux, 1970b), varies over short distances but the overall content of the titaniferous-magnetite remains constant with increasing stratigraphic height, until approximately 200m below the roof where the abundance decreases abruptly (Molyneux, 1970b). Ti content increases in the magnetite as fractional crystallisation increases, and a *fo2* decrease which would suggest depletion in Ti only occurred later, and not during the early stages of magnetite fractionation (Reynolds, 1985). The behaviour of TiO_2 suggests that the residual liquid was augmented by additional magma influxes, or that the processes operative in the melt were very complex.

To summarize, Reynolds (1985) suggests that large-scale *in situ* silicate crystallisation led to an increase in the total Fe content. This led to a density increase of the surrounding melt which formed as a thick layer on the bottom of the magma chamber. This enriched liquid did not mix with the overlying magma, forming an inactive layer from which large volumes of titaniferous-magnetite crystallised. The interaction of factors such as the Fe_2O_3/FeO ratio of the liquid, temperature, *fo2*, and the *fh2o/fh2* ratio also led to large amounts of titaniferous-magnetite crystallising. Magnetite precipitation then lowered the density of the inactive layer until it equaled the density of the overlying magma. Mixing occurred which ended that specific cycle of magnetite layer formation. Fractionation once again became silica dominated.

EXSOLUTION TEXTURES OF TITANIFEROUS-MAGNETITE

Titaniferous-magnetite solid solution is found between the end-members magnetite (Fe_3O_4) and ulvöspinel (Fe_2TiO_4). Exsolution of titaniferous-magnetite shows various textures, depending on the mode of formation, tectonic setting, pressure-temperature, and oxygen fugacity (Petrochilos, 2010).

Titaniferous-magnetite exsolution is considered to be a compositional unmixing, which produces a cloth-textured intergrowth or boxwork structure of two phases that have not interacted or mixed (Figure 4 and Figure 5). The compositions of the two phases are close to the end-members of the solid solution (Petrochilos, 2010). Titaniferous-magnetites that have undergone this exsolution have been observed in massive ore deposits such as the Bushveld Igneous Complex, or, in general, basic plutonic environments (Price, 1980). This has been confirmed by observing these textures in Layer 21 in the Upper Zone.

The resulting exsolution intergrowth texture described is quite rare in the Earth's crust. The present oxidizing conditions favour oxidation of titaniferous-magnetite into a "trellis" type of lamellae due to the ilmenite in the magnetite (Haggerty, 1991). The formation of ilmenite solid solution depletes the host in titanium, reducing the thermodynamic driving force for additional unmixing to occur. Initially-homogeneous titaniferous-magnetite evolves into other phases via a process that depends mostly on the current oxidation state of the system. The cloth texture that forms as a result of titaniferous-magnetite unmixing is only visible in certain conditions (Petrochilos, 2010).

Experimental studies of the titaniferous-magnetite solid solution series show that the critical solution temperature of impurity-bearing titaniferous-magnetite solvus occurs either above or below the Curie temperature (TC) of exsolved magnetite grains (Petrochilos, 2010). This titaniferous-magnetite solvus has a critical solution point around 600 ºC or less, with the solvus being skewed slightly more towards the magnetite end-member of the titaniferous-magnetite mixture (Lindsley, 1981) (Figure 6). The Curie temperature of the ulvöspinel is -153 ºC, and the Curie temperature of the magnetite is near 580 ºC. The Curie temperature of intermediate titaniferous-magnetite compositions are considered to be linearly proportional to the ratio of the ulvöspinel to magnetite components (Merrill and McElhinny, 1983).

As reported by Deer *et al.,* (1962), and Frost & Lindsley (1991), titaniferous-magnetite found in natural systems usually contain impurities. This changes the consolute temperature of titaniferous-magnetite, which is presumed to be higher in Al-bearing oxides. This is proven by the consolute temperature of magnetite-hercynite ($FeAl_2O_4$) solid solution, which is approximately 850 ºC (Turnock and Eugster, 1962).

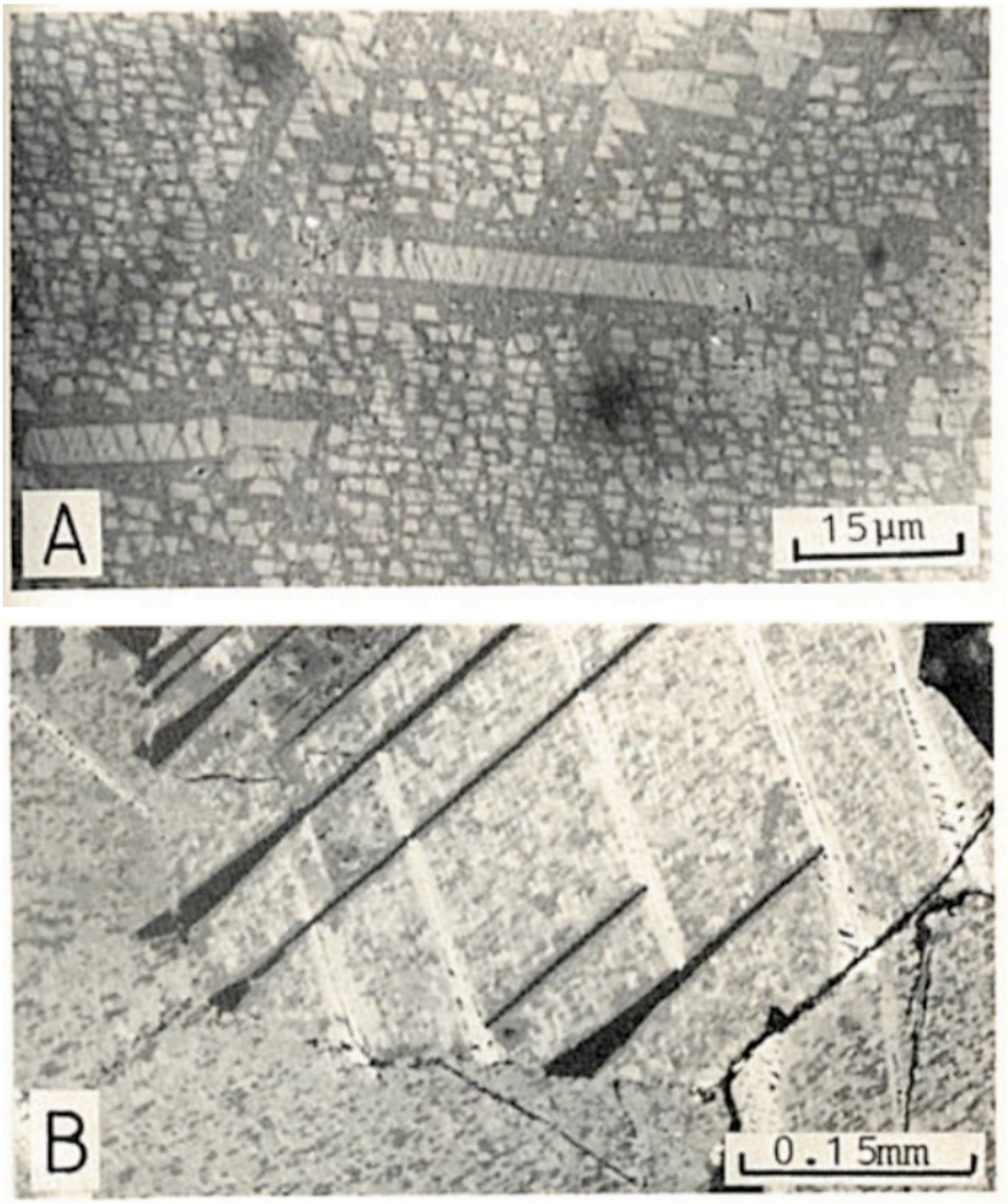

Figure 4. Photomicrographs showing exsolution textures of high titanium magnetite. (A) Ulvöspinel is dark in colour and magnetite is light in colour. Exsolution has resulted in the cloth texture. (B). Ilmenite "trellis" texture present as broad angled lines. The blotchy appearance seen in this photograph was reported due to the oxidation of ulvöspinel intergrowths into ilmenite. (Reynolds, 1985).

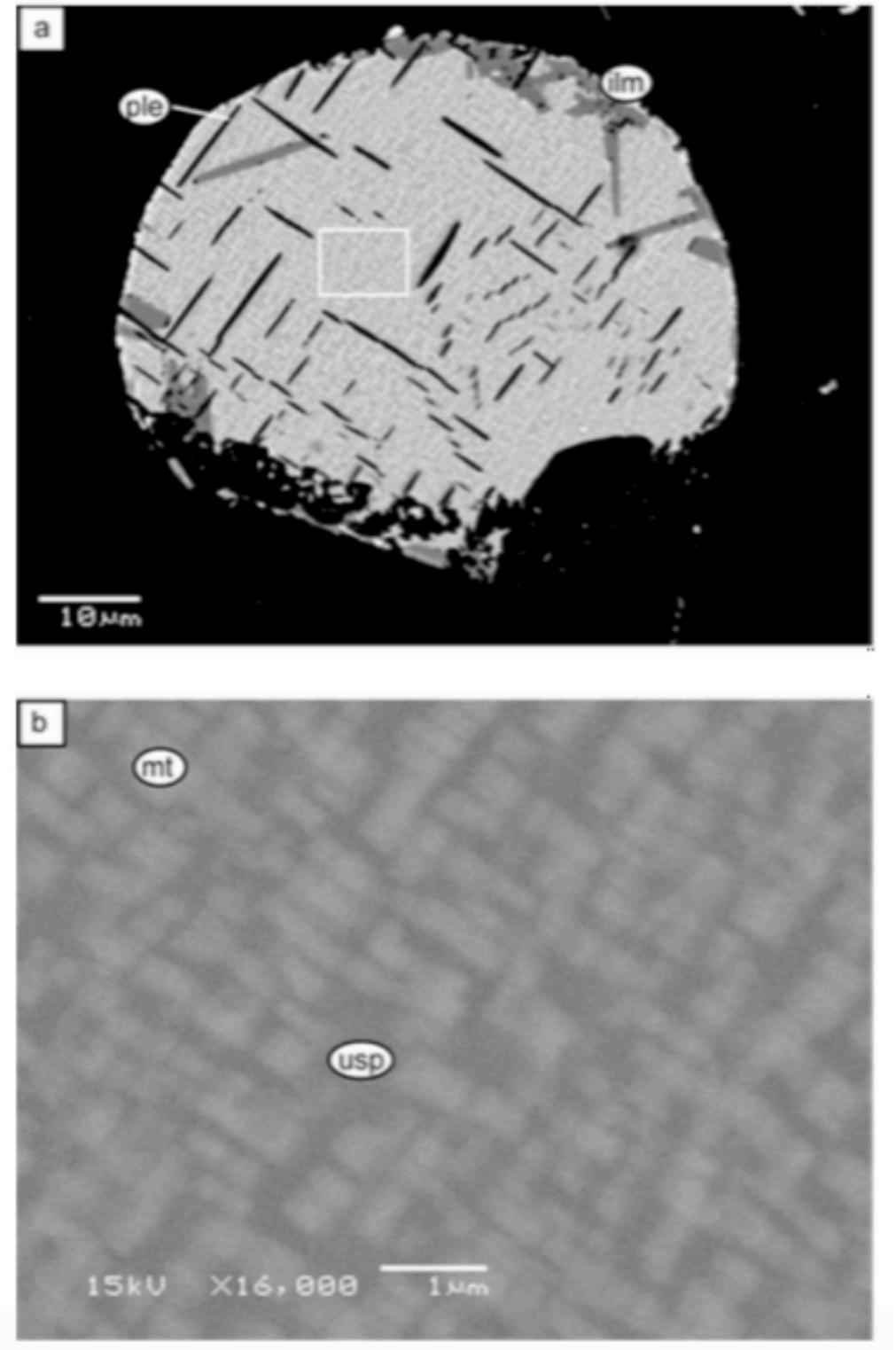

Figure 5. Backscattered images of titaniferous-magnetite grains showing a cloth texture exsolution due to oxidation. (a): An entire titaniferous-magnetite grain. Ilmenite exsolution is also present as a "trellis" texture. The exsolution of titaniferous-magnetite and ilmenite are contrasted. The exsolved phases are magnetite, ulvöspinel, pleonaste, and ilmenite. (b): High magnification of the region shown in (a). This shows the cloth texture that is produced from magnetite-rich end-members in an ulvöspinel-rich host (Petrochilos, 2010).

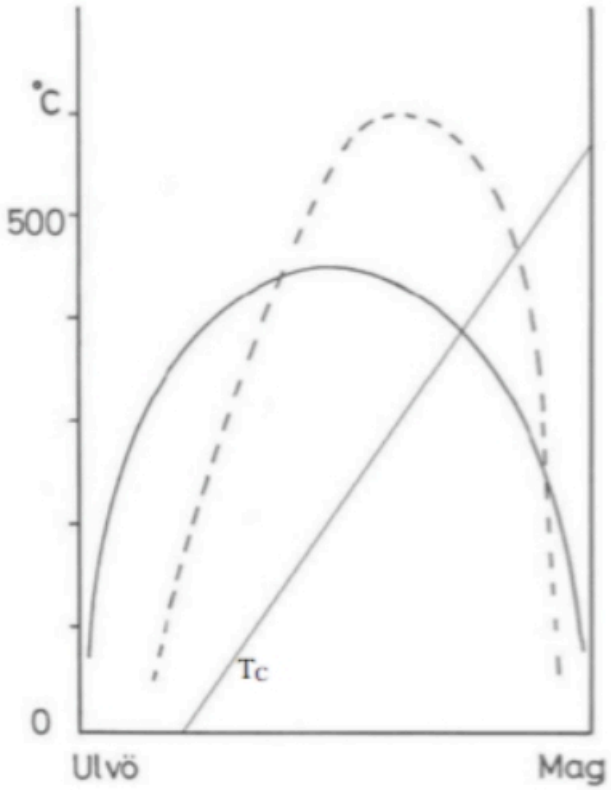

Figure 6. Titaniferous-magnetite solid solution and its representative solvi in a schematic diagram. Curie temperature (TC) is also shown in the diagram. The solvus in dashed line is suggested by Vincent *et al.,* (1957) and the solid line is from Price (1981). Modified from Price (1981).

The mechanism of titaniferous-magnetite exsolution is of importance. Homogenization experiments carried out by Kawai (1956), Vincent *et al.,* (1957), Lindsley (1981), and Price (1981), were used to infer the temperature range and the shape of the titaniferous-magnetite solvus. These types of experiments show that naturally exsolved titaniferous-magnetite grains are annealed at a range of temperatures at various intervals of time, to drive homogenization of the two phases. The homogenization experiments allow mapping of the binary solvus in temperature-composition space.

Two primary mechanisms for titaniferous-magnetite exsolution have been proposed by Gibbs (1961), namely: nucleation and spinodal decomposition. Nucleation is considered to be either heterogeneous or homogeneous. Heterogeneous nucleation would occur when a new phase forms at areas with defects, whilst homogeneous nucleation would occur in uniform bulk material. The mechanism of nucleation leads to a texture in which the new phase is chemically uniform, discrete, and localized in space (Petrochilos, 2010).

A spinodal decomposition mechanism leads to a more chemically non-uniform distribution of the exsolved phase (Yund and McCallister, 1970). Compositional fluctuation in spinodal decomposition is represented by a wavelength as small as 100 Å (Harrison and Putnis, 1999). Exsolution can be either incoherent or coherent. If the exsolution is incoherent, the lattice planes between new phases and matrix phases remain continuous, and the exsolution texture would be in a predictable crystallographic orientation compositional fluctuation in spinodal decomposition. The conditions needed for each mechanism to take place can be seen in the temperature versus composition phase diagram (Figure 7).

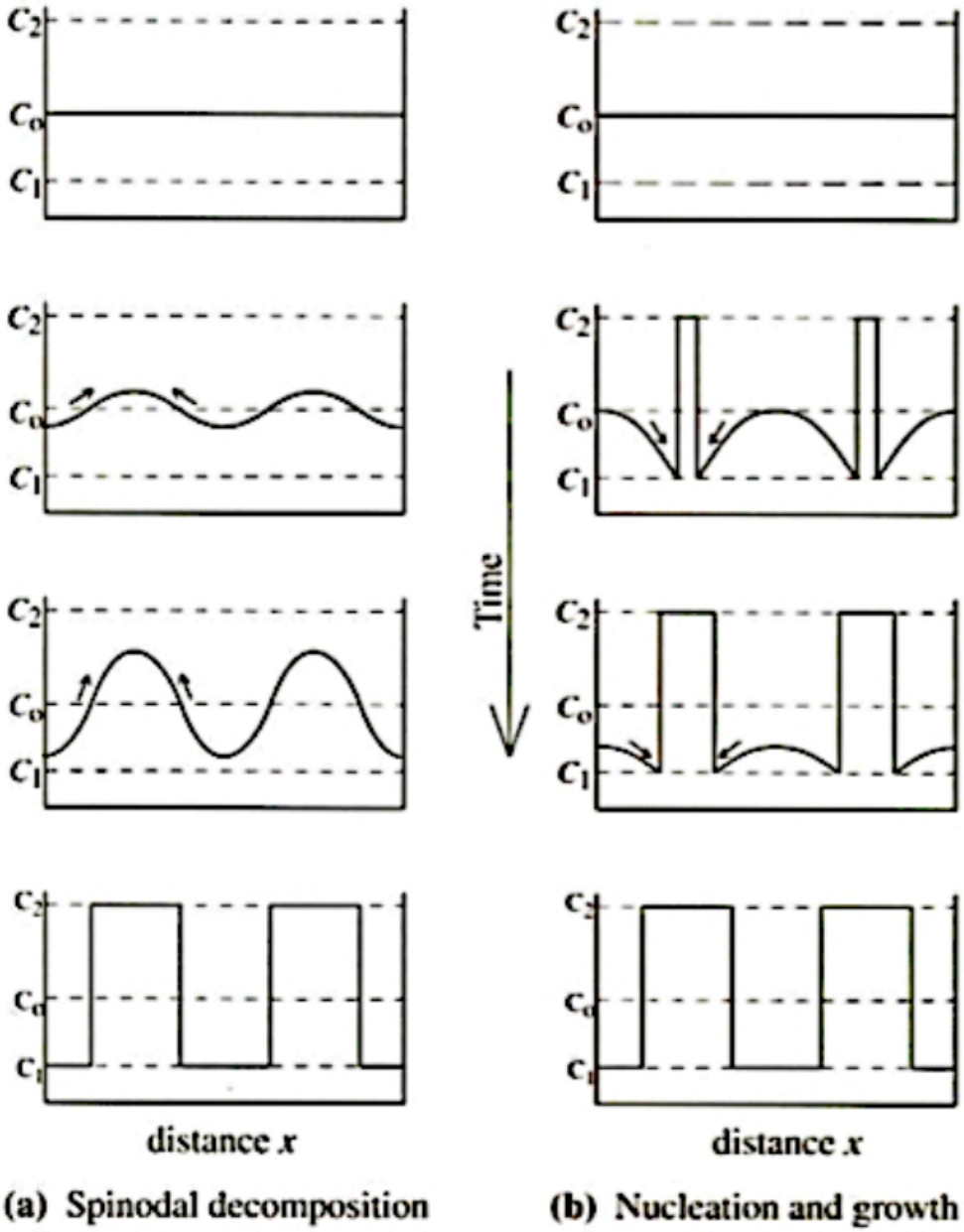

Figure 7. The two mechanisms of exsolution represented in a schematic diagram showing the development of compositional fluctuations. C0 is the initial composition of the solid solution. C1 and C2 are the equilibrium compositions of the exsolved two-phase intergrowth (Petrochilos, 2010).

If the end-member compositions and the mechanism of exsolution are known, it will allow the mapping of a solvus that corresponds to a particular mechanism (Figure 7), specifically for titaniferous-magnetite solid solution (Petrochilos, 2010). A nucleation mechanism can occur anywhere within the chemical solvus, but a spinodal decomposition mechanism is limited to the field within the chemical spinodal. Coherent exsolution is constrained at lower temperature due to strain energy contributing to the free energy of the solid solution. The upper limit below which spinodal decomposition or coherent nucleation can take place are defined as the coherent solvus and spinodal.

Currently, the kinetics of spinel oxide exsolution has not been extensively researched and provides no constraints on hypotheses. Petrochilos (2010) theorised that the exsolution mechanism could be determined through observing the evolution of the bulk magnetic properties of samples, and that the Curie temperature was of vital importance. The magnetic properties of titaniferous-magnetite are beyond the scope of this dissertation, but is discussed here as part of the experimental work of Petrochilos (2010). Theory suggests that changes in the bulk Curie temperature could indicate the emergence of either titaniferous-magnetite or magnetite during the incipient stages of exsolution. If the exsolving phase evolves gradually from titaniferous-magnetite toward magnetite with an increasing volume fraction at a given temperature, then the exsolution mechanism is spinodal decomposition. If the exsolving phase composition is immediately rich in the magnetite component and unvarying through time, then the mechanism is more consistent with the nucleation mechanism (Petrochilos, 2010).

This study aims to analyse 10 sections made from samples of Layer 21. These samples were obtained from the BK1 borehole taken on the Bierkraal farm. Petrological and geochemical analysis of these sections and samples hope to provide more insight into the exsolution textures of titaniferous-magnetite in Layer 21 of the Bushveld Igneous Complex.

CHAPTER 3 METHODOLOGY

SAMPLING

Three deep boreholes were drilled in the Bierkraal area, cutting through the Upper Zone in the Western Limb of the Rustenburg Layered Suite (Britt, 2015). The holes were drilled by SACS; and provided research material from an area where the outcrop of Bushveld Igneous Complex rocks is poor. BK1, a 1230m vertical section through the top of the Upper Zone, has been extensively logged in order to identify layers and cycles throughout the sequence. BK1 was drilled through the felsic roof rocks of the Rashoop Granophyre Suite and intersected the Rustenburg Layered Suite at approximately 412m (SACS, 1980). Core logging followed the SACS subdivisions, with the succession showing three main rock types present, namely anorthosite, gabbros, and magnetite (Britt, 2015). On a broad scale, the rock sequence is similar to the typical rock sequences in the eastern limb of the Bushveld Complex (Reynolds, 1985).

Samples for chemical and petrographic analyses of Layer 21 were taken at intervals between 1425-1432m along BK1. 21 polished thin sections were prepared from the samples.

MICROSCOPY

21 polished thin sections were made from the core samples collected from Layer 21. The petrographic study of these thin sections aimed to identify minerals, examine textural relations, estimate modal proportions of the mineral assemblage, and identify and interpret changes throughout the sequence.

SCANNING ELECTRON MICROSCOPE

Element data, images, and line scans were collected for thin sections 2 MG 1.1 - 2 MG 2.8 using a JEOL JSM IT300 at the Department of Metallurgy at the University of Pretoria. Analytic conditions used during the analysis was an acceleration voltage of 15,0 kV. Each thin section was carbon coated.

Thin section examination was used to identify changes in elemental abundance throughout the sequence. The SEM imaging and line scan analysis using AzTec Version 3.0 also allowed for identification of various forms of exsolution, which sparked major interest in the textures shown by the oxides, specifically titaniferous-magnetite.

CHAPTER 4 RESULTS

MINERALOGY

Several points were analysed on each thin section with an SEM in order to observe the titaniferous-magnetite change, including variations between ulvöspinel, magnetite, and ilmenite. Each thin section will be discussed separately. The original classification grouped all analysis from the exsolved area as ulvöspinel. This was determined to be incorrect when considering the homogenous unmixing and the two end-members presenting themselves as the cloth like intergrowth.

2 MG 1.3

Thin section 2 MG 1.3 was sampled from a depth of 1425.7m in the Upper Zone.

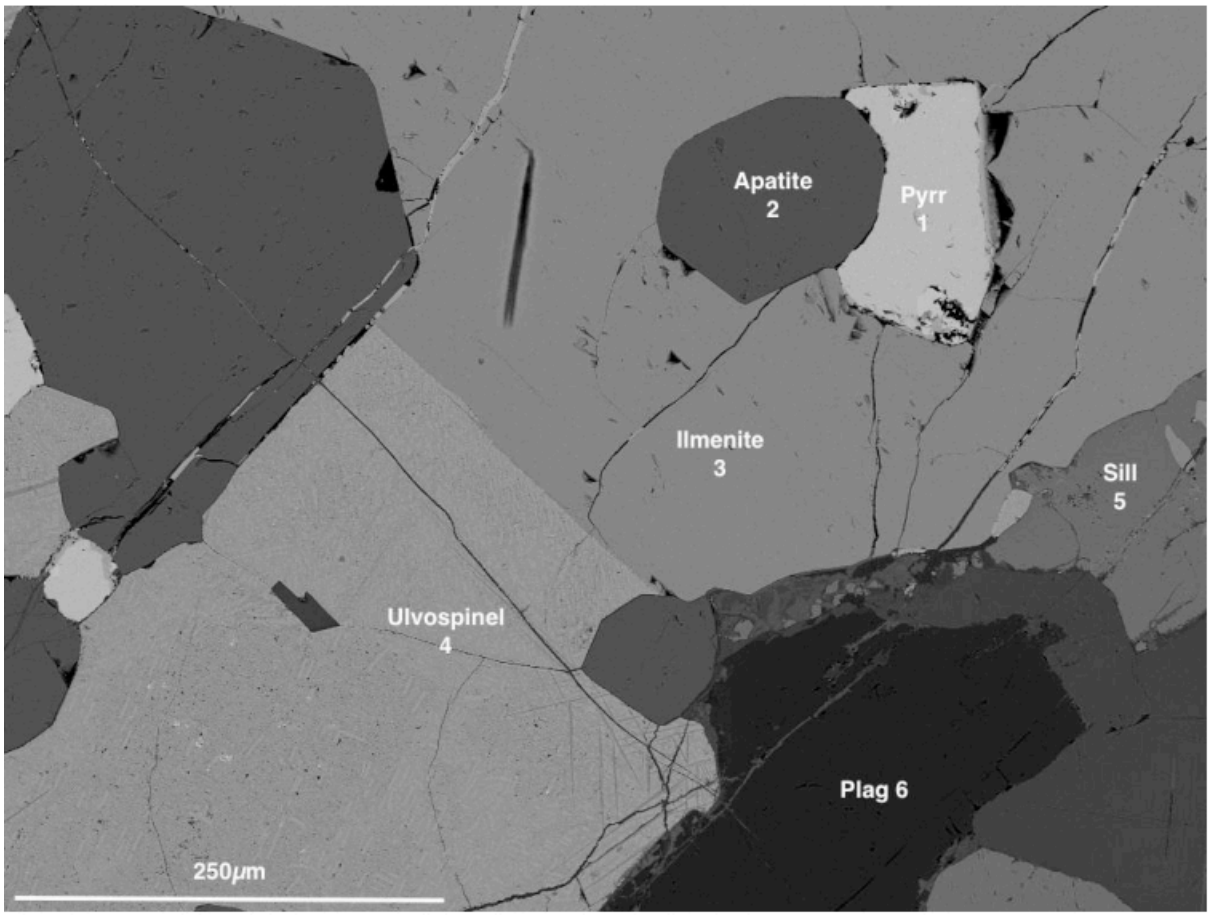

Figure 8. A SEM image of slide 2 MG 1.3 showing a cloth texture exsolution of titaniferous-magnetite grains together with various other minerals. The exsolved phases are magnetite and ulvöspinel. Apatite=Apatite; Ilmenite=Ilmenite; Plag=Plagioclase; Pyrr=Pyrrhotite; Sill=a Silicate; Ulvospinel=Ulvöspinel.

The titaniferous-magnetite in Figure 8 shows the cloth texture which forms due to the exsolution of titaniferous-magnetite on a large scale. Ilmenite is present in the image but "trellis" type exsolution of ilmenite cannot be seen. Pyrrhotite is present as a sulphide body, together with plagioclase and another silicate. In Figure 9, Figure 10, Figure 11, and Figure 12 the same minerals appear as in Figure 8, and also similar titaniferous-magnetite exsolution. Ilmenite is only spotted Figure 8 and not in the other images.

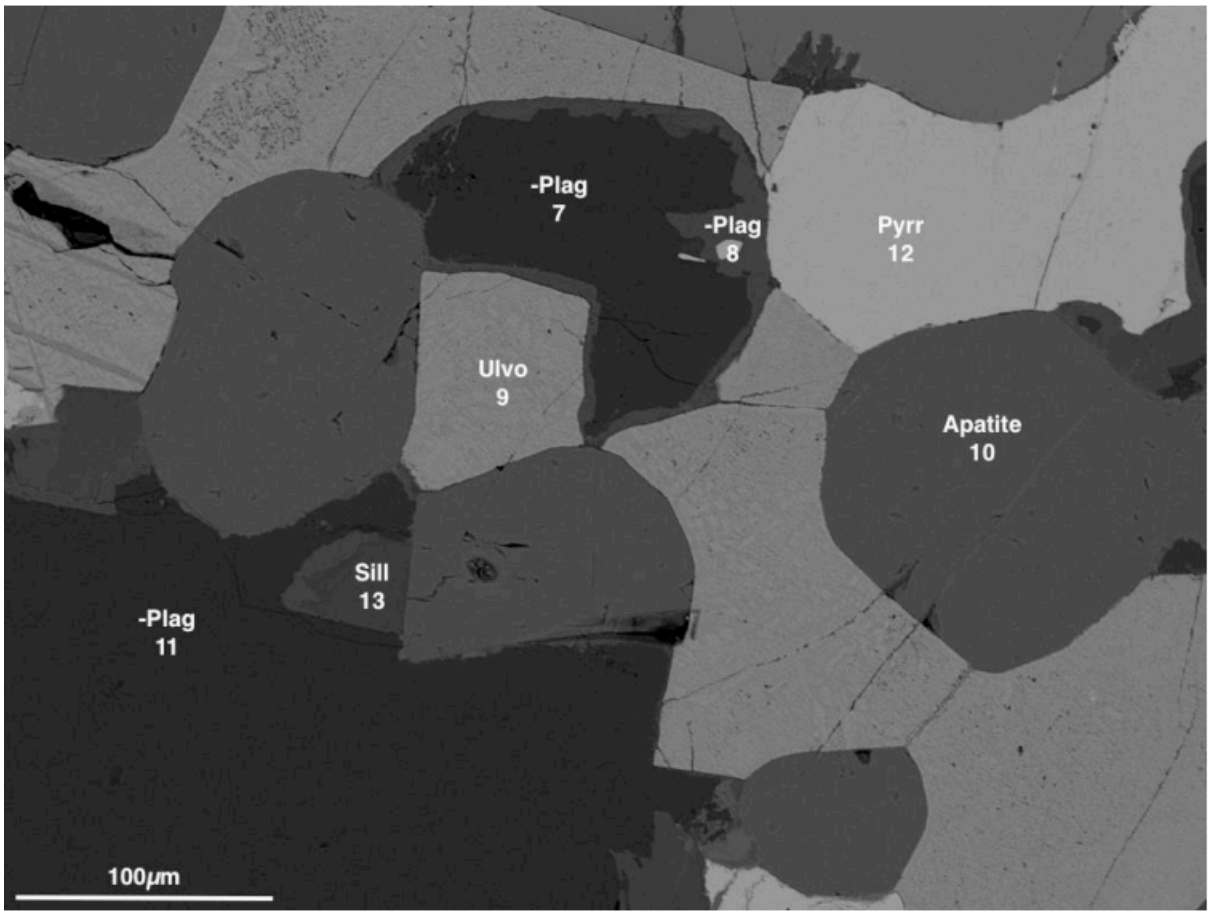

Figure 9. SEM image of slide 2 MG 1.3 showing large plagioclase grains, a cloth texture exsolution of titaniferous-magnetite grains, and various other minerals. The exsolved phases are magnetite, ulvöspinel and ilmenite. Apatite=Apatite; Plag=Plagioclase; Pyrr=Pyrrhotite; Sill=a Silicate; Ulvo=Ulvöspinel.

The exsolved titaniferous-magnetite grains are generally large and subhedral. Figure 10 and Figure 12 indicate extensive cracks or infiltration of another mineral into the titaniferous-magnetite grain. In most figures, plagioclase forms a rim around the titaniferous-magnetite grains. Magnetite appears between two silicate grains in Figure 12, suggesting that the mineral either filled empty space during formation or infiltrated between the two silicate grains.

Table 13 in Appendix A gives the elemental weight percentages measured by the SEM for each grain. Recalculated values of the results of the titaniferous-magnetite grains are reported as oxides in tabular form as seen in Table 1. The analysis number correlates to the labeled value on each image.

Table 1. Elemental weight percentages of the titaniferous-magnetite analysis (Figure 8 and Figure 9) recalculated as an oxide. Only elements of importance have been listed.

Figure 8				
Spectrum	**Al2O3**	**SiO2**	**FeO**	**TiO2**
4	3,514	0	72,517	18,332
Figure 9				
9	3,533	0,214	71,760	18,932

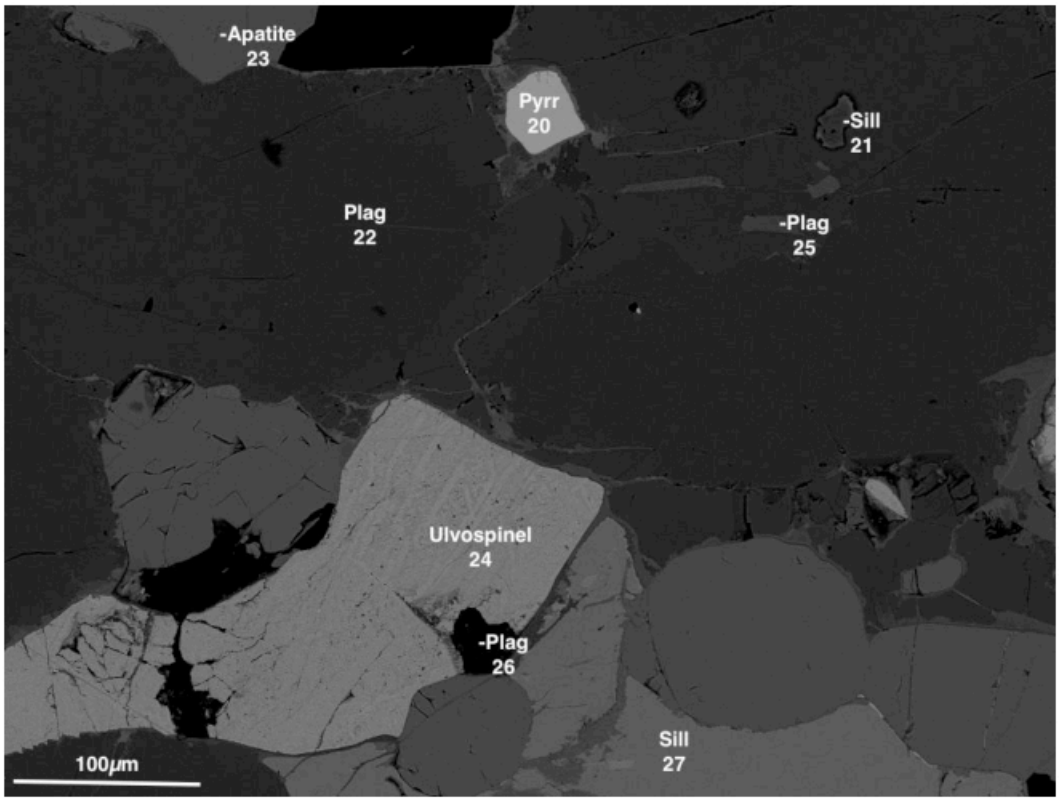

Figure 10. SEM image of slide 2 MG 1.3 showing large plagioclase grains with various silicate grains. Exsolution of titaniferous-magnetite can be seen at (24). The exsolved phases are magnetite and ulvöspinel. Apatite=Apatite; Plag=Plagioclase; Pyrr=Pyrrhotite; Sill=a Silicate; Ulvöspinel=Ulvöspinel.

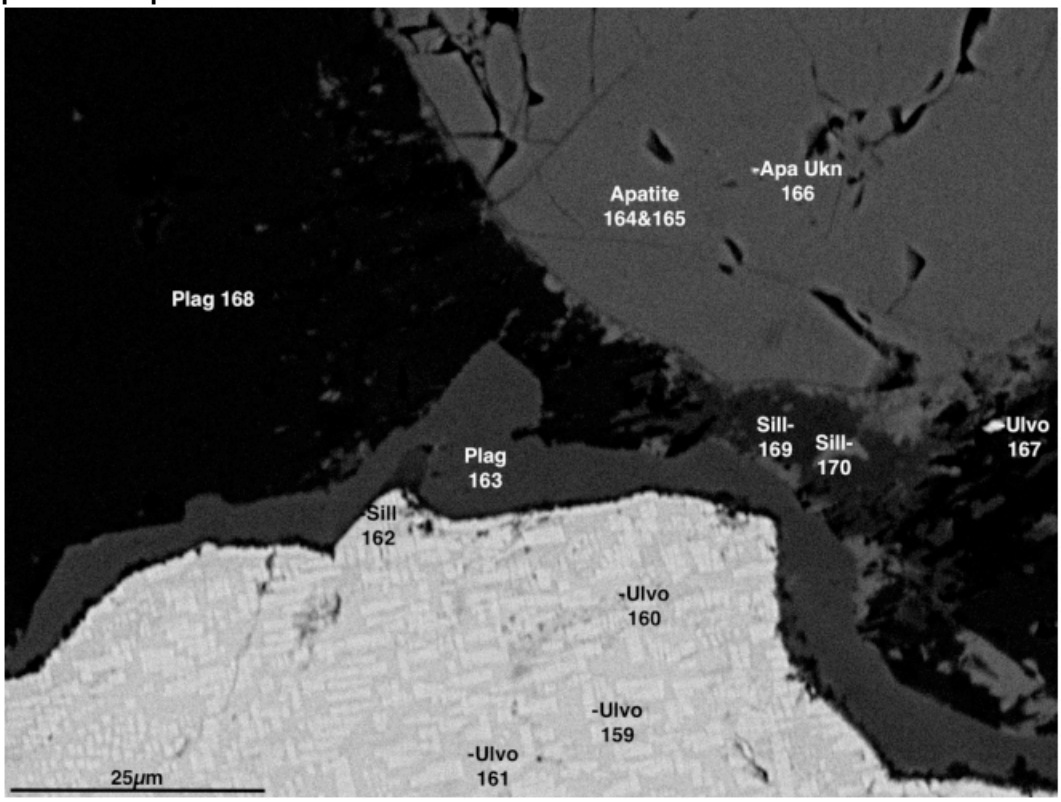

Figure 11. SEM image of slide 2 MG 1.3 showing a cloth texture exsolution of a titaniferous-magnetite grain. A silicate and plagioclase forms a ring around the titaniferous-magnetite grain. The exsolved phases are magnetite and ulvöspinel. Apatite=Apatite; Apa Ukn=Apatite Unknown; Plag=Plagioclase; Pyrr=Pyrrhotite; Sill=a Silicate; Ulvöspinel=Ulvöspinel.

Figure 11 shows a higher magnification of the titaniferous-magnetite grain and the cloth texture exsolution. The exsolution texture is not uniform; showing areas with more densely packed square prisms and sparse areas with rectangular prisms. This change can be seen throughout the sequence, being more prominent in certain images than others.

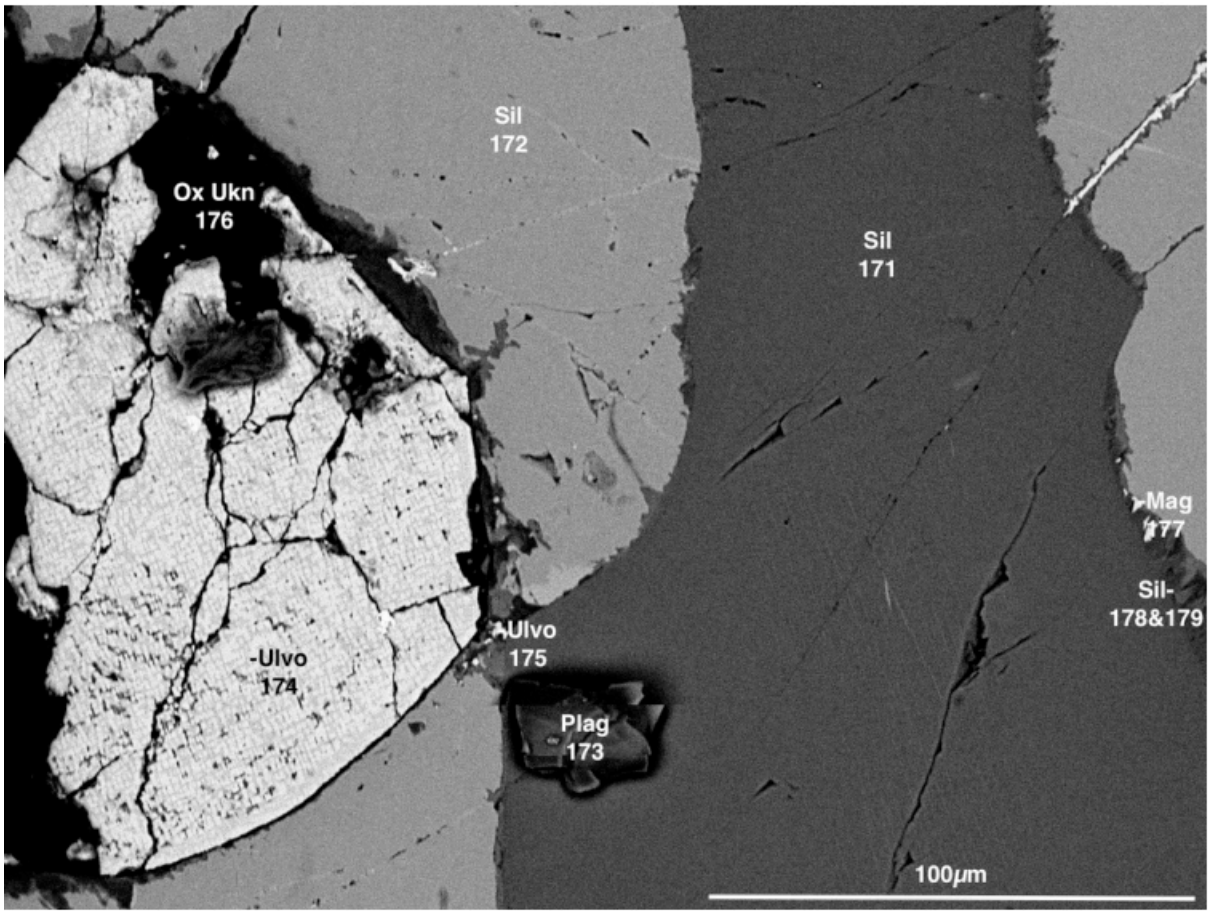

Figure 12. SEM image of slide 2 MG 1.3 showing a cracked titaniferous-magnetite grain surrounded by various other minerals. The exsolved phases presented by the cloth texture are magnetite and ulvöspinel. Apatite=Apatite; Mag=Magnetite; Ox Ukn=Oxide Unknown; Plag=Plagioclase; Pyrr=Pyrrhotite; Sill=a Silicate; Ulvöspinel=Ulvöspinel.

Table 2. Elemental weight percentages of the titaniferous-magnetite analysis (Figure 10, Figure 11, and Figure 12) recalculated as an oxide. Only elements of importance have been listed.

Spectrum	Al2O3	SiO2	FeO	TiO2
Figure 10				
24	3,401	0,321	71,510	18,367
Figure 11				
159	1,455	0	83,623	10,325
160	3,741	1,347	70,513	22,836
161	4,402	0,556	69,683	22,400
167	7,160	12,235	70,403	4,170
Figure 12				
174	0	1,134	0,513	82,927
175	5,438	1,908	7,978	78,250

2 MG 1.6

Thin section 2 MG 1.6 was sampled from a depth of 1425.7m in the Upper Zone.

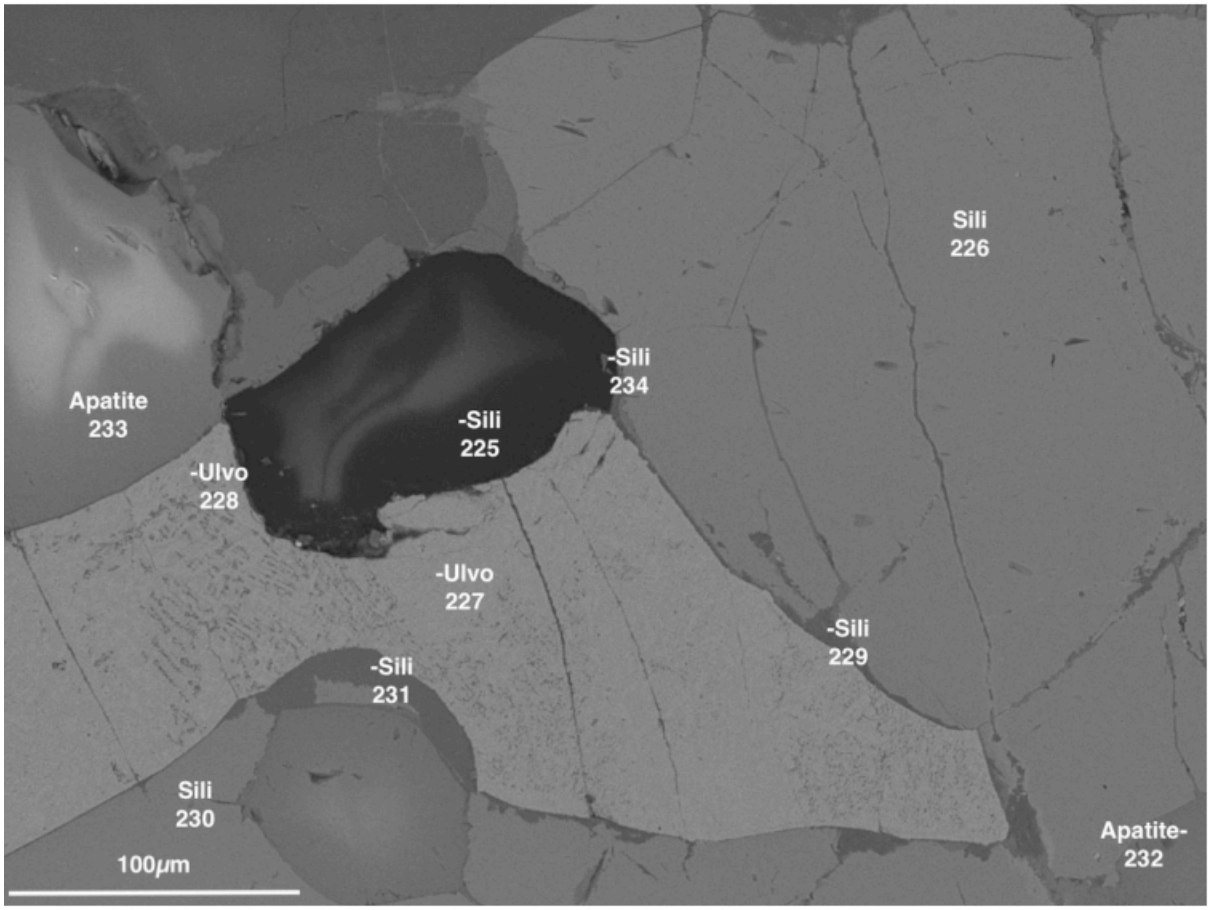

Figure 13. SEM image of slide 2 MG 1.6 showing a cloth texture exsolution of titaniferous-magnetite grains together with large silicate grains and apatite. The exsolved phases are magnetite and ulvöspinel. Apatite=Apatite; Plag=Plagioclase; Sill=a Silicate; Ulvöspinel=Ulvöspinel.

Figure 13 shows no “trellis” type exsolution present in the titaniferous-magnetite grain. Figure 14, however, does show a small amount of ilmenite exsolution as indicated in red. The silicates continue to form a rim around the titaniferous-magnetite grain in each figure. The appearance of small, dark spots can be seen in the titaniferous-magnetite grains. Figures 9 and 10 also show these dark spots in localised positions across the grains.

Figure 14 shows a mineral included in the silicates and titaniferous-magnetites. These inclusions seem to be localised, and are not present throughout the titaniferous-magnetite grains. Both Figure 13 and Figure 14 show the presence of similar minerals to slide 2 MG 1.3, although no sulphides could be identified.

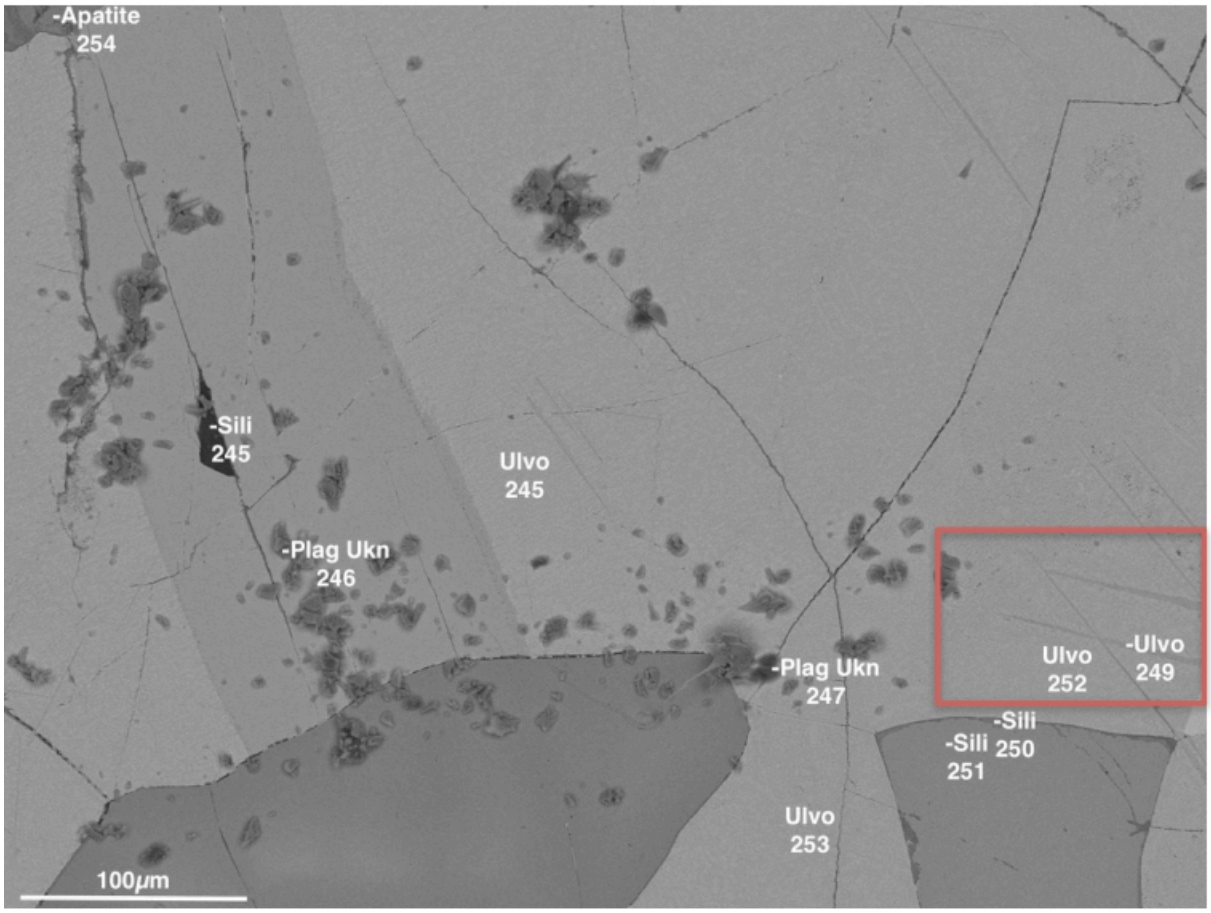

Figure 14. A SEM image of slide 2 MG 1.6 showing a spotty formation of plagioclase grains. The exsolved titaniferous-magnetite grain is large, and ilmenite is present as "trellis" type exsolution (indicated in red). The exsolved phases are magnetite and ulvöspinel. Apatite=Apatite; Sill=a Silicate; Ulvo=Ulvöspinel.

Table 3. Elemental weight percentages of the titaniferous-magnetite analysis (Figure 13 and Figure 14) recalculated as an oxide. Only elements of importance have been listed.

Spectrum	MgO	Al2O3	SiO2	FeO	TiO2
Figure 13					
227	0	3,193	0,984	62,479	26,403
228	2,968	5,612	3,787	69,645	9,292
Figure 14					
248	0	3,496	0	74,218	17,515
249	0	6,934	0	55,760	36,498
252	0	3,042	0	69,580	24,702
253	0	1,493	0,642	84,780	9,958

2 MG 1.8

Thin section 2 MG 1.8 was sampled from a depth of 1426.4m in the Upper Zone.

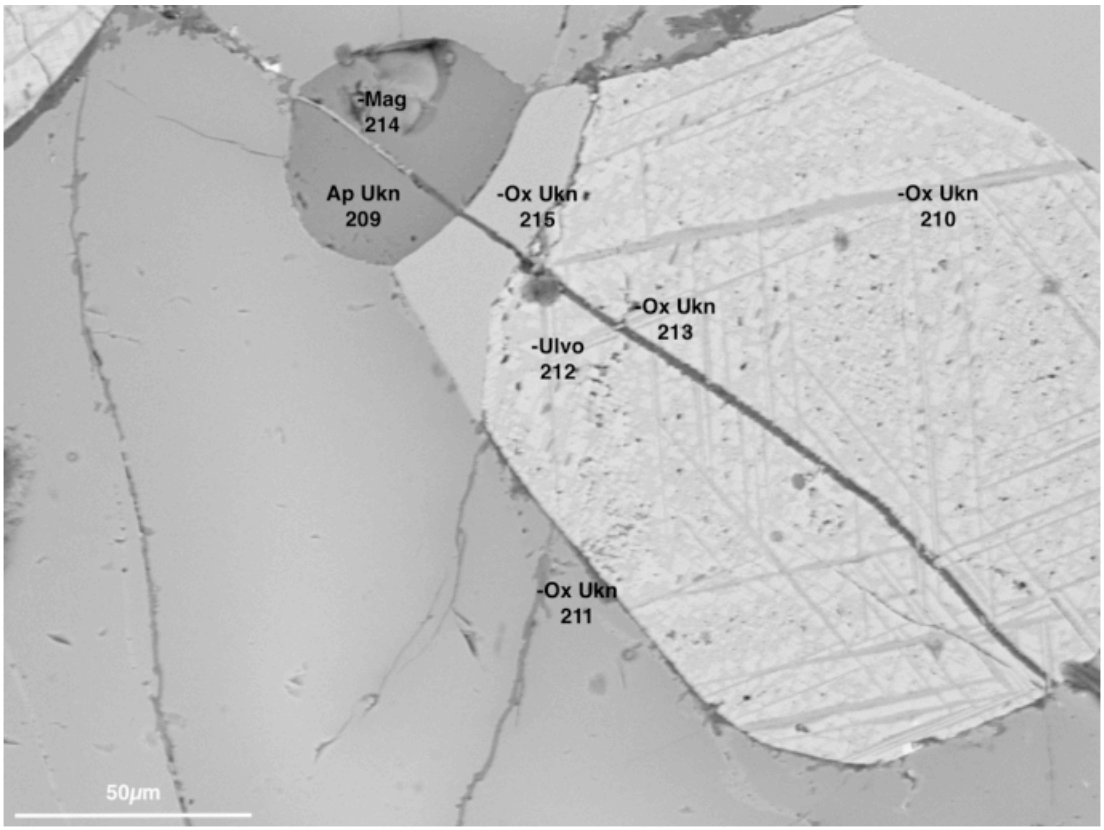

Figure 15. SEM image of slide 2 MG 1.8 showing a cloth texture exsolution of a titaniferous-magnetite grain as well as ilmenite "trellis" type exsolution. The exsolved phases are magnetite and ulvöspinel. Apatite=Apatite; Ilmenite=Ilmenite; Mag=Magnetite; Plag=Plagioclase; Pyrr=Pyrrhotite; Sill=a Silicate; Ulvo=Ulvöspinel.

Figure 15 shows an exsolved titaniferous-magnetite grain as well as a "trellis" type texture as a result of the exsolution of ilmenite. Here, the "trellis" type texture is found throughout the titaniferous-magnetite grain and not localised in a region as seen in Figure 14. No sulphides are present.

Magnetite is present in Figure 15, Figure 16, and Figure 17. Figure 16 shows the cloth texture exsolution of titaniferous-magnetite, but without any ilmenite exsolution. Figure 17 shows a large pyrrhotite grain together with plagioclase and silicates. A dark mineral shows small inclusions throughout the image, but this was not analysed.

Table 4. Elemental weight percentages of the titaniferous-magnetite analysis (Figure 15, Figure 16, and Figure 17) recalculated as an oxide. Only elements of importance have been listed.

Spectrum	MgO	Al2O3	SiO2	FeO	TiO2
Figure 15					
212	0	4,992	0,435	57,104	17,130
Figure 17					
299	0	0	0	38,600	4,747

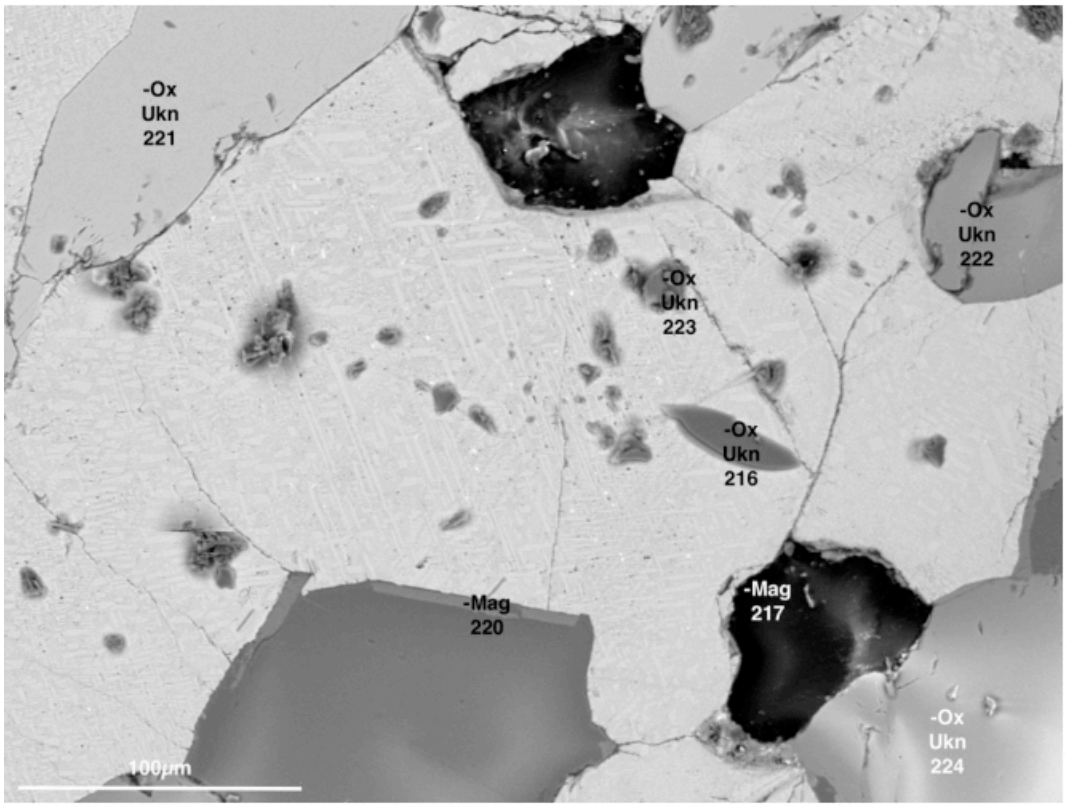

Figure 16. SEM image of slide 2 MG 1.8 showing a cloth texture exsolution of titaniferous-magnetite grains together with various other minerals. The exsolved phases are magnetite and ulvöspinel. Apatite=Apatite; Ilmenite=Ilmenite; Plag=Plagioclase; Pyrr=Pyrrhotite; Sill=a Silicate; Ulvo=Ulvöspinel.

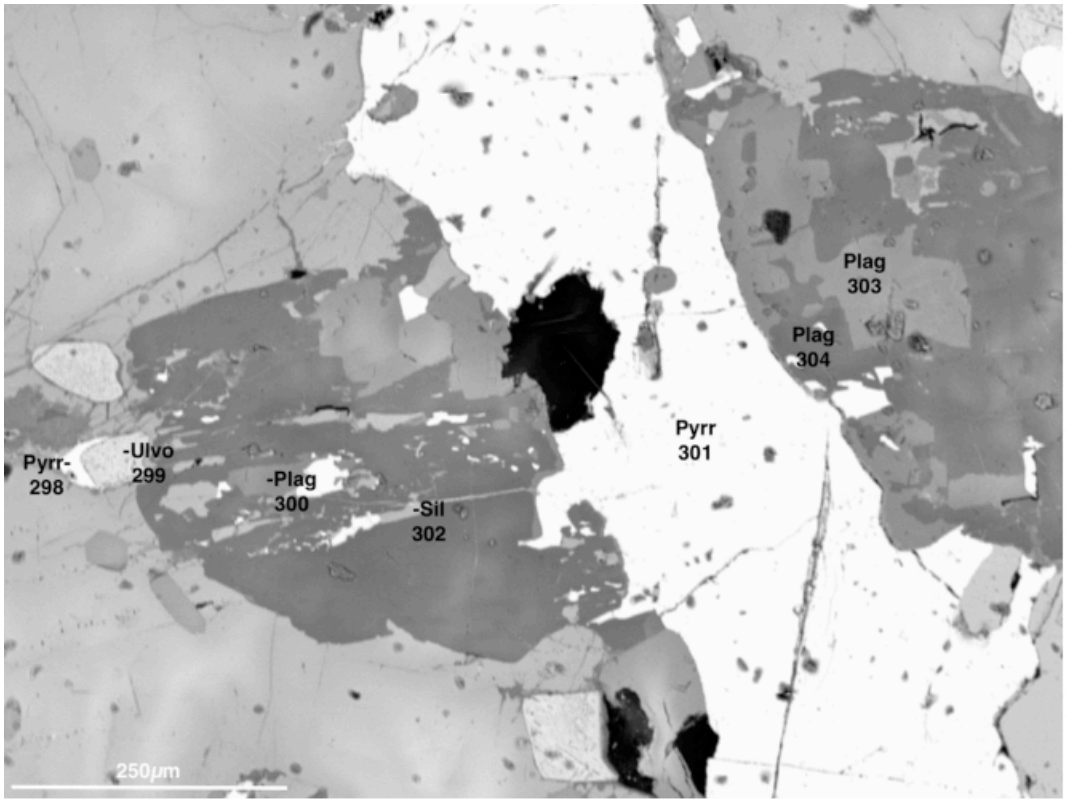

Figure 17. SEM image of slide 2 MG 1.8 showing a large pyrrhotite grain together with plagioclase and silicate grains. A small titaniferous-magnetite grain is visible. Plag=Plagioclase; Pyrr=Pyrrhotite; Sill=a Silicate; Ulvo=Ulvöspinel.

2 MG 2.0

Thin section 2 MG 2.0 was sampled from a depth of 1426.8m in the Upper Zone.

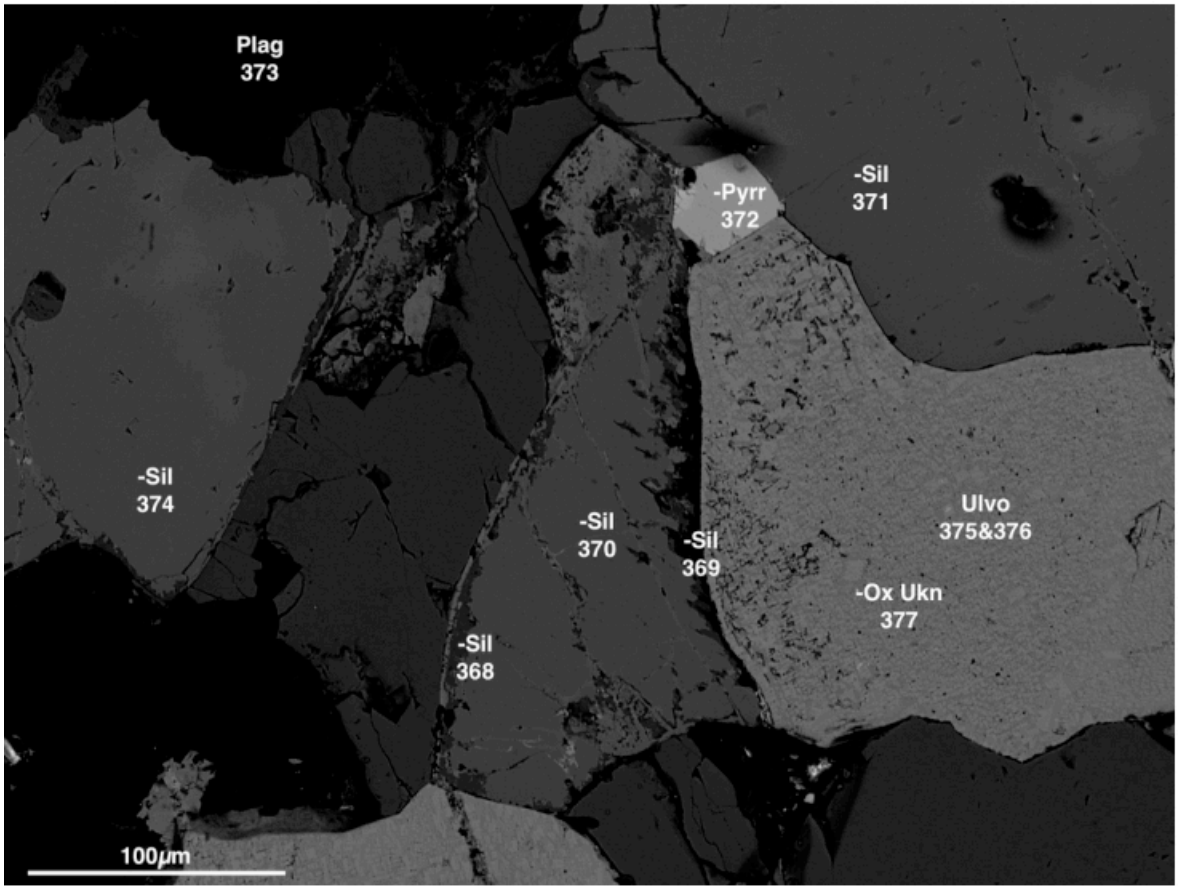

Figure 18. SEM image of slide 2 MG 2.0 showing a cloth texture exsolution of titaniferous-magnetite grains, surrounded by a silicate and plagioclase. The exsolved phases are magnetite and ulvöspinel. Plag=Plagioclase; Ox Ukn=Oxide Unknown; Pyrr=Pyrrhotite; Sill=a Silicate; Ulvo=Ulvöspinel.

Figure 18 shows the reemergence of sulphides over the 4m interval from 2 MG 1.8 to 2 MG 2.0. Titaniferous-magnetite grains continue to show a cloth like exsolution texture, with the titaniferous-magnetite grain surrounded by a silicate. The small, dark spots are present in Figure 18, but not in Figure 19.

The grains in Figure 19a were not analysed, but Figure 19b shows a high magnification of a region indicated by the red rectangle. No “trellis” type texture is visible, which indicates a lack of ilmenite at this depth. The exsolution texture in Figure 19b is relatively uniform, with some minor change of the prisms towards the bottom left of the image.

Various images have labels indicating an “unknown” analysis. These unknown minerals have been grouped in with specific elements, but their analyses indicate that they do not perfectly match the minerals they are grouped with. This could be for various reasons, such as the SEM spectra clipping over two minerals, problems with the thin section carbon coating, or internal SEM problems.

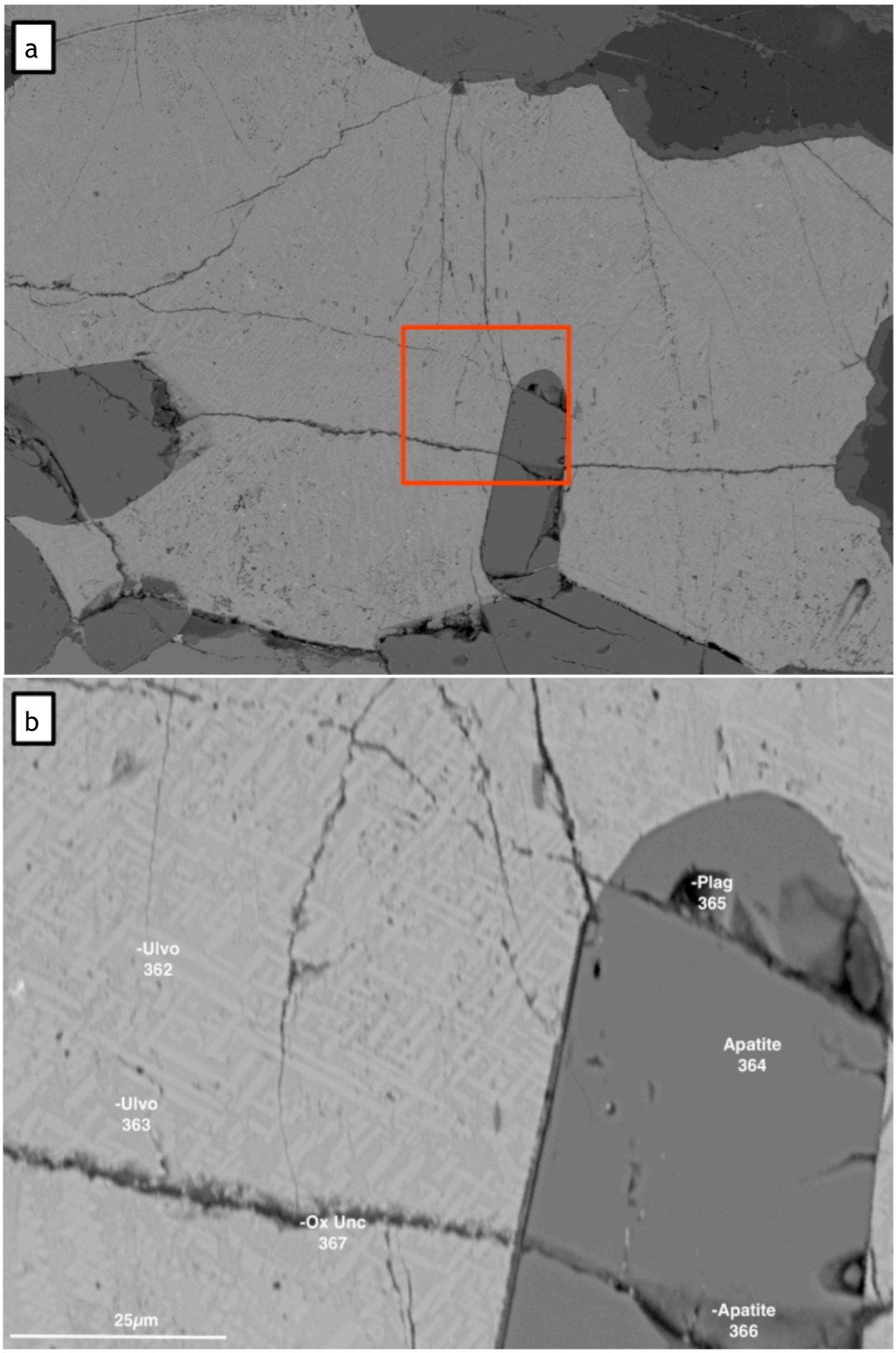

Figure 19. SEM image of slide 2 MG 2.0 showing titaniferous-magnetite grains which are exsolved. (a): A large titaniferous-magnetite grain together with other minerals. (b): A high magnification image of a region indicated by the red rectangle. The prisms formed by the exsolution can be clearly seen. The exsolved phases are magnetite and ulvöspinel. Apatite=Apatite; Plag=Plagioclase; Ulvo=Ulvöspinel.

Table 5. Elemental weight percentages of the titaniferous-magnetite analysis (Figure 18 and Figure 19) recalculated as an oxide. Only elements of importance have been listed.

Spectrum	MgO	Al2O3	SiO2	FeO	TiO2
Figure 18					
375	0	0	0	70,366	9,954
376	0	3,809	0,250	60,735	20,546
Figure 19					
362	0	1,481	0,272	71,342	10,688
363	0	4,270	0,313	57,105	22,337

2 MG 2.2A

Thin section 2 MG 2.2a was sampled from a depth of 1427.2m in the Upper Zone.

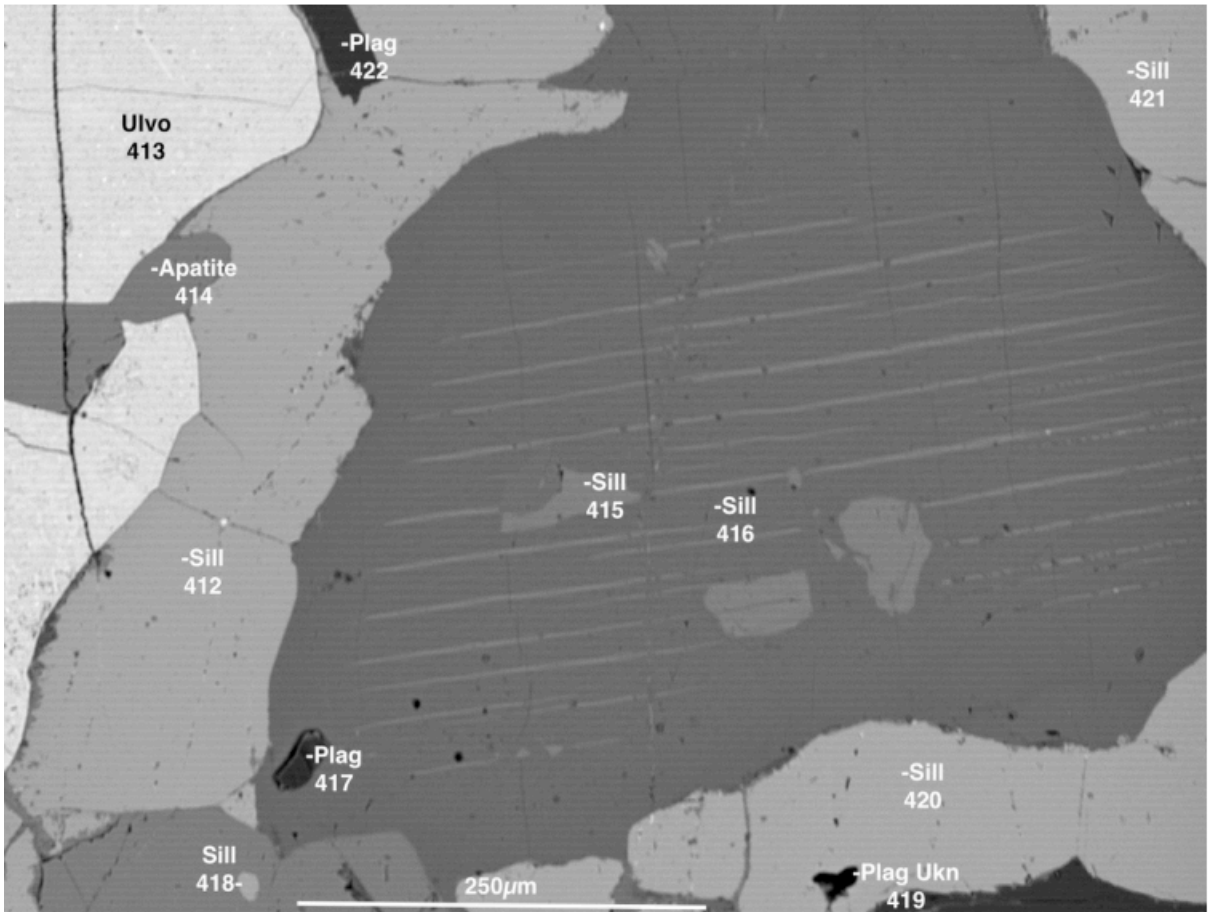

Figure 20. SEM image of slide 2 MG 2.2a showing the exsolution of a silicate, in this case orthopyroxene. The cloth-like texture of titaniferous-magnetite exsolution is also visible. The exsolved phases are magnetite (white) and ulvöspinel (darker). Apatite=Apatite; Plag=Plagioclase; Sill=a Silicate; Ulvo=Ulvöspinel.

Ilmenite is not visible in any images collected form 2 Mg 2.2a, but was identified in the line scans that are discussed later in this section. An exsolved silicate grain is indicated by Figure 20, together with exsolved titaniferous-magnetite grains. Plagioclase and silicates are present as found in every image.

Figure 21 is a higher magnification image of an exsolved titaniferous-magnetite grain. Prisms alternate in size as well as in angle throughout the grain. Certain parts of the grain once again indicate darker spots. This dark spots are not systematic throughout the mineral, but rather localised in two areas, with some minor emergences throughout the rest of the grain. These dark spots are considered to be holes, which may be due to the leaching of sulphides, indicated by the small, light grains in the image. The cloth texture prism change is very clear in Figure 23, showing various titaniferous-magnetite grains. These grains exhibit areas with smaller, blocky prisms, and areas with longer, rectangular prisms. The other exsolved phases are localised as all other images show.

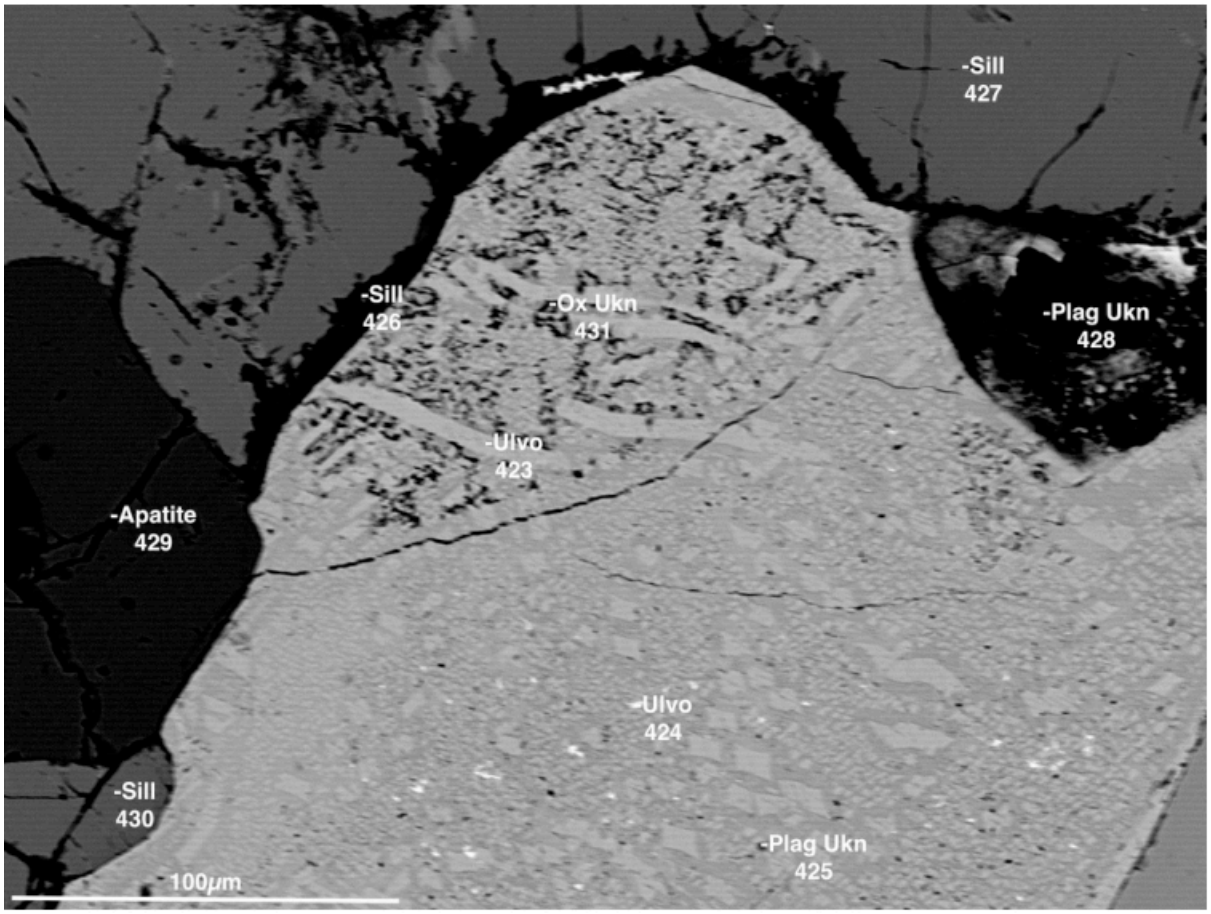

Figure 21. SEM image of slide 2 MG 2.2a showing a high magnification image of the cloth texture exsolution of a titaniferous-magnetite grain. The exsolved phases are magnetite and ulvöspinel. Apatite=Apatite; Plag=Plagioclase; Sill=a Silicate; Ulvöspinel=Ulvöspinel.

Figure 22 shows the presence of pyrrhotite, but once again only as a small grain. Here the titaniferous-magnetite grain exhibits less than a subhedral structure, but rather a more anhedral structure. A silicate has formed a similar rim around the titaniferous-magnetite grain as seen in previous slides. Pyrrhotite is also present in Figure 24, having a subhedral shape.

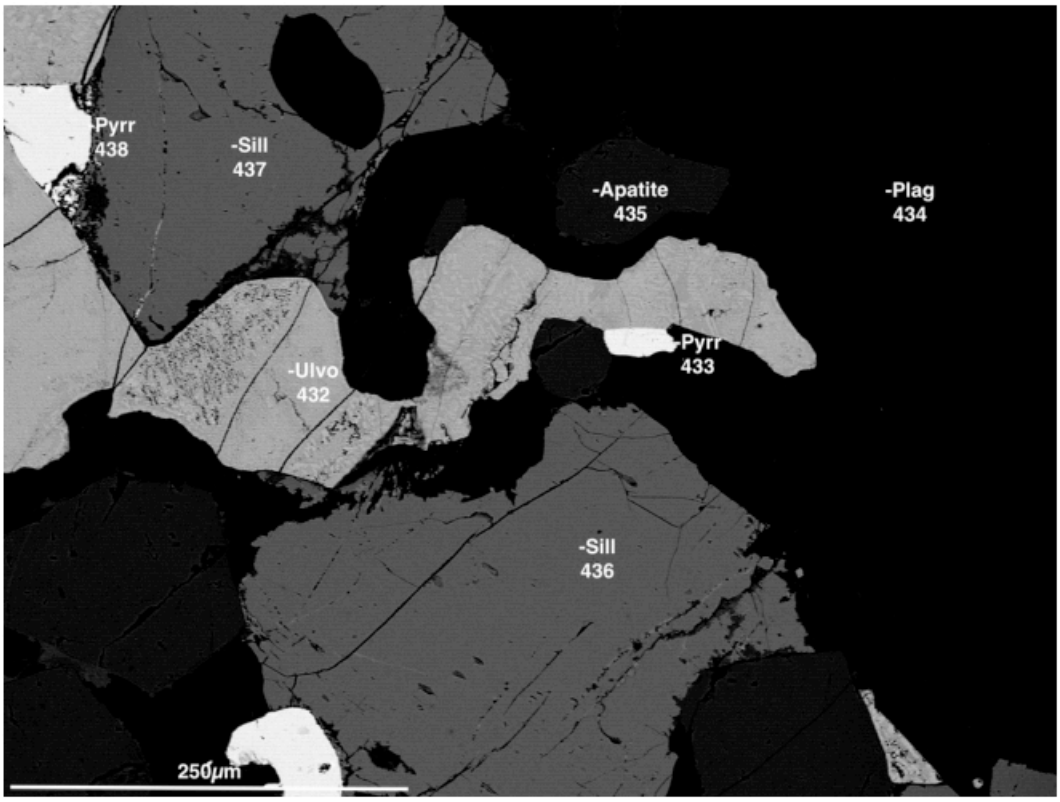

Figure 22. SEM image of slide 2 MG 2.2a showing a large plagioclase grain with a titaniferous-magnetite grain, silicates and pyrrhotite. Apatite=Apatite; Plag=Plagioclase; Pyrr=Pyrrhotite; Sill=a Silicate; Ulvo=Ulvöspinel.

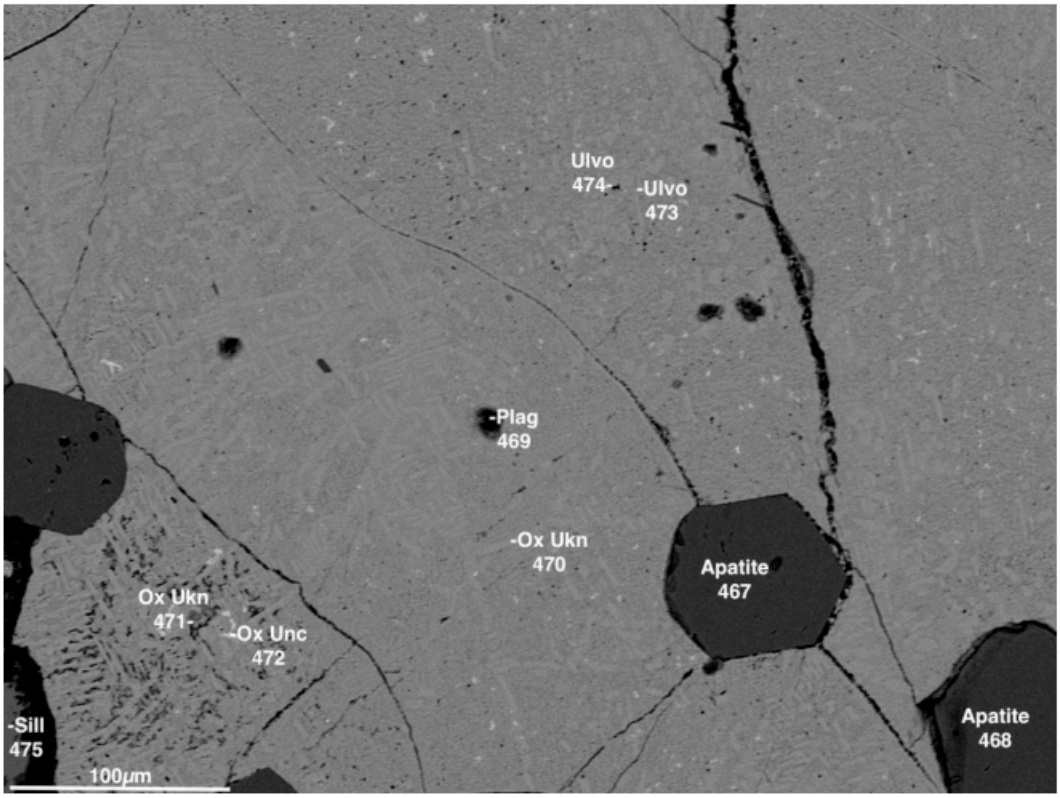

Figure 23. SEM image of slide 2 MG 2.2a showing various titaniferous-magnetite grains. The cloth texture exsolution is clearly visible, with variations between grains. The exsolved phases are magnetite and ulvöspinel. Apatite=Apatite; Plag=Plagioclase; Sill=a Silicate; Ulvo=Ulvöspinel.

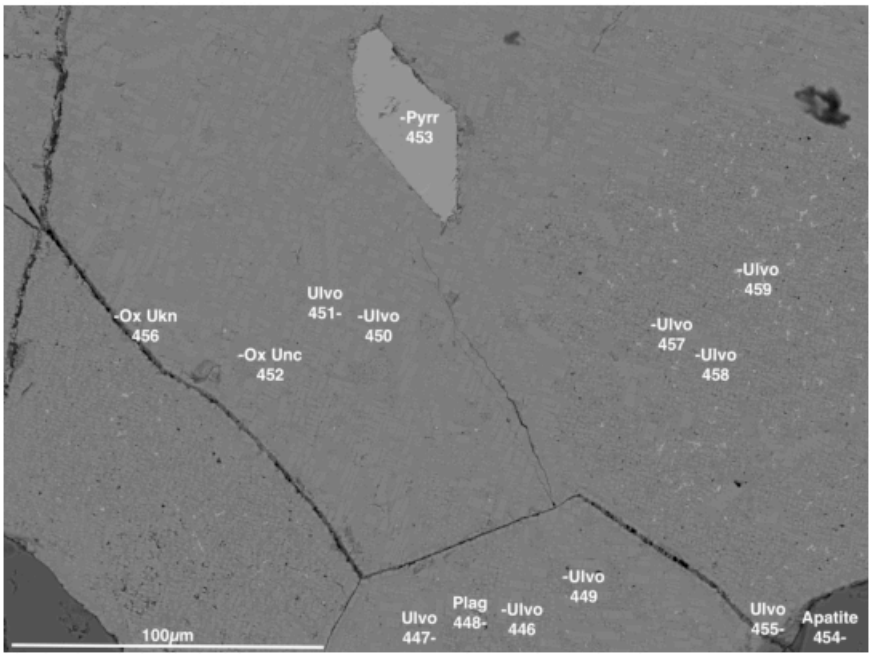

Figure 24. SEM image of slide 2 MG 2.2a showing various titaniferous-magnetite grains with a cloth texture exsolution that varies from grain to grain. The exsolved phases are magnetite and ulvöspinel. Apatite=Apatite; Plag=Plagioclase; Sill=a Silicate; Ulvo=Ulvöspinel.

Table 6. Elemental weight percentages of the titaniferous-magnetite analysis (Figure 20, Figure 21, Figure 22, Figure 23, and Figure 24) recalculated as an oxide. Only elements of importance have been listed.

Spectrum	MgO	Al2O3	SiO2	FeO	TiO2
Figure 20					
413	0	4,434	0,301	61,569	0,289
Figure 21					
423	0	0	0,320	74,061	0,232
424	0	2,364	0,362	69,509	0,301
Figure 22					
432	0	3,939	0,273	62,430	0,355
Figure 23					
473	0	2,250	0,347	65,700	0,487
474	0	4,398	0,944	61,700	0,570
Figure 24					
446	0	0	0	70,805	0,300
447	0	3,280	0	61,705	0,333
449	0	1,900	0	87,270	0,370
450	0	3,280	0	60,710	0,333
451	0	3,940	0	61,059	0,440
455	0	0,438	1,634	81,650	0,284
457	0	2,358	1,480	74,146	0,360
458	0	3,109	0	62,303	0,334
459	0,847	5,446	0	70,127	0,319

2 MG 2.2B

Thin section 2 MG 2.2b was sampled from a depth of 1427.3m in the Upper Zone.

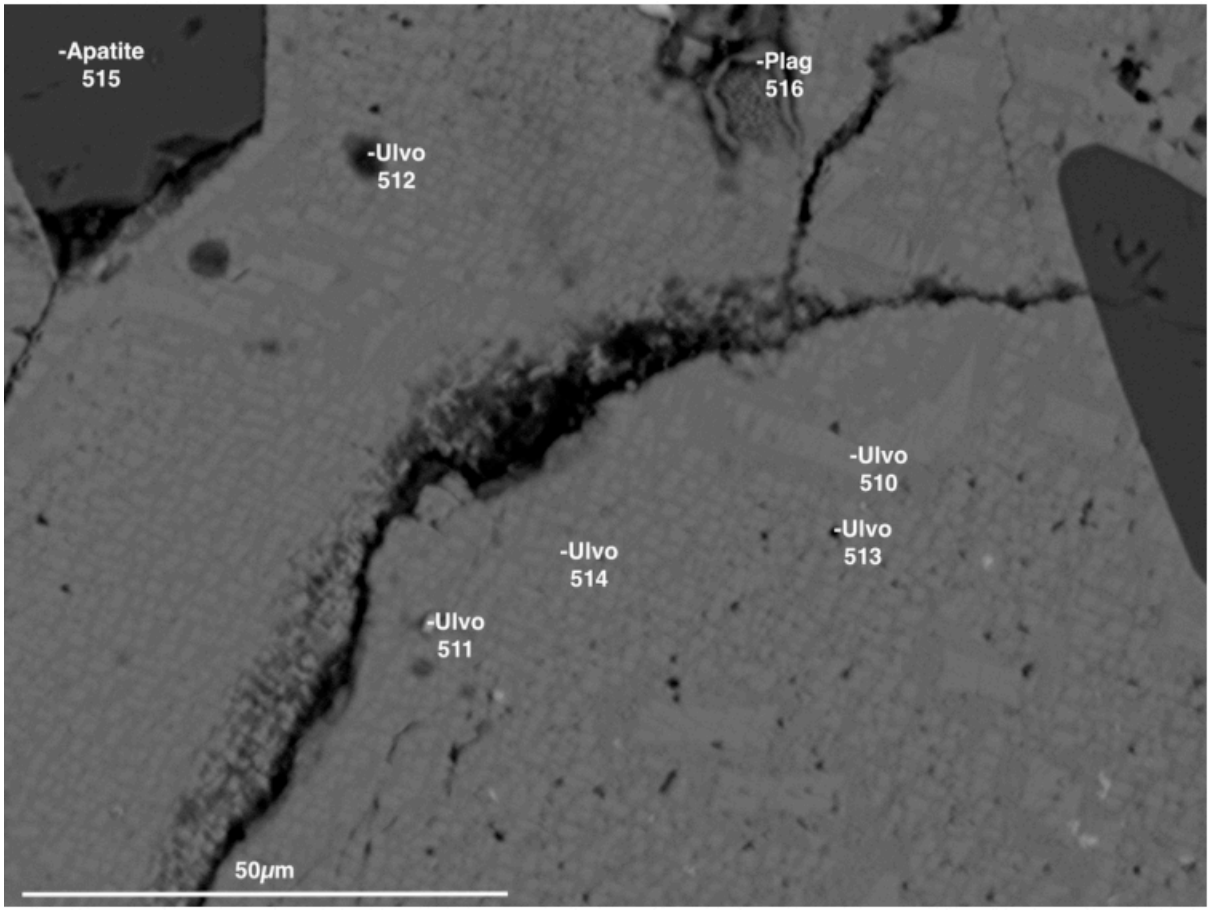

Figure 25. SEM image of slide 2 MG 2.2b showing a cloth texture exsolution of titaniferous-magnetite grains together with apatite and plagioclase. The exsolved phases are magnetite and ulvöspinel. Apatite=Apatite; Plag=Plagioclase; Sill=a Silicate; Ulvo=Ulvöspinel.

Titaniferous-magnetite grains in Figure 25, Figure 26, Figure 27, Figure 28, and Figure 29 exhibit the same cloth texture in titaniferous-magnetite grains. The holes are still present, but to a lesser extent. Figure 29 shows a greater amount of the holes, once again localised to a specific area on the titaniferous-magnetite grain. The small sulphides are also absent in some images, but is seen in large abundance in Figure 28.

Ilmenite is present in Figure 26, but no “trellis” type exsolution is seen. Pyrrhotite is still present in some figures. Figure 27 shows what appears to be either a magnetite vein or an inclusion of magnetite.

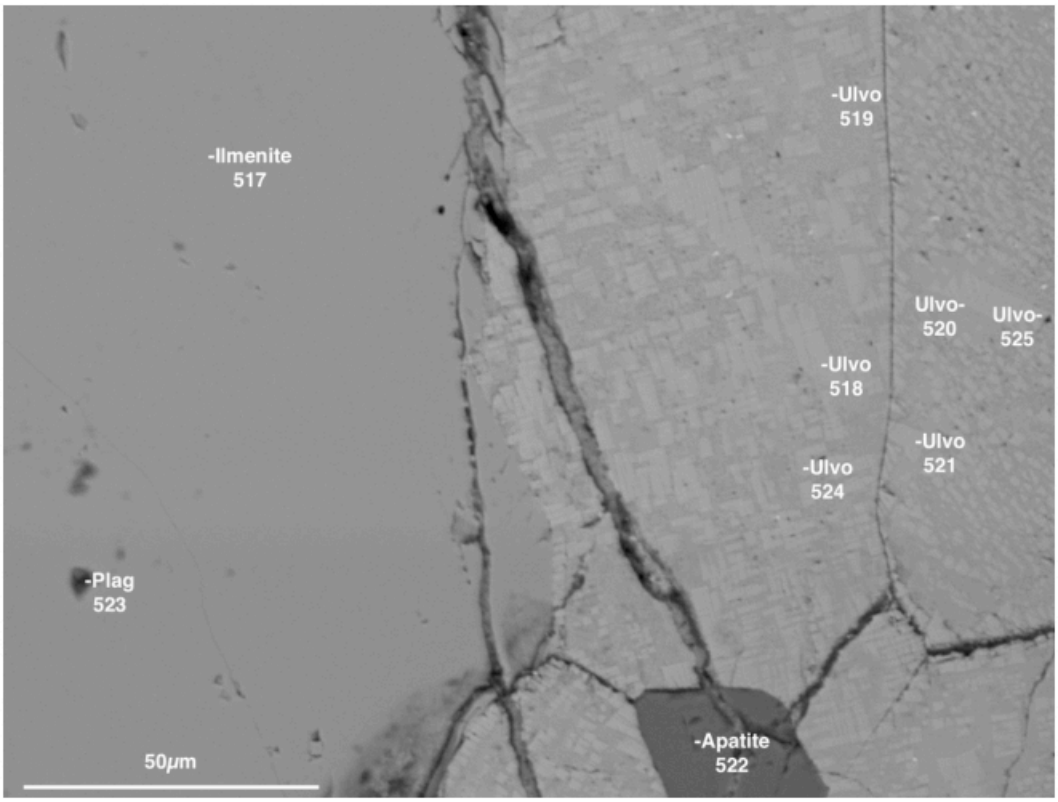

Figure 26. SEM image of slide 2 MG 2.2b showing an ilmenite grain next to an exsolved titaniferous-magnetite grain. The exsolved phases are magnetite and ulvöspinel. Apatite=Apatite; Ilmenite=Ilmenite; Plag=Plagioclase; Ulvo=Ulvöspinel.

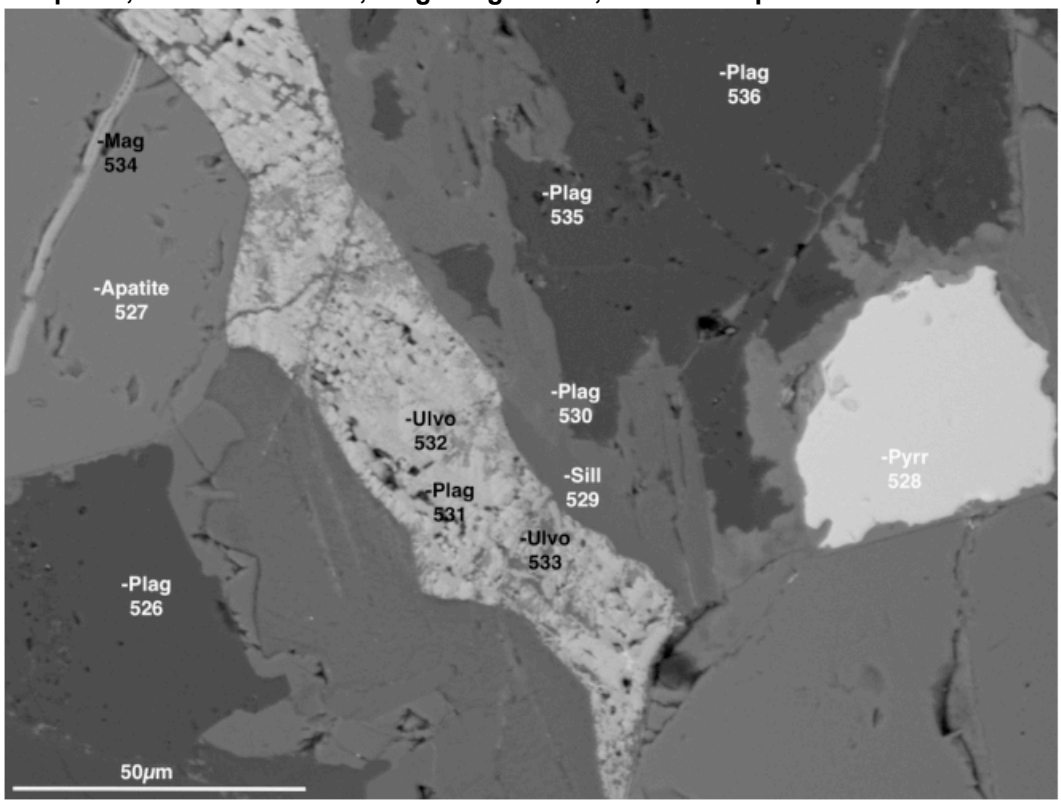

Figure 27. SEM image of slide 2 MG 2.2b showing a cloth texture exsolution of a titaniferous-magnetite grain. Magnetite is present as a vein through an apatite grain. The exsolved phases are magnetite and ulvöspinel. Apatite=Apatite; Mag=Magnetite; Plag=Plagioclase; Pyrr=Pyrrhotite; Sill=a Silicate; Ulvo=Ulvöspinel.

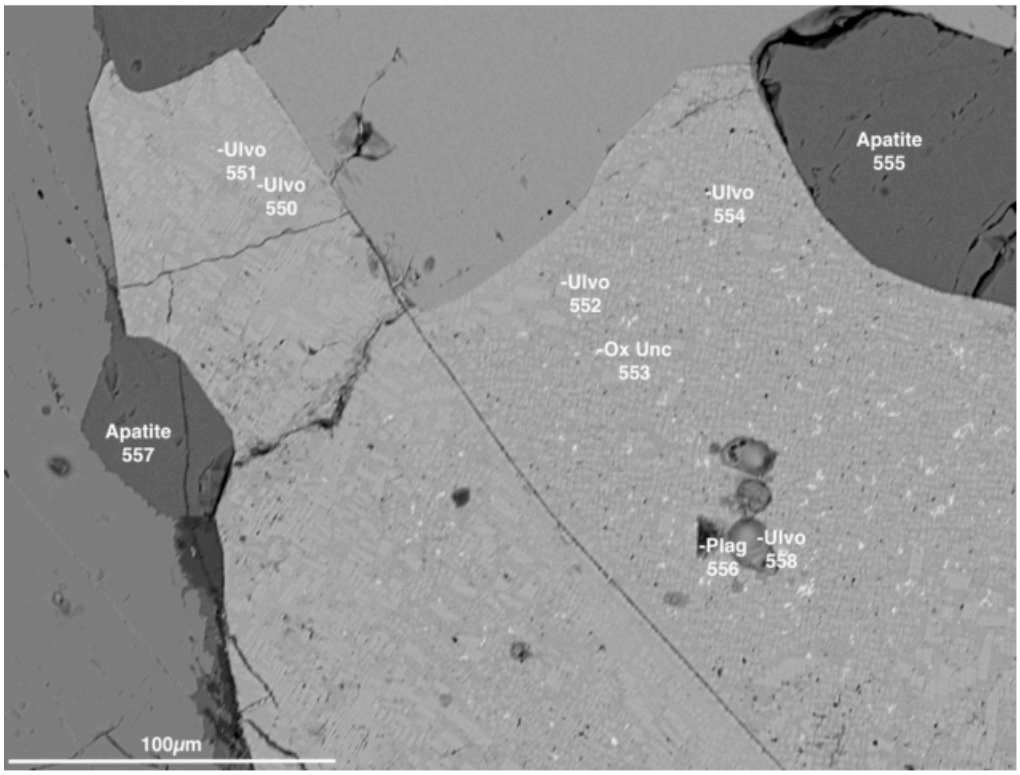

Figure 28. SEM image of slide 2 MG 2.2b showing a cloth texture exsolution of titaniferous-magnetite grains together with various other minerals. The exsolution shows small changes between different grains. The exsolved phases are magnetite and ulvöspinel. Apatite=Apatite; Plag=Plagioclase; Ulvo=Ulvöspinel.

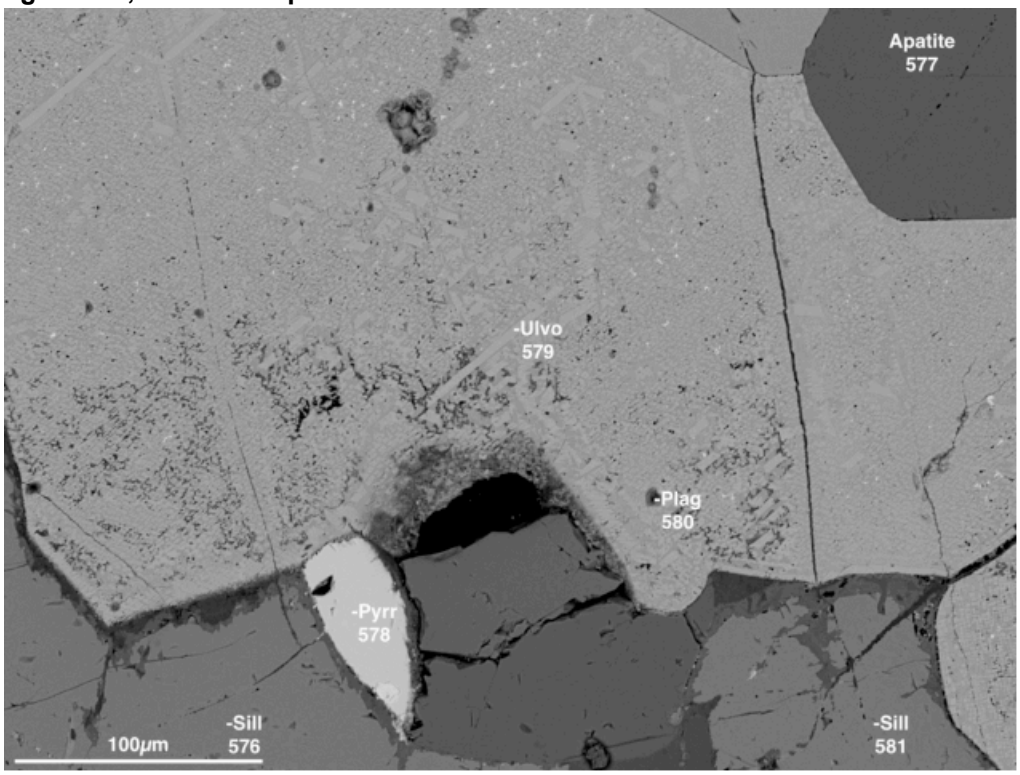

Figure 29. SEM image of slide 2 MG 2.2b showing a large titaniferous-magnetite grain with a cloth texture exsolution. The exsolved phases are magnetite and ulvöspinel. Apatite=Apatite; Plag=Plagioclase; Pyrr=Pyrrhotite; Ulvo=Ulvöspinel.

Table 7. Elemental weight percentages of the titaniferous-magnetite analysis (Figure 25, Figure 26, Figure 27, Figure 28, and Figure 29) recalculated as an oxide. Only elements of importance have been listed.

Spectrum	MgO	Al2O3	SiO2	FeO	TiO2
Figure 25					
510	0	2,142	0,427	80,393	10,995
511	0	2,632	3,249	88,793	14,744
512	0	3,638	3,794	71,797	20,098
513	0	3,378	0,537	71,118	17,511
514	0	2,233	0,559	76,198	15,342
Figure 26					
518	0	1,574	0,361	81,535	9,935
519	0	4,680	0	67,755	22,830
520	0	3,375	0,337	67,988	24,080
521	0	1,451	0,338	82,685	8,810
524	0	5,106	1,269	73,016	15,025
525	0	3,671	1,131	68,754	16,587
Figure 27					
532	0	1,124	0,558	85,409	7,085
533	1,813	12,296	13,606	45,663	15,257
Figure 28					
550	0	2,091	0,335	77,459	14,713
551	0	3,980	0,312	67,552	26,563
552	0	0	0	81,237	9,272
554	0	3,512	3,400	62,975	20,336
558	0	0	0,926	81,069	1,408
Figure 29					
579	0	0,594	0,359	81,803	10,663

2 MG 2.4

Thin section 2 MG 2.4 was sampled from a depth of 1427.6m in the Upper Zone.

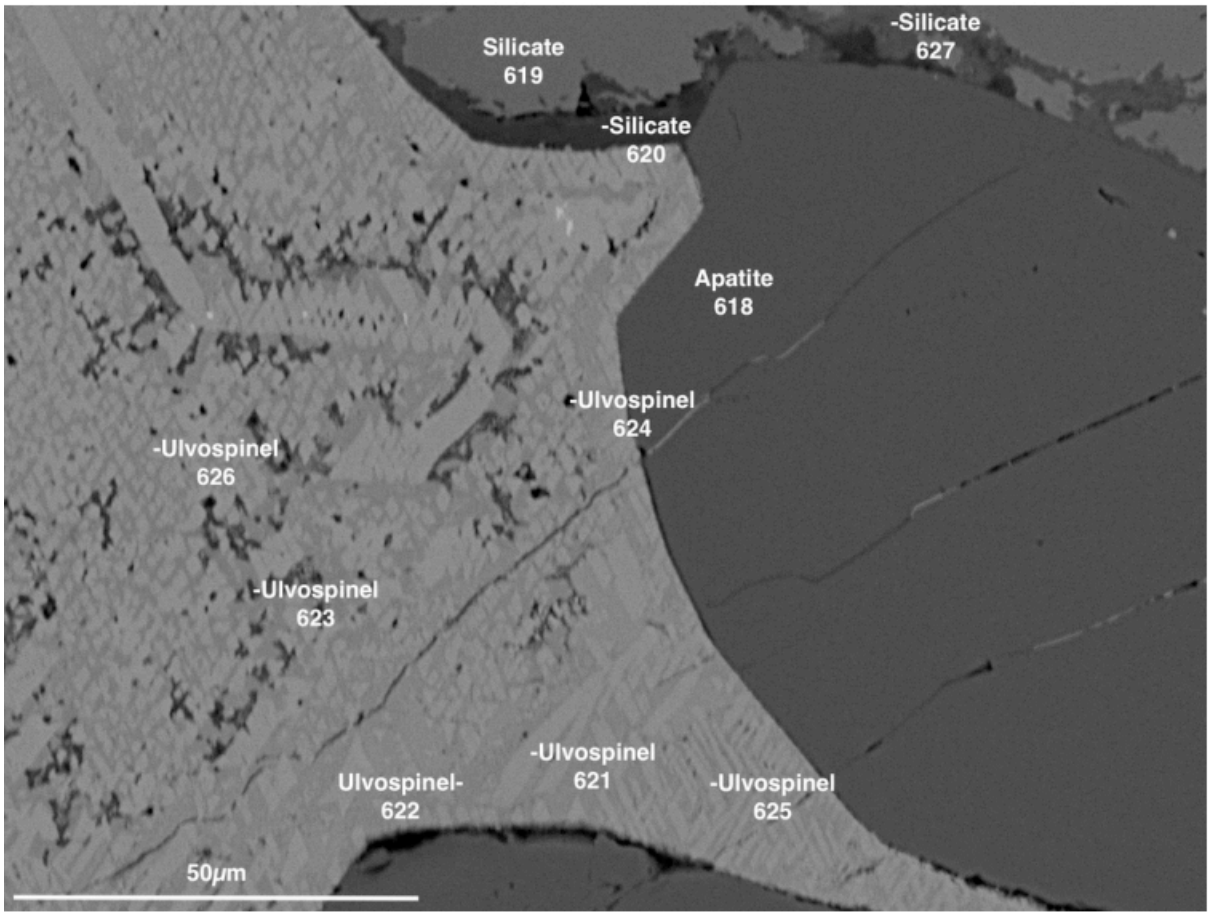

Figure 30. SEM image of slide 2 MG 2.4 showing a titaniferous-magnetite grain next to an apatite grain. A clear change in the cloth texture exsolution can be seen. The exsolved phases are magnetite and ulvöspinel. Apatite=Apatite; Silicate=a Silicate; Ulvospinel=Ulvöspinel.

Figure 30 shows the cloth exsolution texture found in titaniferous-magnetite grains, and also distinctly shows prism changes in the texture. The small holes are present, but only a few emergences of the small sulphides. A silicate rim is present around the titaniferous-magnetite grain, but this does not seem to form between the titaniferous-magnetite and the apatite grain.

Figure 31 shows pyrrhotite in a similar subhedral shape as in previous slides. Cloth texture exsolution shows localised darker areas, with a central area showing no small holes and elongated prisms. An area of the titaniferous-magnetite grain seems to be infiltrated by an unknown oxide body, appearing corroded.

Figure 32 shows the reemergence of the “trellis” type texture, although ilmenite is not present elsewhere in the images. The small holes are still present, and a distinct cut off of these holes can be seen in Figure 33. Magnetite is identified in Figure 24; with a similar infiltrating or included appearance as in slide 2 MG 2.2b.

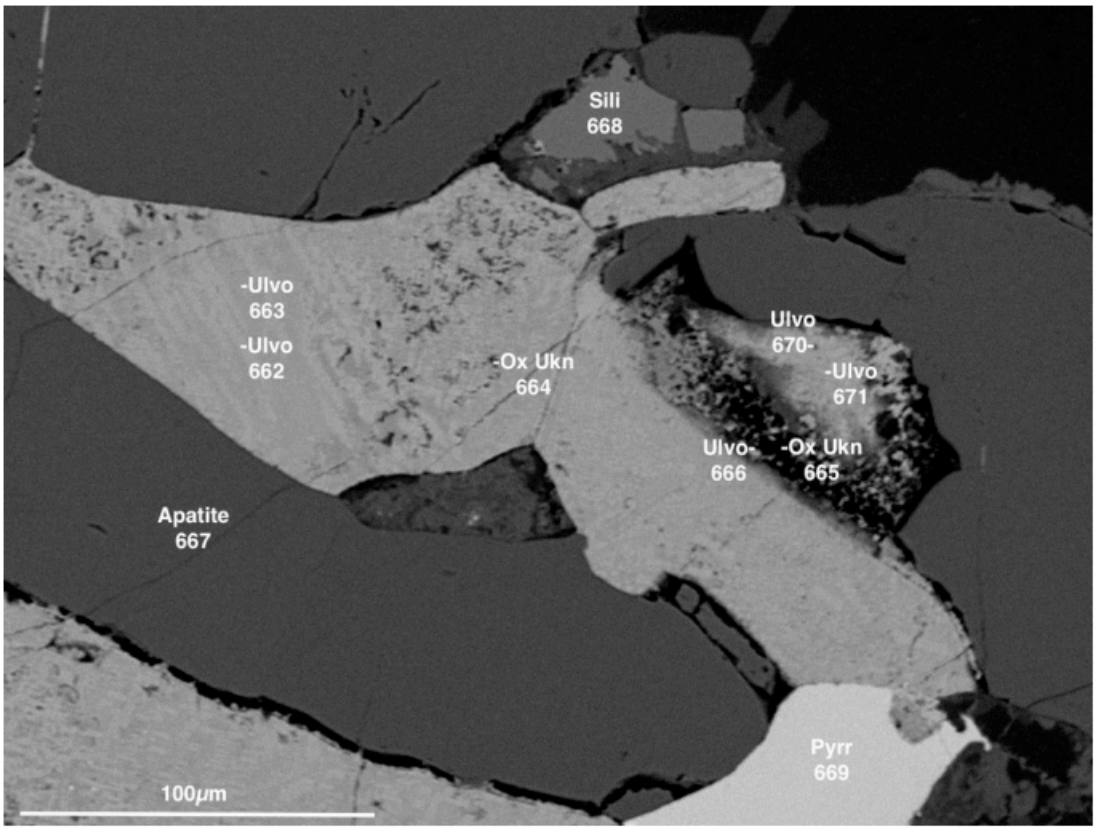

Figure 31. SEM image of slide 2 MG 2.4 showing ulvöspinel with apatite and silicates. The exsolved phases are magnetite and ulvöspinel. Apatite=Apatite; Pyrr=Pyrrhotite; Sill=a Silicate; Ulvo=Ulvöspinel.

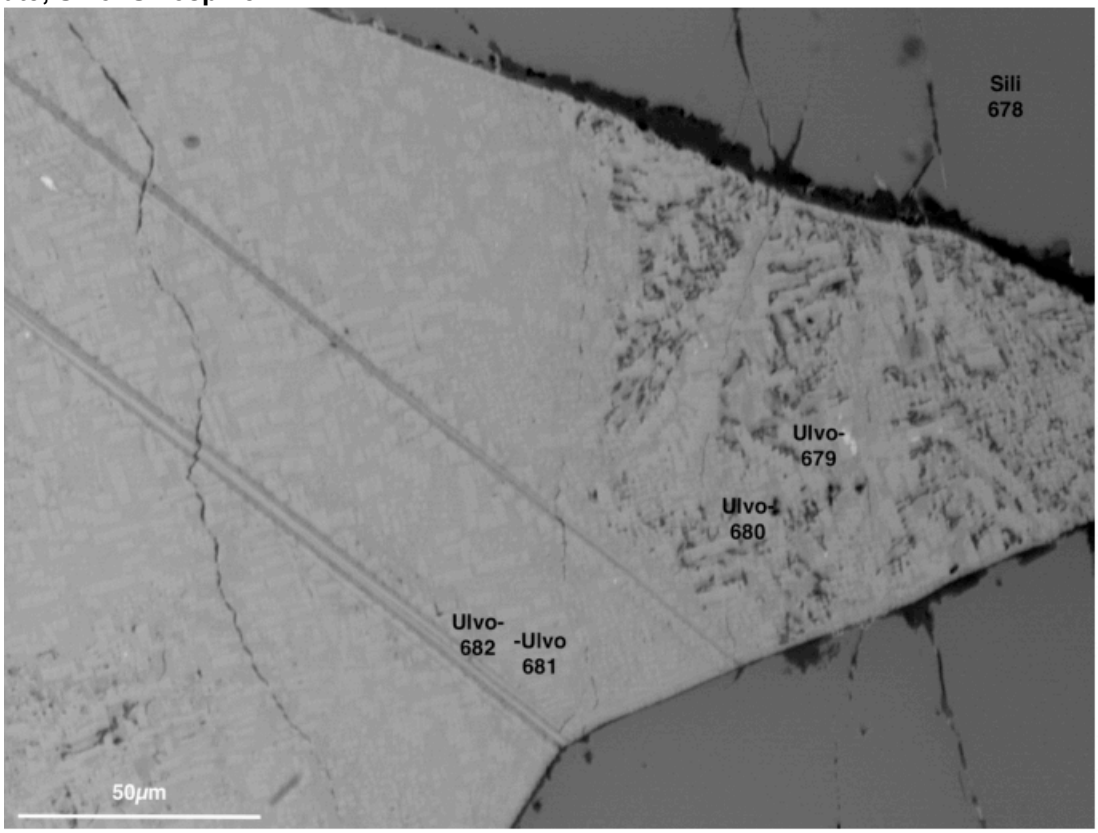

Figure 32. SEM image of slide 2 MG 2.4 showing a reemergence of "trellis" type texture due to ilmenite. Cloth texture exsolution of the titaniferous magnetite grain is still present. The exsolved phases are magnetite and ulvöspinel. Sill=a Silicate; Ulvo=Ulvöspinel.

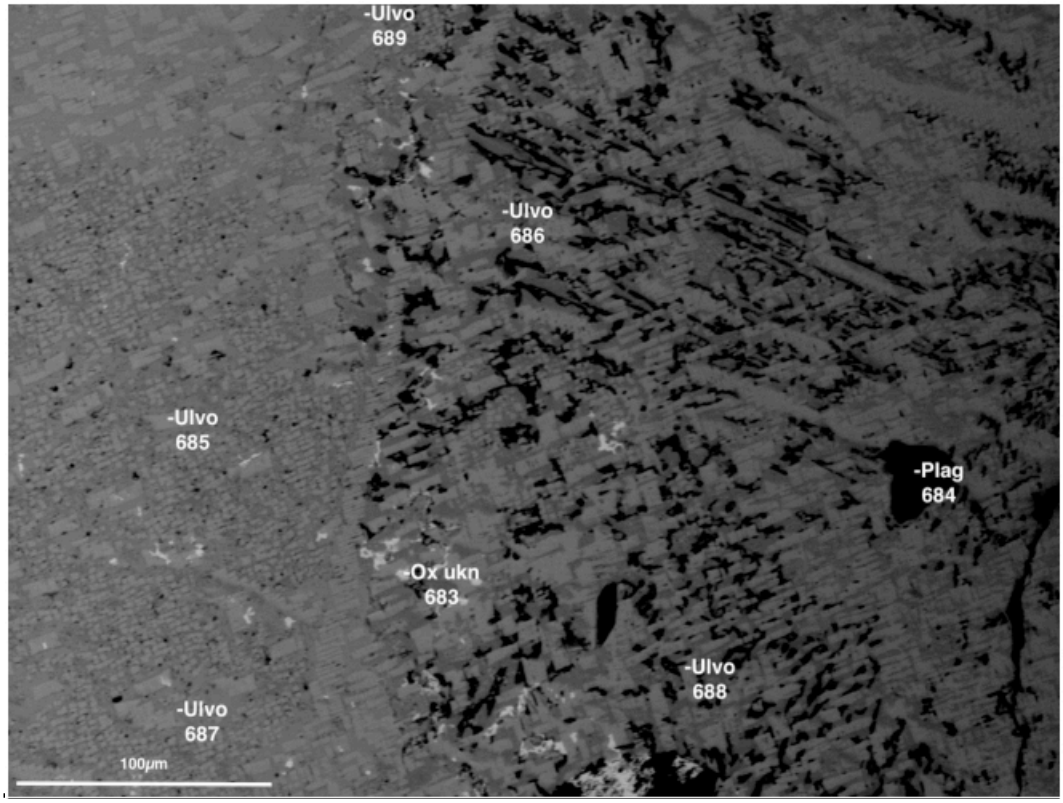

Figure 33. SEM image of slide 2 MG 2.4 showing a magnified titaniferous-magnetite grain with a lighter area and a darker area. The exsolved phases are magnetite and ulvöspinel. Apatite=Apatite; Ilmenite=Ilmenite; Plag=Plagioclase; Pyrr=Pyrrhotite; Sill=a Silicate; Ulvo=Ulvöspinel.

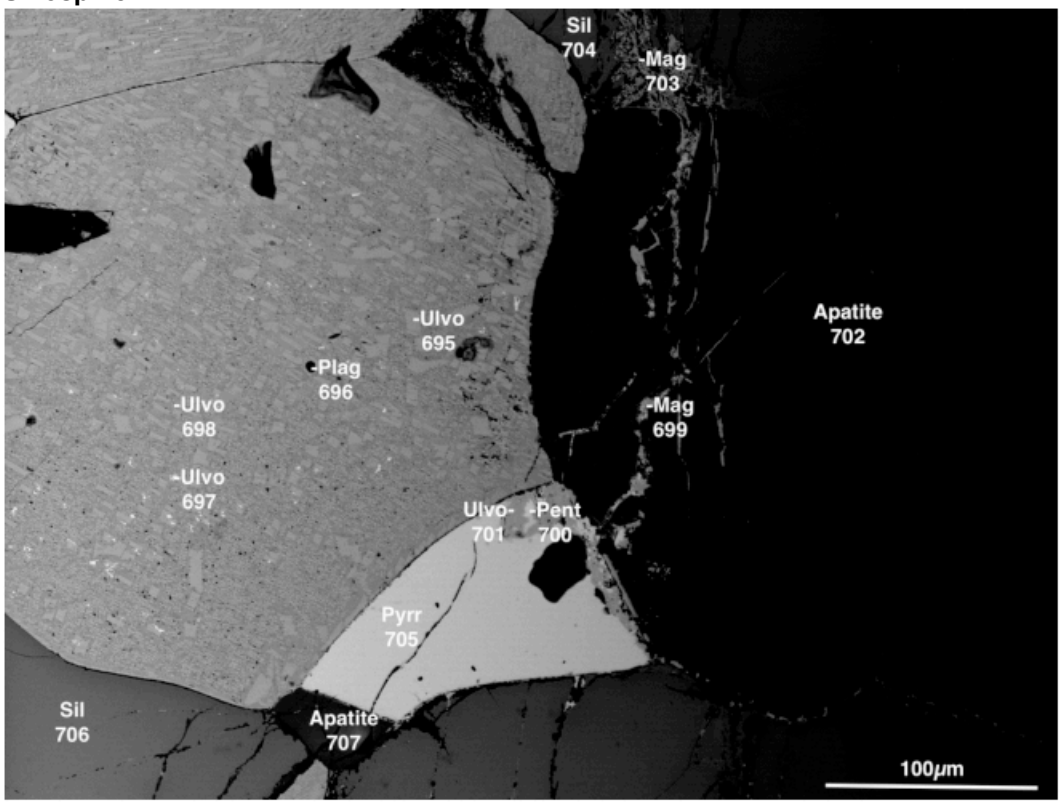

Figure 34. SEM image of slide 2 MG 2.4 showing a titaniferous-magnetite grain next to a large apatite grain. Cloth texture exsolution is visible. The exsolved phases are magnetite and ulvöspinel. Apatite=Apatite; Plag=Plagioclase; Mag=Magnetite; Pent=Pentlandite; Pyrr=Pyrrhotite; Sill=a Silicate; Ulvo=Ulvöspinel.

Table 8. Elemental weight percentages of the titaniferous-magnetite analysis (Figure 30, Figure 31, Figure 32, Figure 33, and Figure 34) recalculated as an oxide. Only elements of importance have been listed.

Spectrum	MgO	Al2O3	SiO2	FeO	TiO2
Figure 30					
621	0	1,871	0	41,340	10,626
622	0	2,496	0,361	75,305	17,373
623	3,434	9,709	6,268	74,002	3,170
624	0	2,654	1,150	68,673	17,260
625	0	3,218	0	73,014	17,874
626	0	0,402	0,863	59,617	32,274
Figure 31					
662	0	1,681	0,385	79,740	12,365
663	0	4,576	0	68,172	23,991
666	0	1,088	2,418	79,814	1,885
670	3,957	0	0,617	60,662	20,789
671	0	0,739	0,475	82,115	13,763
Figure 32					
679	0	1,120	0,378	80,706	12,697
680	0	0	1,410	80,948	8,904
681	0	1,712	0,356	80,433	12,327
682	0	4,080	0	69,099	22,304
Figure 33					
685	0	0	0	82,306	8,580
686	0	0	0,267	59,177	34,365
687	0	4,491	0	68,278	22,925
688	0	1,301	0,670	83,887	6,911
Figure 34					
695	0	1,907	0,223	80,818	10,883
697	0	2,089	0,245	96,792	5,602
698	0	4,081	0	66,656	23,073

2 MG 2.6

Thin section 2 MG 2.6 was sampled from a depth of 1428m in the Upper Zone.

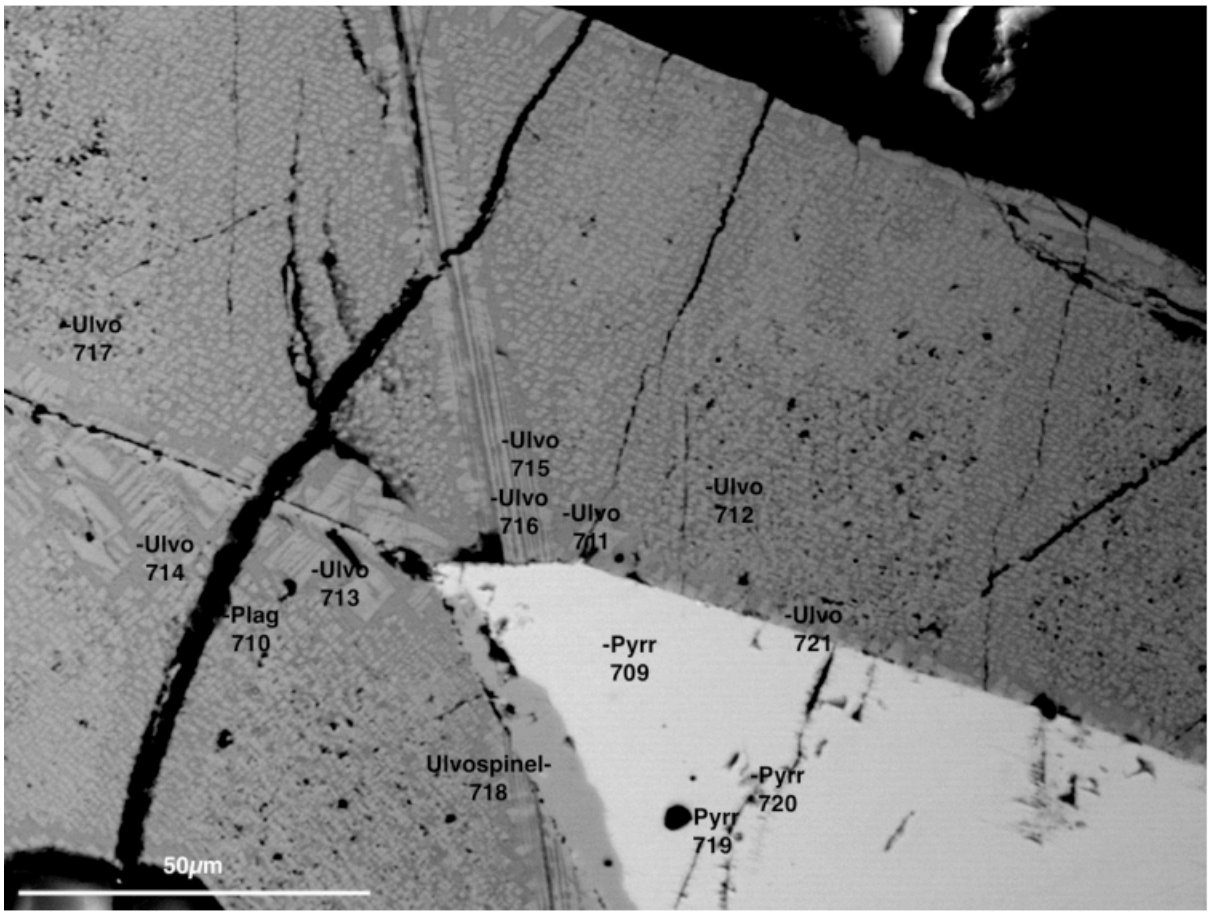

Figure 35. SEM image of slide 2 MG 2.6 showing multiple titaniferous-magnetite grains next to a pyrrhotite grain. Cloth texture exsolution is visible. The exsolved phases are magnetite and ulvöspinel. Plag=Plagioclase; Pyrr=Pyrrhotite; Ulvo/Ulvospinel=Ulvöspinel.

Figure 35, Figure 36, and Figure 39 show a distinct change in the prism shapes of the cloth texture exsolution throughout the titaniferous-magnetite grains. Some of the prisms are rectangular and in close proximity. Other prisms are more rectangular and sparsely located. Figure 35 shows in interesting cloth texture appearance at a grain boundary, with the square prisms appearing after the rectangular prisms. This is not a distinct pattern, as Figure 36 and Figure 39 show mixtures of the prisms. The small holes in the cloth texture exsolution can be seen throughout the images, although the small sulphide grains are limited to Figure 36.

Plagioclase, pyrrhotite, apatite, and silicates are still present. Figure 38 shows an apatite grain included in a relatively round pyrrhotite grain. This could indicate that apatite formed before pyrrhotite formed.

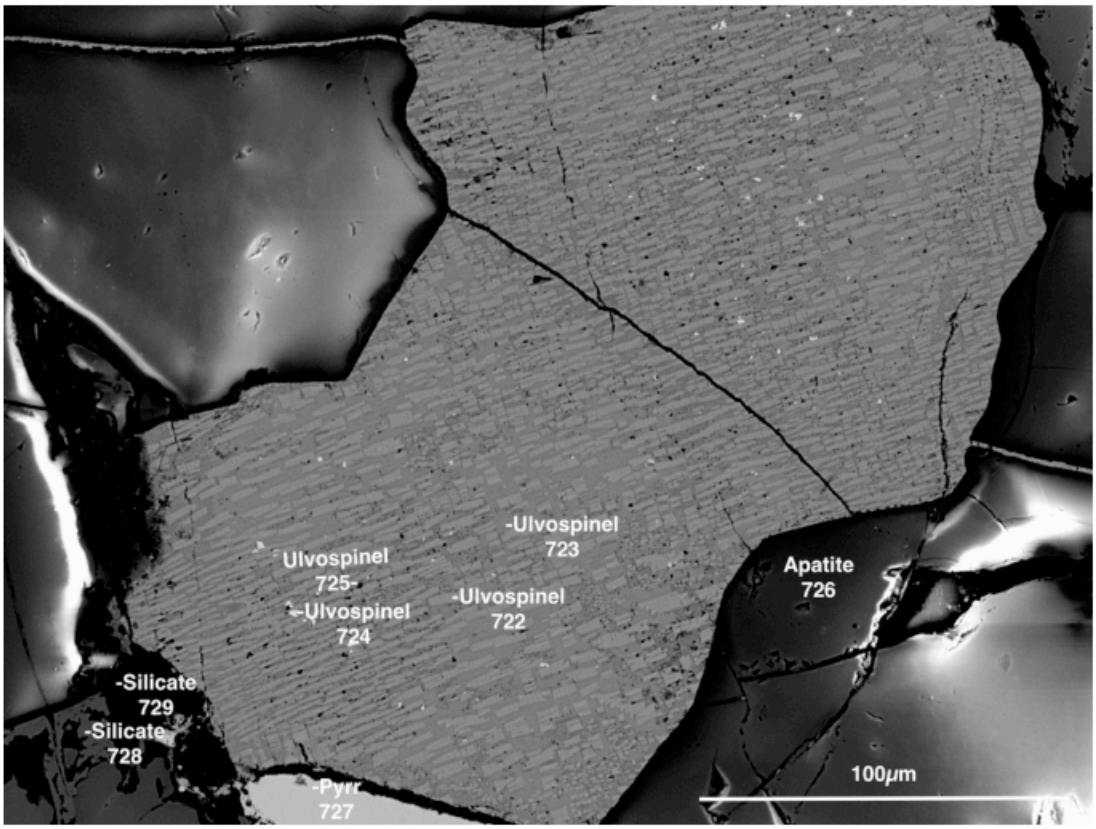

Figure 36. SEM image of slide 2 MG 2.6 showing a cloth texture exsolution of a titaniferous-magnetite grain. The exsolved phases are magnetite and ulvöspinel. Apatite=Apatite; Pyrr=Pyrrhotite; Silicate=a Silicate; Ulvospinel=Ulvöspinel.

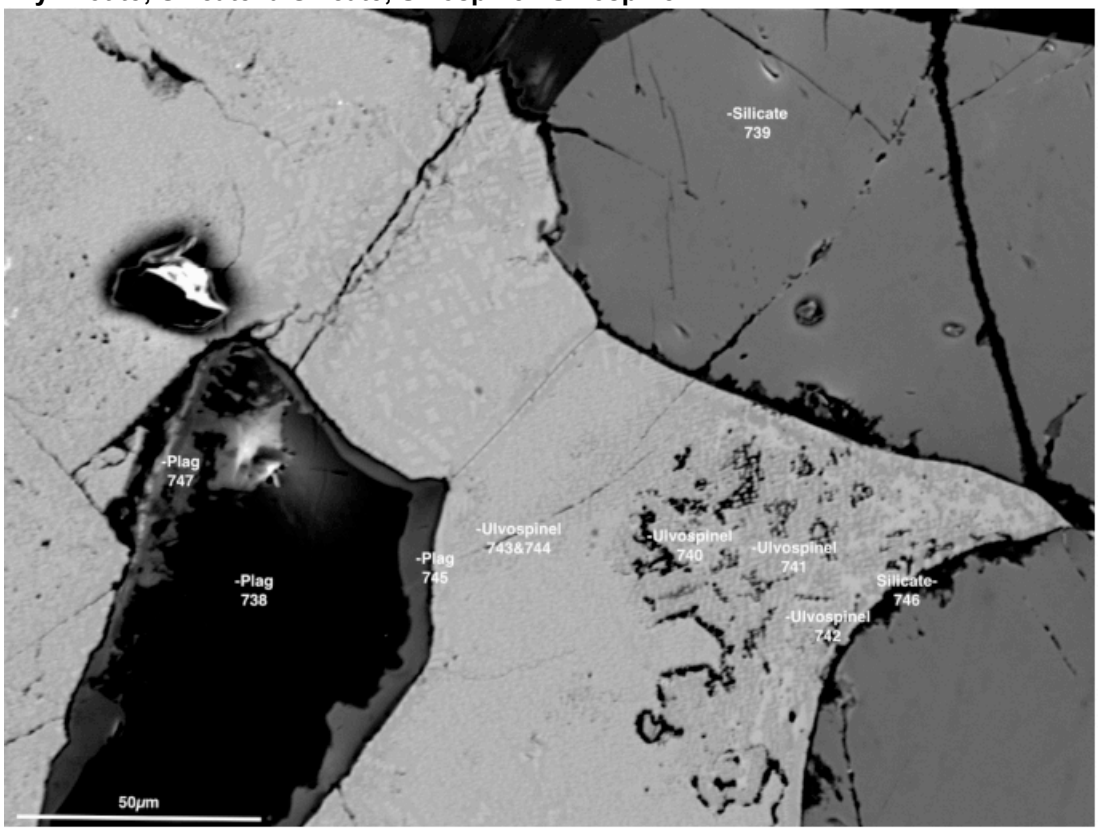

Figure 37. SEM image of slide 2 MG 2.6 showing changes in cloth texture exsolutions of titaniferous-magnetite grains. The exsolved phases are magnetite and ulvöspinel. Plag=Plagioclase; Sill=a Silicate; Ulvospinel=Ulvöspinel.

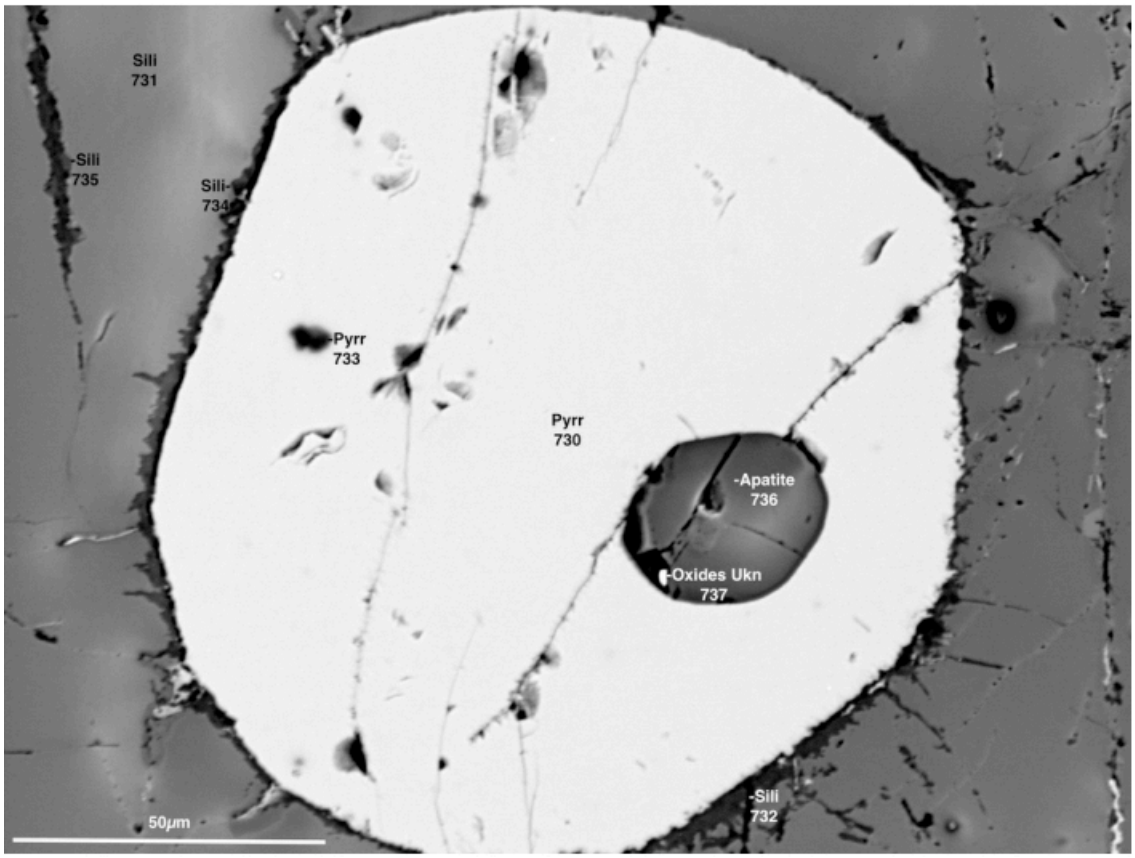

Figure 38. SEM image of slide 2 MG 2.6 showing a relatively round pyrrhotite grain with apatite and silicates. Apatite=Apatite; Pyrr=Pyrrhotite; Sill=a Silicate.

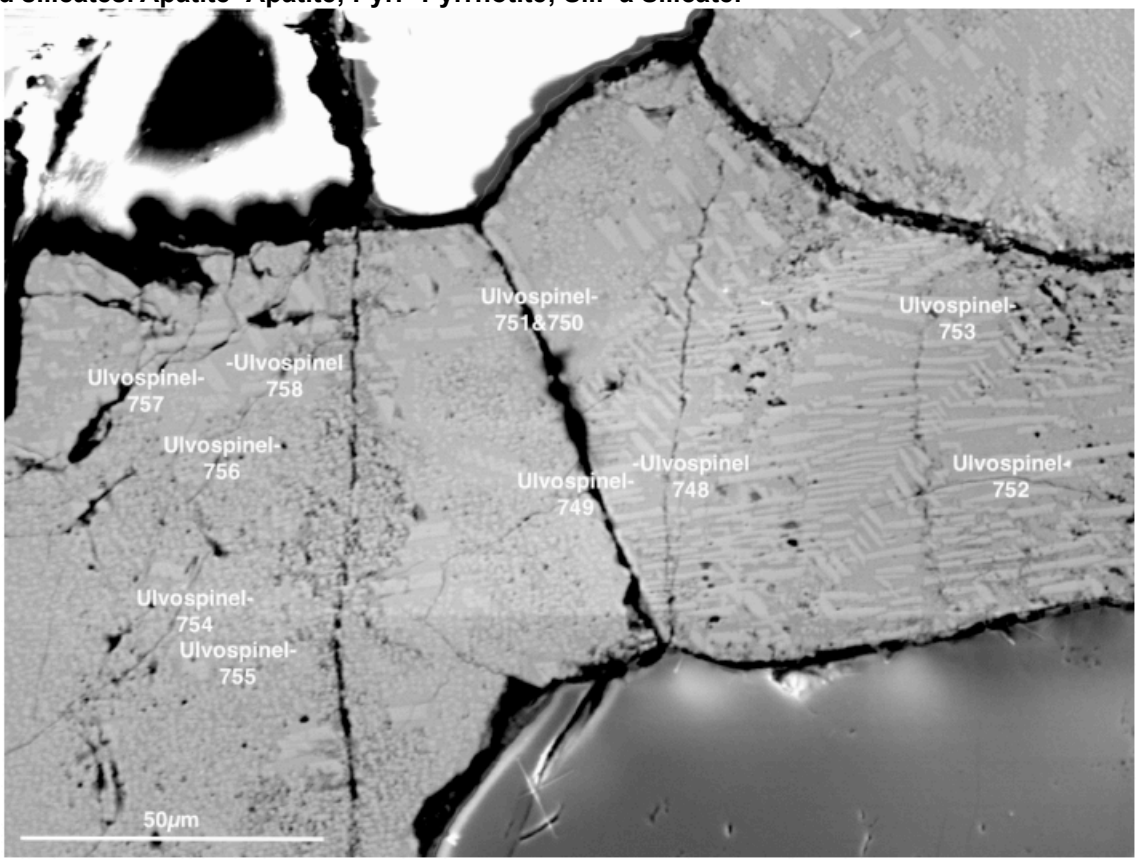

Figure 39. SEM image of slide 2 MG 2.6 showing titaniferous-magnetite grains and changes in the cloth texture exsolution. The exsolved phases are magnetite and ulvöspinel. Ulvospinel=Ulvöspinel.

Table 9. Elemental weight percentages of the titaniferous-magnetite analysis (Figure 35, Figure 36, Figure 37, Figure 38, and Figure 39) recalculated as an oxide. Only elements of importance have been listed.

Spectrum	MgO	Al2O3	SiO2	FeO	TiO2
Figure 35					
711	0	3,751	0	63,823	23,671
712	0	3,160	0,222	72,411	14,279
713	0	0	0	76,165	10,878
714	0	4,265	0	62,207	23,837
715	0	3,927	0	62,403	22,216
716	0	2,327	0	63,712	21,888
717	0	2,476	0	62,627	26,249
718	0	0	0,269	87,927	0,402
Figure 36					
722	0	1,492	0,307	76,979	11,583
723	0	4,414	0	64,259	23,005
724	0	2,548	0,418	81,932	0,277
725	0	2,245	5,114	63,151	20,506
Figure 37					
740	0	0,902	0,511	85,482	9,347
741	0	0,175	1,151	55,885	28,204
742	0	0,411	0,288	58,061	29,201
743	0	1,966	0,334	71,799	13,778
744	0	3,900	0,288	61,169	23,116
Figure 39					
748	0	2,460	0,314	68,755	15,434
749	0	4,632	0,360	62,701	21,290
750	0	4,489	0	60,694	22,164
751	0	3,527	0,292	63,489	20,834
752	0	2,356	0,271	75,969	9,413
753	0	1,662	0	56,880	24,724
754	0	0	0	65,070	14,721
755	0	4,100	0,312	61,976	21,682
756	0	2,315	0,289	62,525	18,864
757	0	4,358	0,380	60,478	22,668
758	0	0,541	0,380	58,969	23,302

2 MG 2.8

Thin section 2 MG 2.8 was sampled from a depth of 1428.5m in the Upper Zone.

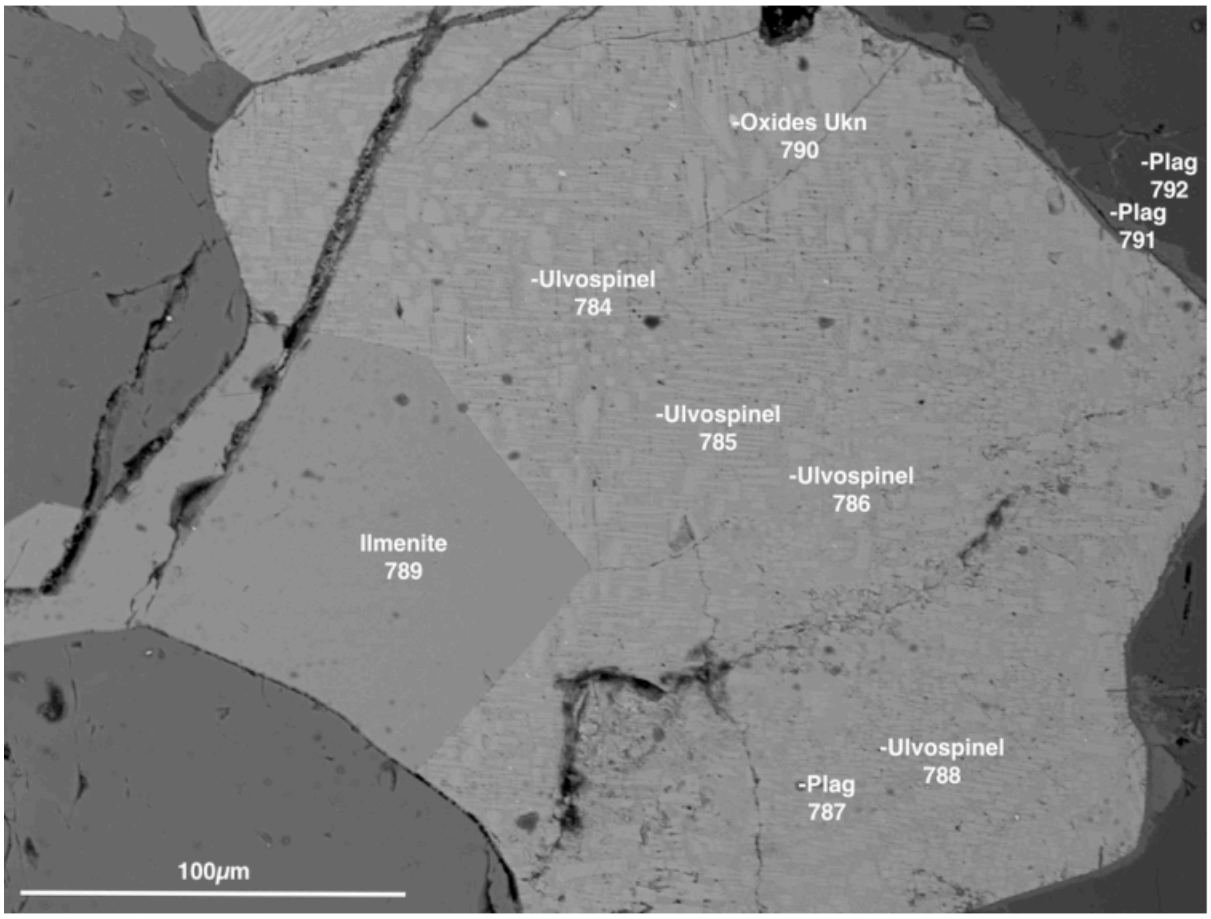

Figure 40. SEM image of slide 2 MG 2.8 showing a cloth texture exsolution of magnetite grains together with various other minerals. The exsolved phases are magnetite and ulvöspinel. Apatite=Apatite; Ilmenite=Ilmenite; Plag=Plagioclase; Pyrr=Pyrrhotite; Sill= a Silicate; Ulvospinel=Ulvöspinel.

Ilmenite is anhedral in shape in Figure 40, yet no “trellis” type exsolution is visible in these images. Figure 40, Figure 41, and Figure 42 show a cloth texture exsolution of titaniferous-magnetite. The exsolution texture continues to exhibit changes in prism size, shape, and proximity. The small holes are still present, but the small sulphides are not visible. Titaniferous-magnetite exsolution is a lot less pronounced in Figure 41 compared to Figure 43, although the magnification is the same.

Figure 40 shows a plagioclase rim around the titaniferous-magnetite, with Figures 41 ad 42 showing a silicate rim. Figure 42 also shows an area where one silicate seems to have infiltrated another silicate.

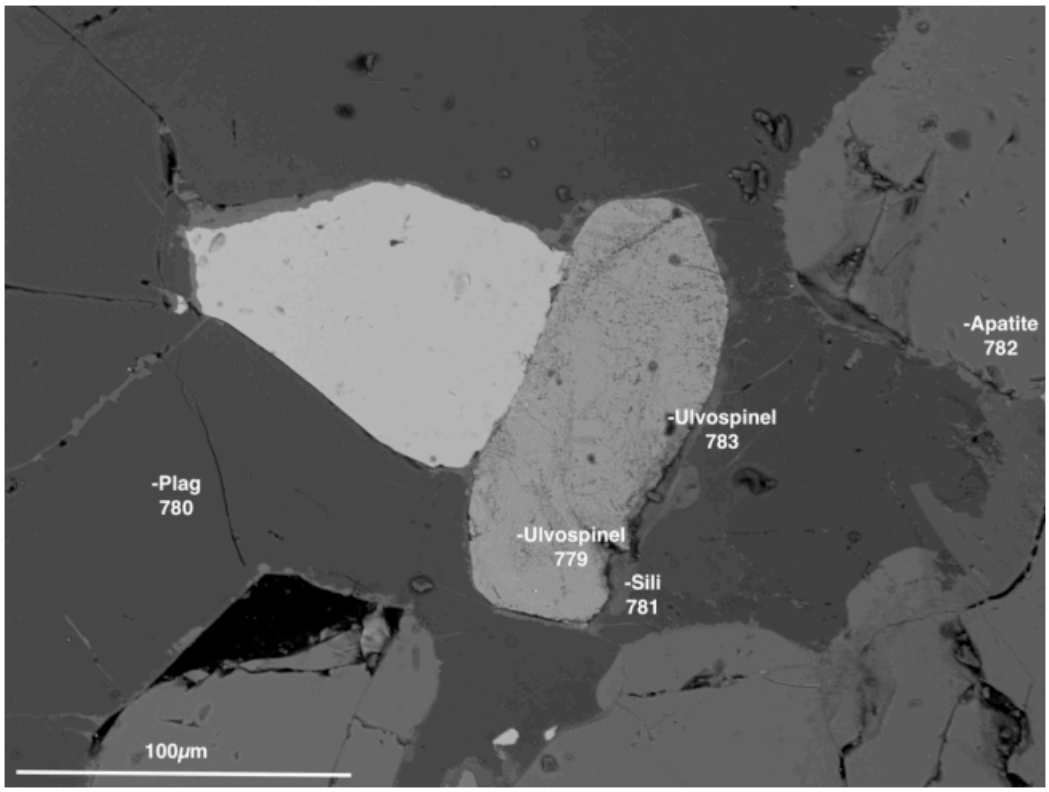

Figure 41. SEM image of slide 2 MG 2.8 showing a cloth texture exsolution of magnetite grains together with various other minerals. The exsolved phases are magnetite and ulvöspinel. Apatite=Apatite; Ilmenite=Ilmenite; Plag=Plagioclase; Pyrr=Pyrrhotite; Sill=a Silicate; Ulvospinel=Ulvöspinel.

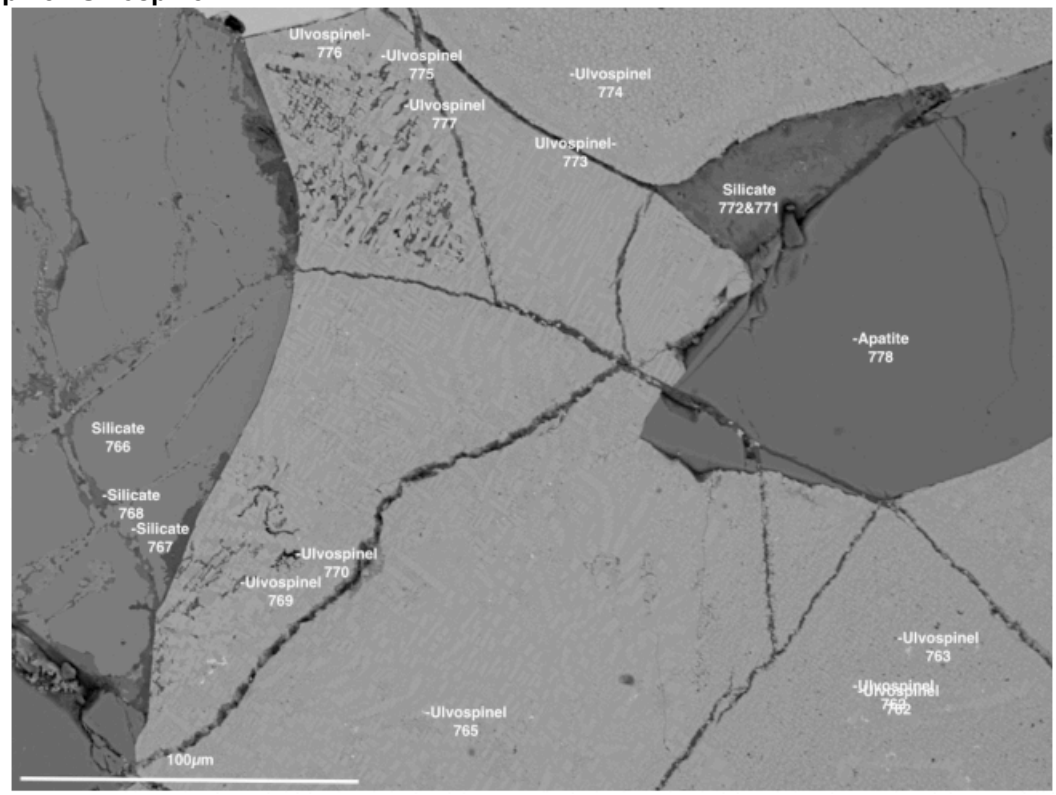

Figure 42. SEM image of slide 2 MG 2.8 showing a cloth texture exsolution of magnetite grains together with various other minerals. The exsolved phases are magnetite and ulvöspinel. Apatite=Apatite; Ilmenite=Ilmenite; Plag=Plagioclase; Pyrr=Pyrrhotite; Sill=a Silicate; Ulvospinel=Ulvöspinel.

Table 10. Elemental weight percentages of the titaniferous-magnetite analysis (Figure 40, Figure 41, and Figure 42) recalculated as an oxide. Only elements of importance have been listed.

Spectrum	MgO	Al2O3	SiO2	FeO	TiO2
Figure 40					
784	0	1,379	0,299	85,874	7,240
785	0	1,184	0,299	80,493	11,741
786	0	4,156	0,278	67,670	24,371
788	0	2,930	1,434	84,746	14,382
Figure 41					
779	0	2,268	0,257	68,809	22,672
783	0	5,971	5,477	64,434	35,551
Figure 42					
762	0	3,722	0	73,974	16,531
763	0	2,362	0,578	72,739	17,582
764	0	3,364	0,321	68,706	22,588
765	0	1,303	0,364	83,336	10,290
769	7,512	14,833	11,252	56,027	5,021
770	0	2,229	1,497	68,698	31,471
773	0	1,530	0,385	80,998	11,927
774	0	3,685	0,406	67,270	23,516
775	0	1,474	0,428	82,169	9,825
776	0	3,307	0,363	65,547	24,538
777	9,385	9,579	9,775	40,212	27,871

2 MG 1.1

Thin section 2 MG 1.1 was sampled from a depth of 1429.7m in the Upper Zone.

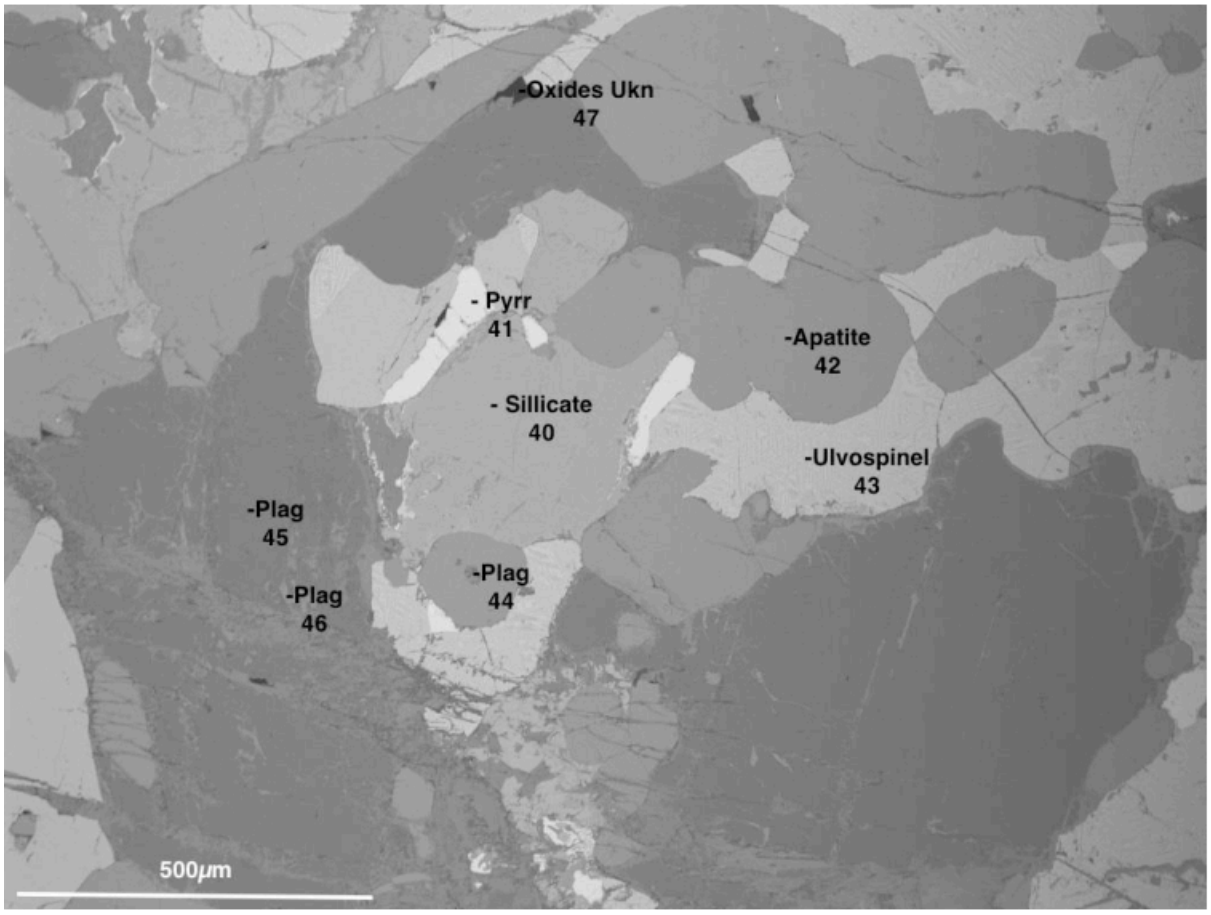

Figure 43. SEM image of slide 2 MG 1.1 showing various minerals together with an area that seems to be altered by the movement of a liquid. Apatite=Apatite; Plag=Plagioclase; Pyrr=Pyrrhotite; Sill=a silicate; Ulvospinel=Ulvöspinel.

Figure 43 shows the titaniferous-magnetite grain together with plagioclase, apatite, silicates, pyrrhotite, and an unknown oxide. The cloth texture exsolution is still present, but very light at 500µm. There appears to be an infiltration through the plagioclase grains, but this is only localised at the bottom of the image. This same infiltration of hydrothermal alteration can be seen in Figure 45, but to a greater extent.

Figure 44, Figure 45, and Figure 46 show grains with almost only “trellis” type exsolution. This contrasts with the cloth texture exsolution which was dominant in the previous slides. Figure 48 shows both “trellis” type exsolution as well as cloth texture exsolution. Ilmenite is also present as grains. Plagioclase and apatite are included inside some of the titaniferous-magnetite grains.

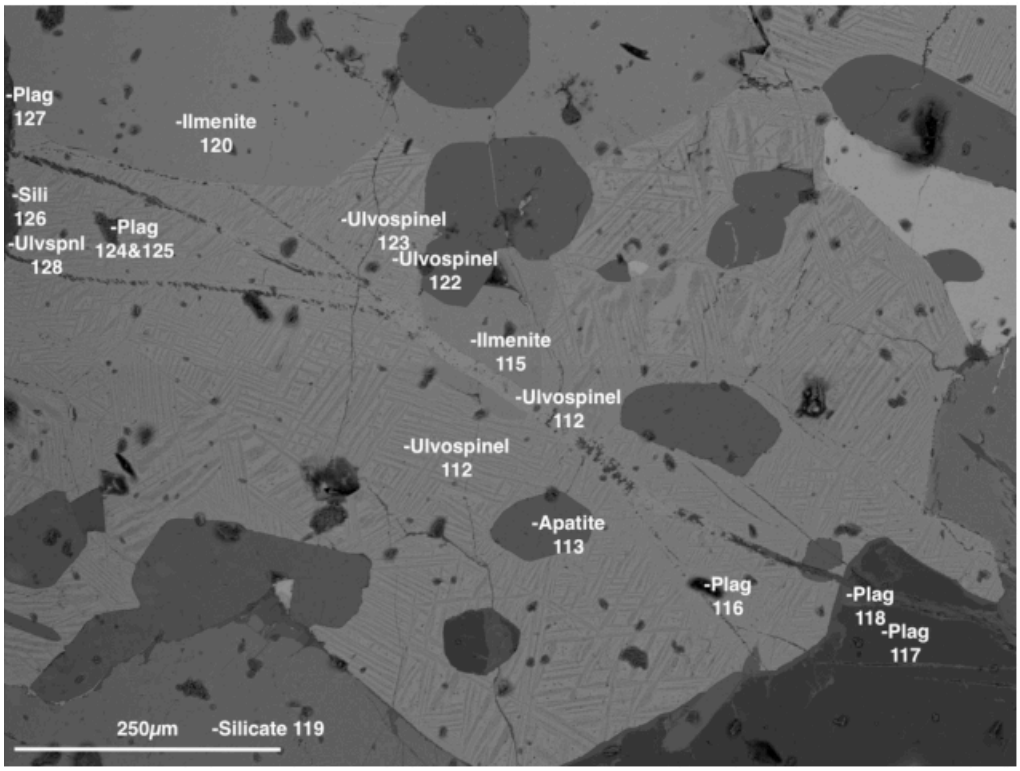

Figure 44. SEM image of slide 2 MG 1.1 showing a change in the cloth texture exsolution of titaniferous-magnetite. Ilmenite exsolution is also present as a "trellis" texture. The exsolved phases are magnetite, ulvöspinel and ilmenite. Ilmenite=ilmenite; Plag=Plagioclase; Ulvospinel=Ulvöspinel.

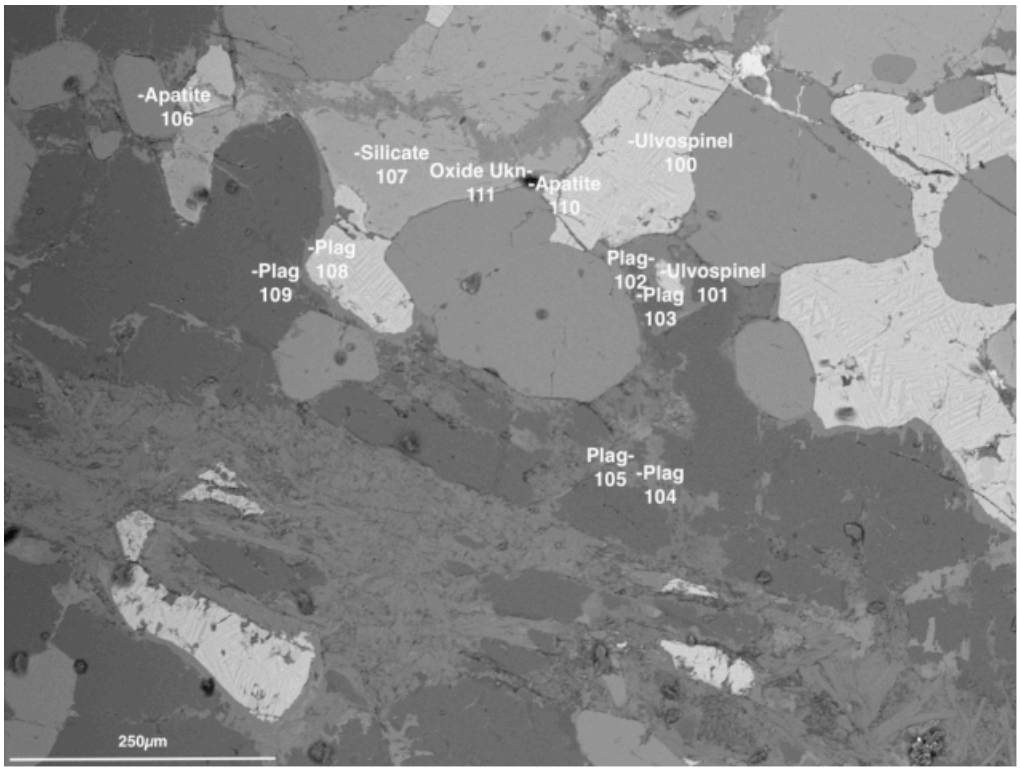

Figure 45. SEM image of slide 2 MG 1.1 showing a cloth texture exsolution of titaniferous-magnetite grains. Ilmenite exsolution is also present as a "trellis" texture. The exsolved phases are magnetite, ulvöspinel and ilmenite. Ilmenite=ilmenite; Plag=Plagioclase; Ulvospinel=Ulvöspinel.

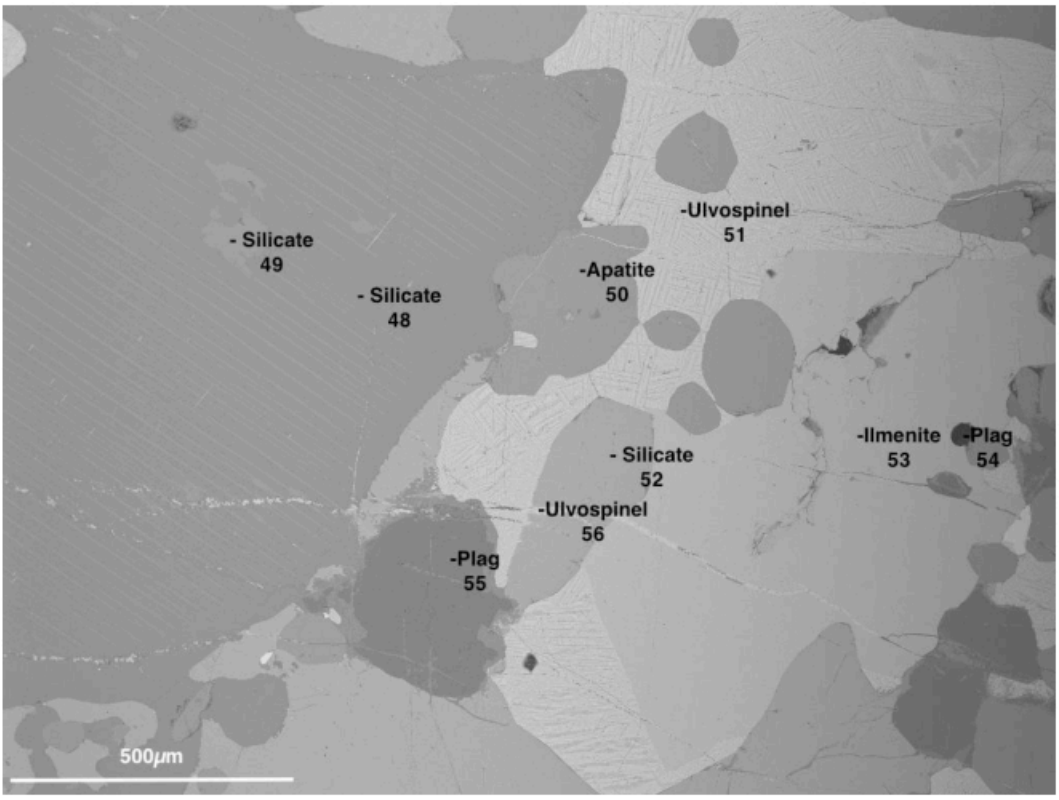

Figure 46. SEM image of slide 2 MG 1.1 showing exsolution of a silicate as well as cloth texture exsolution of titaniferous-magnetite grains. Ilmenite exsolution is also present as a "trellis" texture. The exsolved phases are magnetite, ulvöspinel and ilmenite. Apatite=Apatite; Ilmenite=ilmenite; Plag=Plagioclase; Sill=a silicate; Ulvospinel=Ulvöspinel.

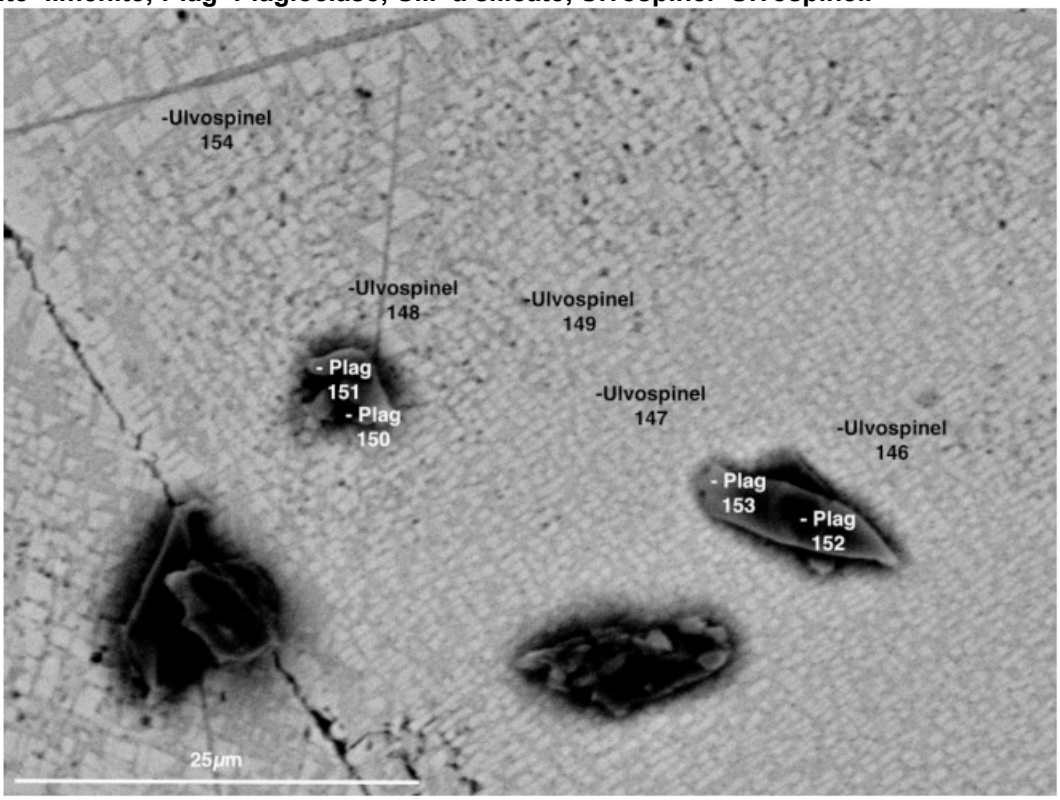

Figure 47. SEM image of slide 2 MG 1.1 showing a cloth texture exsolution of titaniferous-magnetite grains together with plagioclase. The exsolved phases are magnetite and ulvöspinel. Plag=Plagioclase; Ulvospinel=Ulvöspinel.

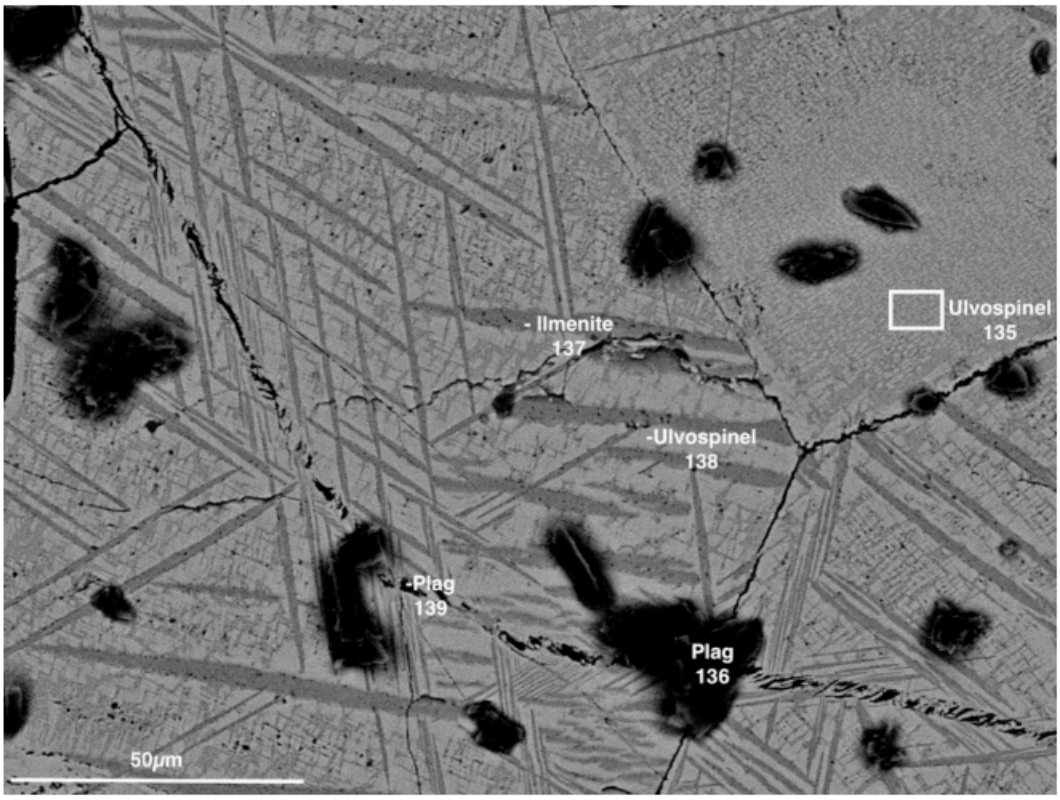

Figure 48. SEM image of slide 2 MG 1.1 showing a cloth texture exsolution of titaniferous-magnetite grains, as well as "trellis" type exsolution of ilmenite. The exsolved phases are magnetite, ulvöspinel, and ilmneite. Ilmneite=ilmenite Plag=Plagioclase; Ulvospinel=Ulvöspinel.

Table 11. Elemental weight percentages of the titaniferous-magnetite analysis (Figure 43, Figure 44, Figure 45, Figure 46, Figure 47, and Figure 48) recalculated as an oxide. Only elements of importance have been listed.

Spectrum	MgO	Al2O3	SiO2	FeO	TiO2
Figure 43					
43	0,348	3,534	0,300	69,542	18,668
Figure 44					
112	0,580	3,855	0,385	70,269	19,317
122	0,116	0,926	0,578	89,724	2,685
123	0,049	5,504	12,742	56,856	6,618
128	5,754	6,594	10,824	69,097	0,867
Figure 45					
100	0,415	3,345	0,364	69,233	20,887
101	0,647	2,152	1,754	68,140	20,436
Figure 46					
51	0,613	3,741	0,342	69,348	18,531
56	0,365	0,416	1,562	91,351	0,234
Figure 47					
146	0,232	2,551	0,556	78,734	14,179
147	0,415	3,458	0,556	68,841	22,536

Spectrum	MgO	Al2O3	SiO2	FeO	TiO2
148	0,713	3,175	0,685	68,462	22,388
149	0,630	4,044	0,449	72,353	19,166
154	0	1,209	0,385	85,093	7,272
Figure 48					
135	0,381	3,250	0,300	72,906	19,116
138	0,199	0,813	0,535	88,726	4,554

THE CHEMISTRY OF TITANIFEROUS-MAGNETITE

Most of the images collected from the SEM analysis show the cloth texture exsolution of titaniferous-magnetite, but this exsolution is not consistent throughout the investigated slides. Line scans were taken of titaniferous-magnetite grains in sections 2 MG 2.2a and 2 MG 2.6 to determine if there are any chemical changes that might explain the inconsistency of the exsolution pattern seen. Line scans were also used to provide more information on the elemental abundances of the titaniferous-magnetite grains.

Figure 49 is a high magnification image of a titaniferous-magnetite grain, focusing on the exsolution pattern that shows a cloth texture with blocky prisms that are in close proximity to one another. Line Data 2 shows the area across which a line scan was taken to investigate the elemental changes across the exsolution. From the line scan data in Figure 50b, it is evident that the Fe content dips across the grey areas and peaks across the lighter prisms. Ti shows the opposite result of Fe, peaking in the grey areas, and dipping across the lighter prisms. This confirms the reported data that the exsolution of the titaniferous-magnetite results in ulvöspinel and magnetite. Very small amounts of carbon are present, but this is due to carbon coating of the slides.

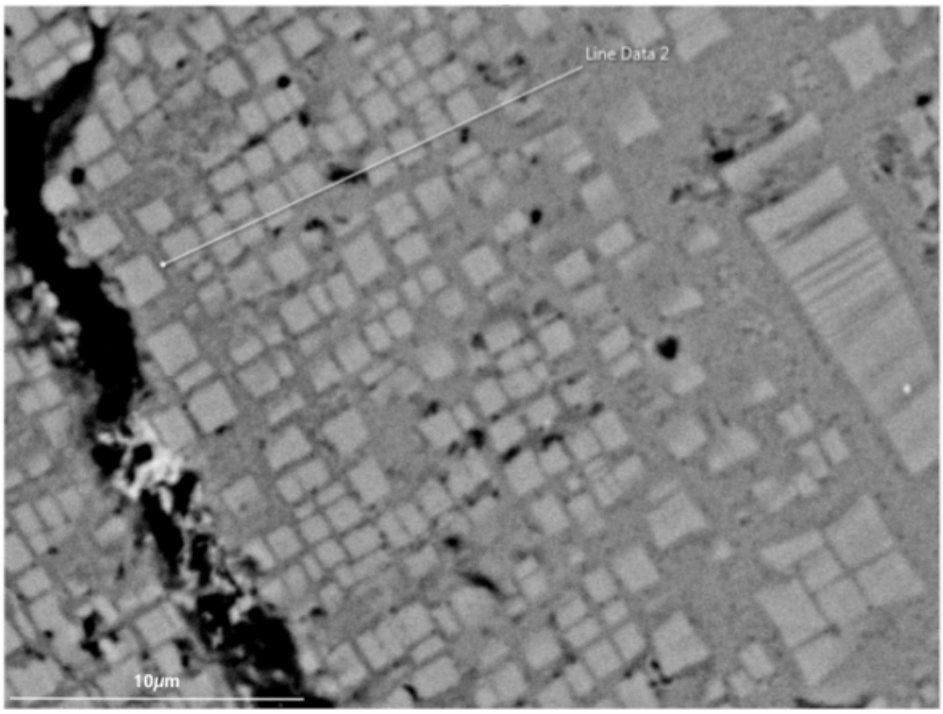

Figure 49. A high magnification SEM image of slide 2 MG 2.2a showing a cloth texture exsolution pattern of titaniferous-magnetite grains, and the area where a line scan of the exsolution pattern was taken.The exsolved phases are magnetite and ulvöspinel.

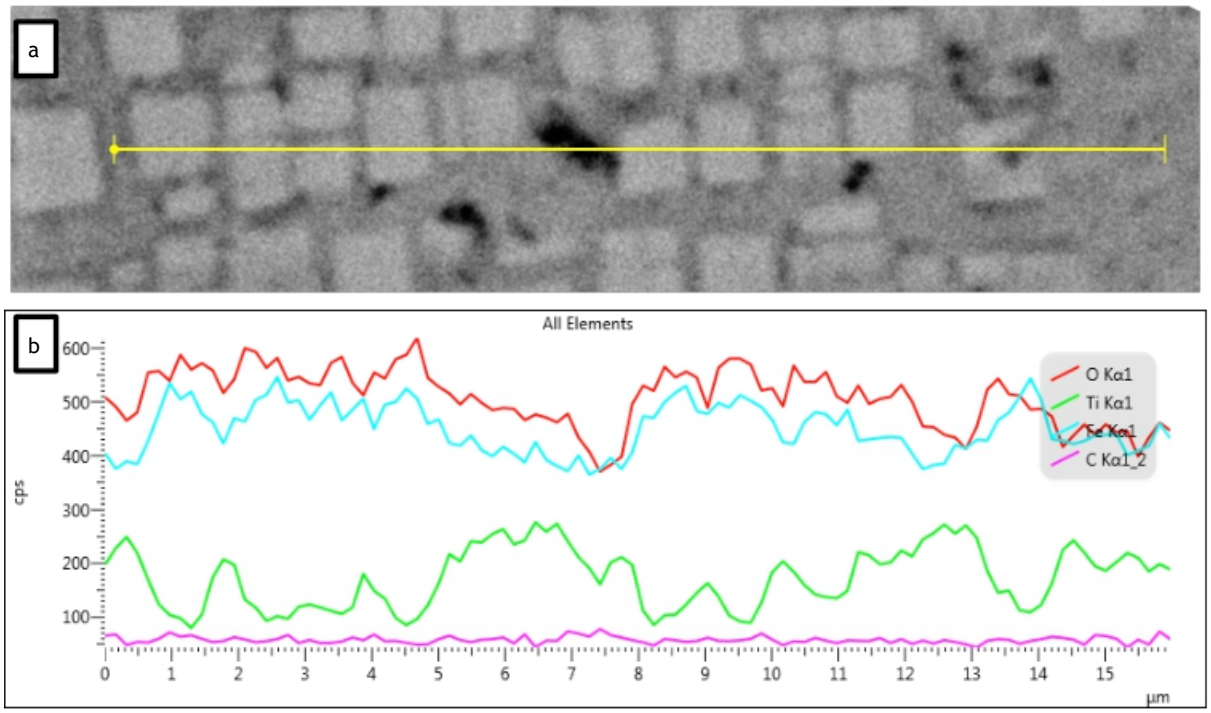

Figure 50. (a): A high magnification SEM image of Figure 49 showing a cloth texture exsolution of a titaniferous-magnetite grain, and the extent of Line Data 2. The exsolved phases are magnetite and ulvöspinel. (b): A line scan of Line Data 2.

Figure 51 is a high magnification image of slide 2 MG 2.2a that clearly shows the variation in the cloth texture exsolution of titaniferous-magnetite between two grains. The top grain shows more elongated prisms compared to the blocky prisms of the bottom grain. The darker phase in the exsolution is also much more prevalent in the top grain.

Figure 52 is a high magnification image of the titaniferous-magnetite grain shown in Figure 51, focusing on the exsolution pattern that shows the cloth texture with elongated prisms that appear sparser at lower magnification. Line Data 3 shows the area across which a line scan was taken to investigate the elemental changes across the exsolution. From the line scan data in Figure 52b, elemental abundances show much higher peaks and dips as compared to the line scan in Figure 50b. Similar Fe dips across the grey areas and peaks across the lighter prisms can be seen. Ti continues to show the opposite result of Fe, peaking in the grey areas, and dipping across the lighter prisms. A big variation is the addition of Al to the scan, which does not seem to follow a distinct pattern like Fe and Ti. Al seems to show dips in the lighter areas (magnetite) and peaks in the grey areas (ulvöspinel), but this is not uniform.

Additional titaniferous-magnetite grains were analysed to see if the addition of Al could be an indicator of the change in the prisms of the exsolution texture (Figure 54 to Figure 60). This was shown to be incorrect as the line scan of Figure 54 does not indicate any Al, although elongated prisms are seen in the exsolution texture. Line scan 11 in Figure 58 once again shows the presence of Al, but at very low rates.

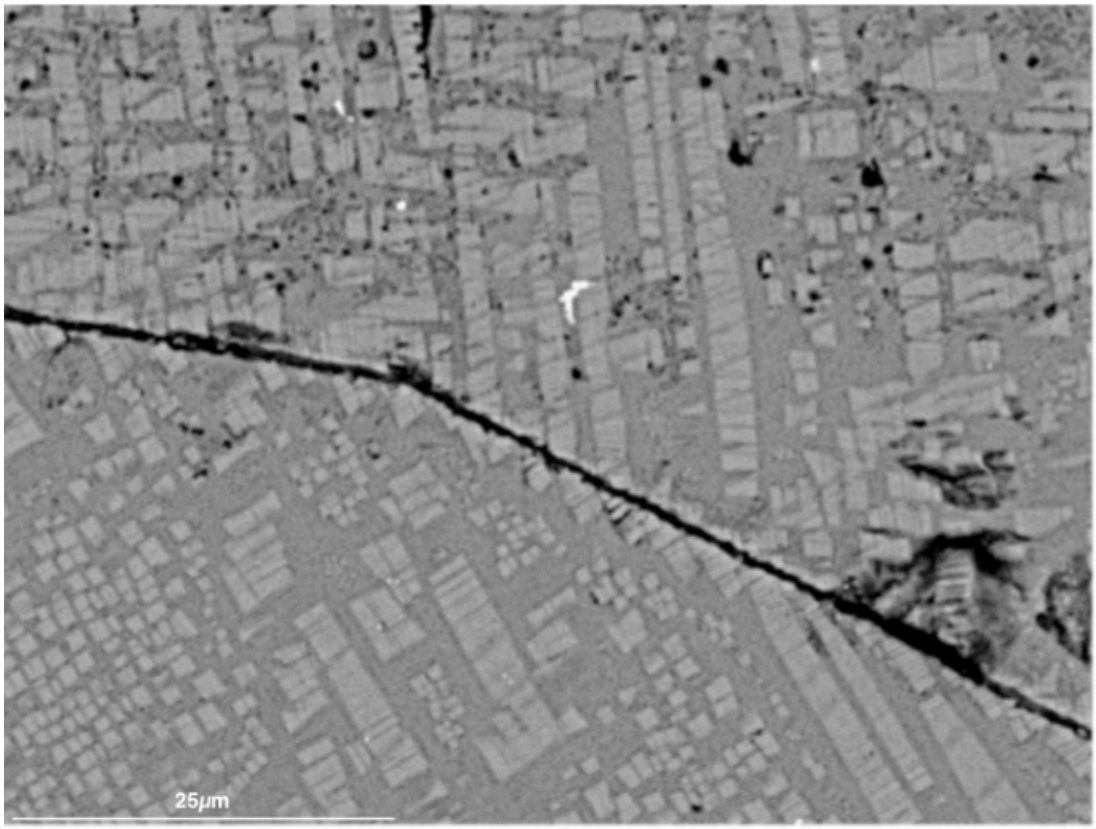

Figure 51. A high magnification SEM image of slide 2 MG 2.2a showing a variation in the cloth texture exsolution pattern of titaniferous-magnetite grains.The exsolved phases are magnetite and ulvöspinel.

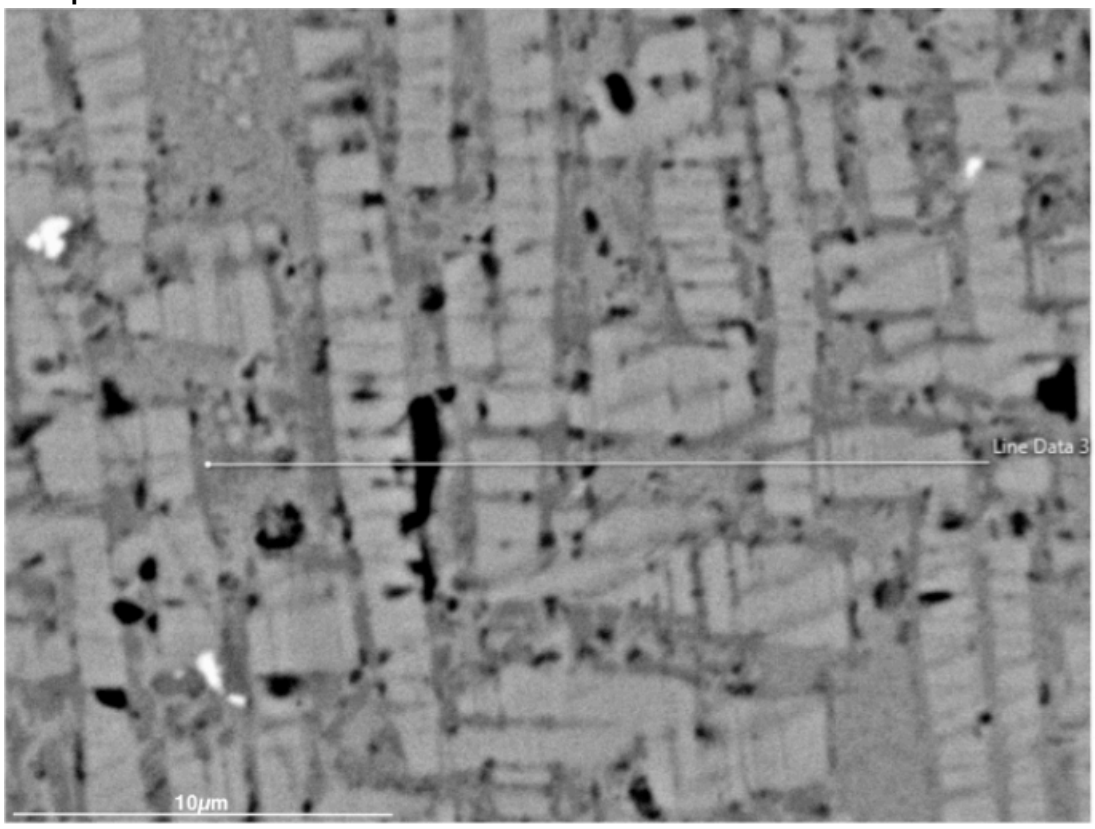

Figure 52. A high magnification SEM image of slide 2 MG 2.2a showing elongated prisms in the cloth texture exsolution pattern of a titaniferous-magnetite grain, and the area where a line scan of the exsolution pattern was taken.The exsolved phases are magnetite and ulvöspinel.

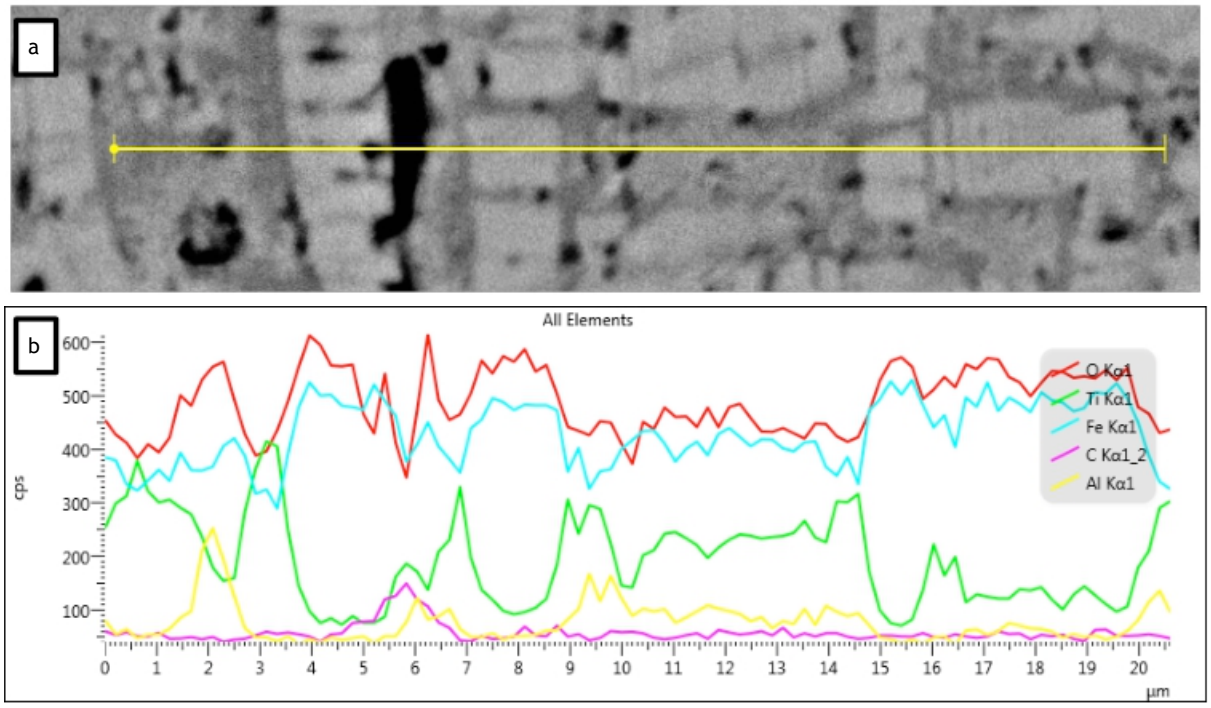

Figure 53. (a): A high magnification SEM image of Figure 51 showing a cloth texture exsolution of a titaniferous-magnetite grain, and the extent of Line Data 3. (b): A line scan of Line Data 3.

The pattern of increased Ti in darker areas and increased Fe in lighter areas of the exsolution pattern remains constant throughout the analysed areas of Figure 54 to Figure 60. It is important to note that although the line scans show similar peaks and dips, the range and rates of the each elemental spectrum changes for every grain. Comparing the Fe line in Figure 53b to Figure 56b, shows a change from a line that is generally flatter and has an average of 500cps, to a line that has much more extensive peaks and dips, and has an average of 400cps.

Figure 57 and Figure 58 shows the emergence of “trellis” type exsolution, which is caused by ilmenite. In some areas the “trellis” type exsolution intersects the cloth texture exsolution, but in other area the exsolution stops before hitting the cloth texture. Similar to the change in prisms that is seen in the cloth texture, “trellis” type texture is also not uniform across a titaniferous-magnetite grain. Line scans across the ilmenite exsolution show the increase and decrease of Ti, although the rate seems to be lower overall compared to scans of only titaniferous-magnetite exsolution.

Figure 63 to Figure 68 were taken from slide 2 MG 1.6 in order to analyse grains from a different depth. These images show a similar pattern of high Ti in the grey areas and high Fe in the lighter areas of the exsolution pattern. The particularly elongated prisms seen in Figure 66 are a new appearance, as these continuous lines have been noted in Figure 21, Figure 30, and Figure 31, but are generally shorter and curved. The line scan in Figure 68 does not show a difference in the Fe-Ti peak patterns, which does not give much information about this change in pattern from one grain to another.

Figure 68b shows a line scan moving over a hole. The sharp drop in elements such as O, Fe, and Ti, and an increase in carbon, confirms this as a hole as the thin sections were carbon coated to allow for SEM analysis. Line scan 15 of Figure 62b shows an analysis across a lighter space, where a drop in other elements are present, with an increase in Fe.

This also provides confirmation as to the small, light dots being sulphide grains in the titaniferous-magnetite grains.

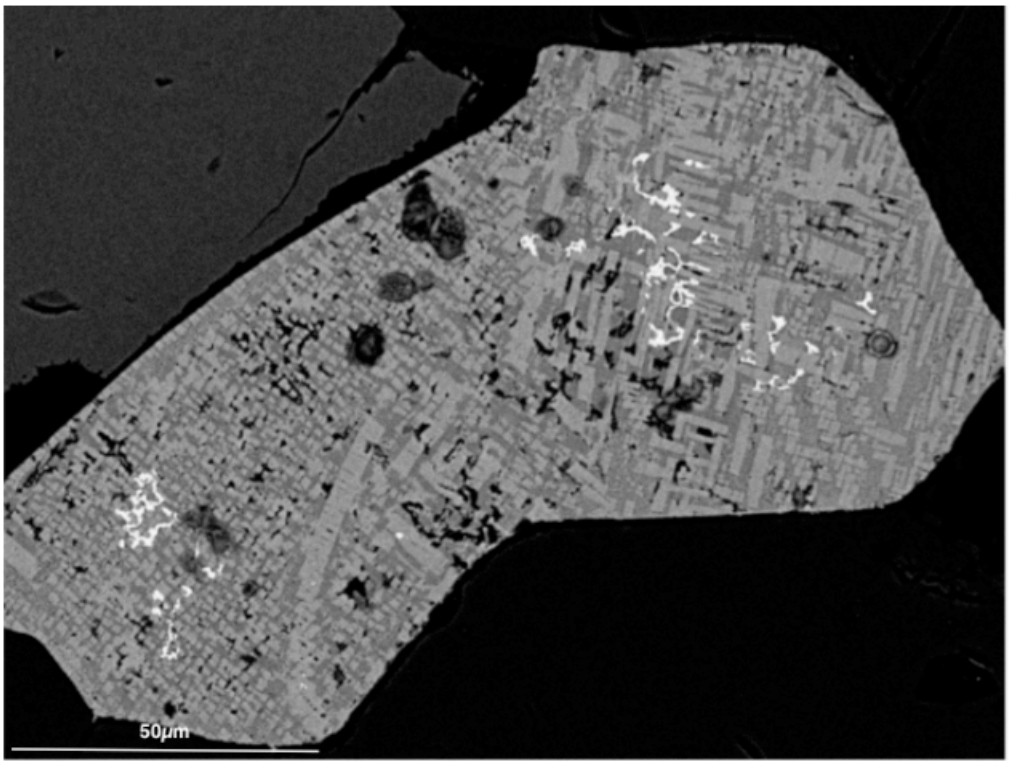

Figure 54. A high magnification SEM image of slide 2 MG 2.2a showing a variation in the cloth texture exsolution pattern in a single titaniferous-magnetite grain.The exsolved phases are magnetite and ulvöspinel.

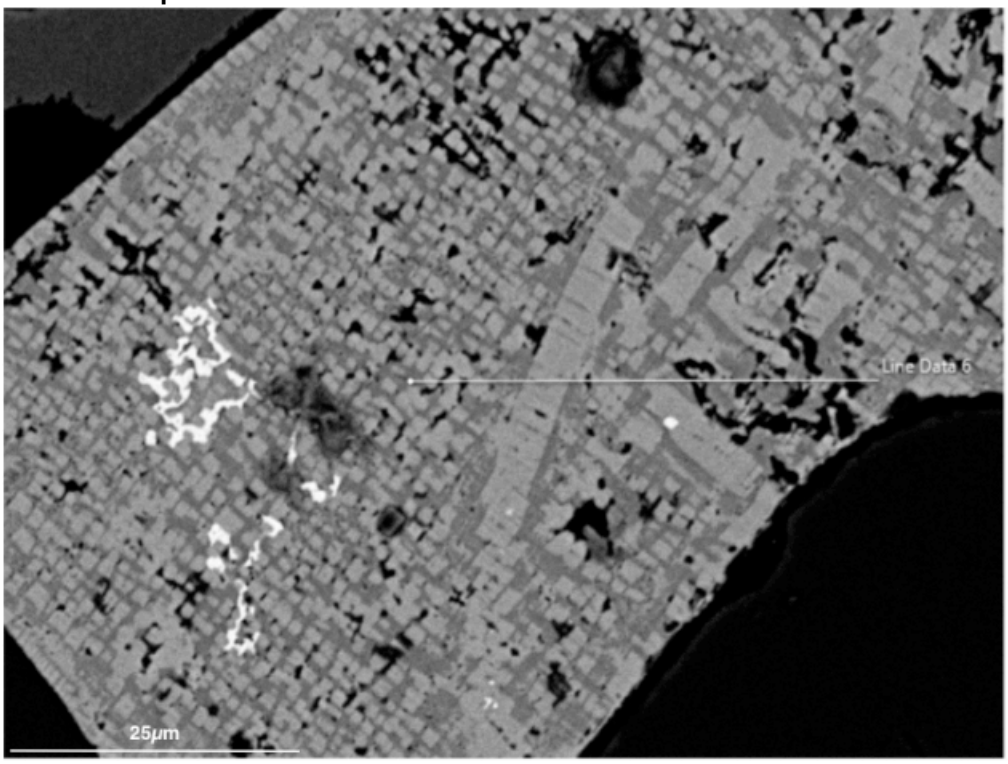

Figure 55. A high magnification SEM image of slide 2 MG 2.2a showing elongated prisms and blocky prisms in the cloth texture exsolution of a titaniferous-magnetite grain, as well as the area where a line scan of the exsolution pattern was taken. The exsolved phases are magnetite and ulvöspinel.

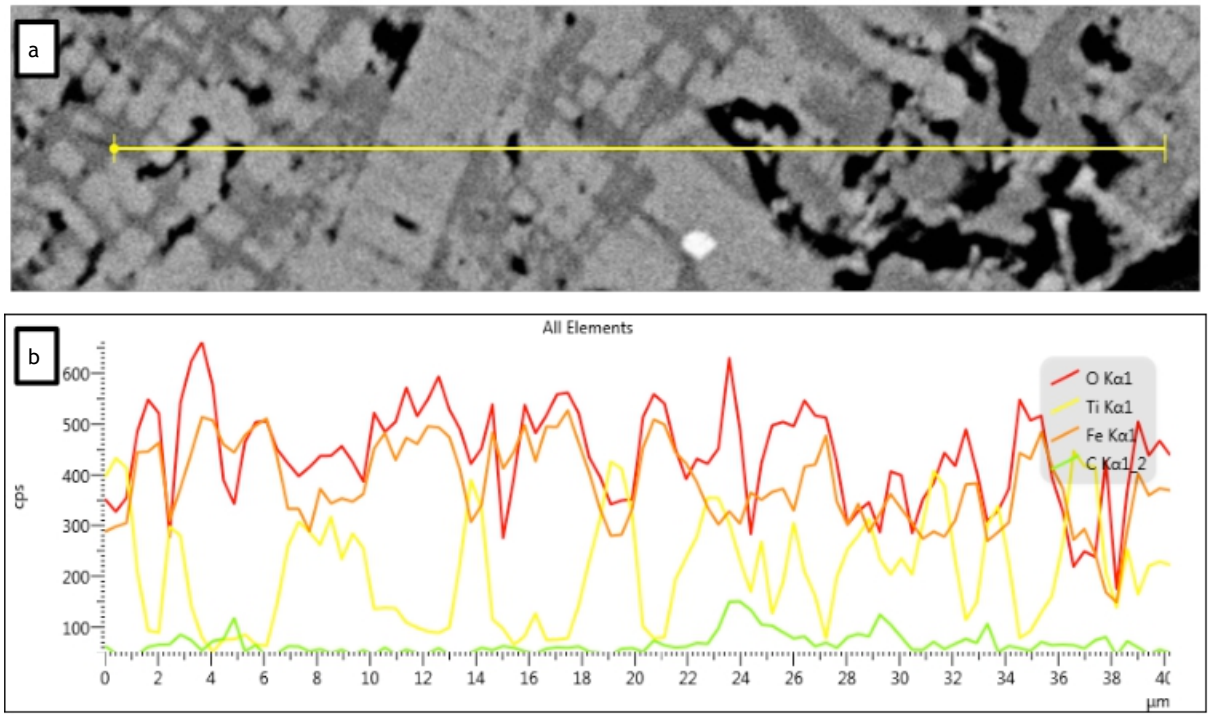

Figure 56. (a): A high magnification SEM image of Figure 54 showing a cloth texture exsolution of a titaniferous-magnetite grain, and the extent of Line Data 6. (b): A line scan of Line Data 6.

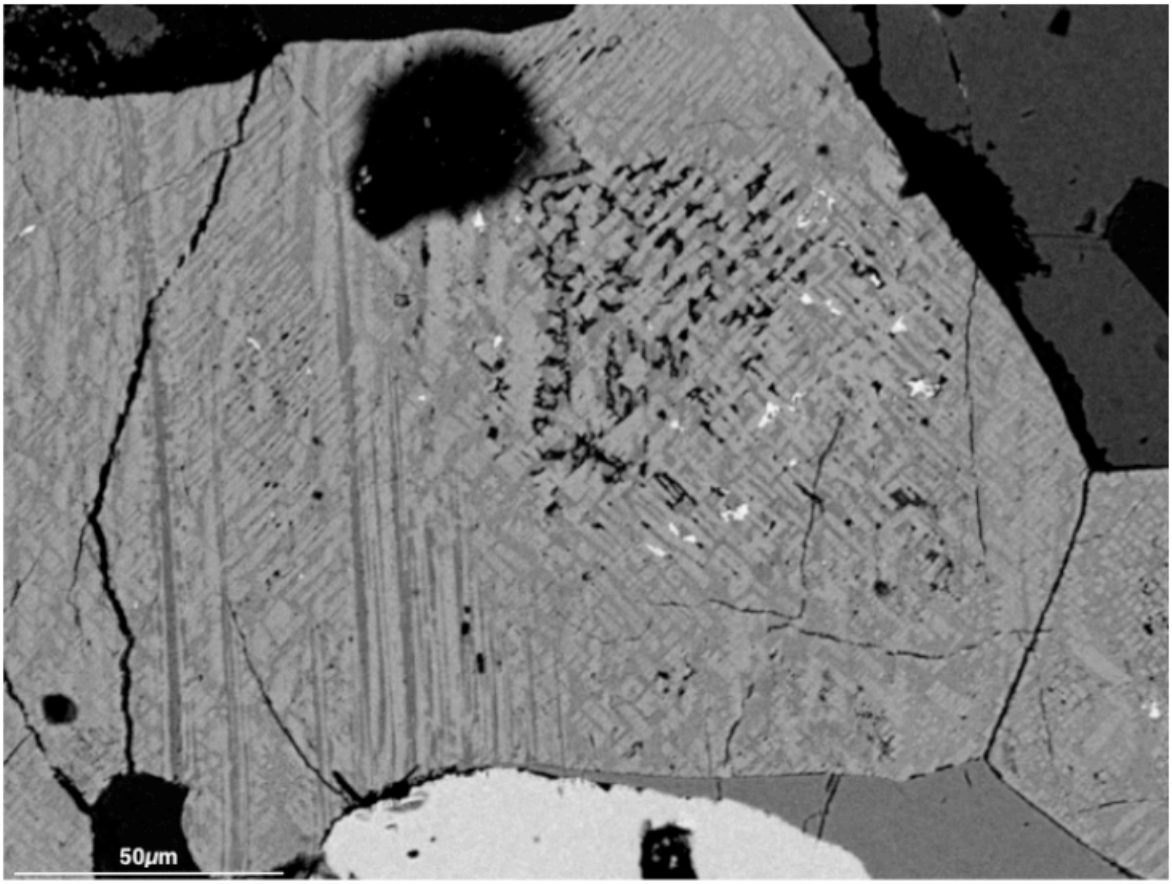

Figure 57. A high magnification SEM image of slide 2 MG 2.2a showing a variation in the cloth texture exsolution pattern in a single titaniferous-magnetite grain, as well as "trellis" type texture due to ilmenite.The exsolved phases are magnetite, ulvöspinel, and ilmenite.

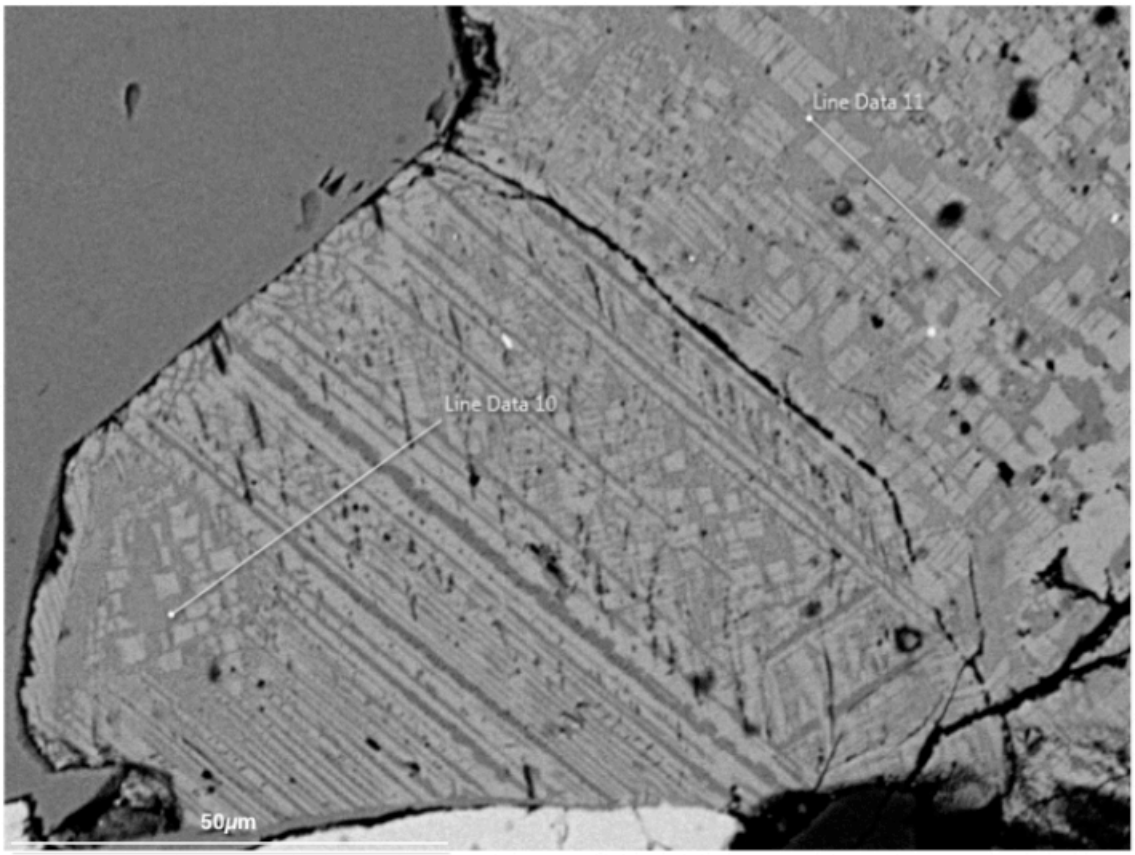

Figure 58. A high magnification SEM image of slide 2 MG 2.2a showing various prisms in the cloth texture exsolution pattern of a titaniferous-magnetite grain, ilmenite "trellis" type exsolution, as well as the area where line scans of the exsolution patterns were taken. The exsolved phases are magnetite, ulvöspinel, and ilmenite.

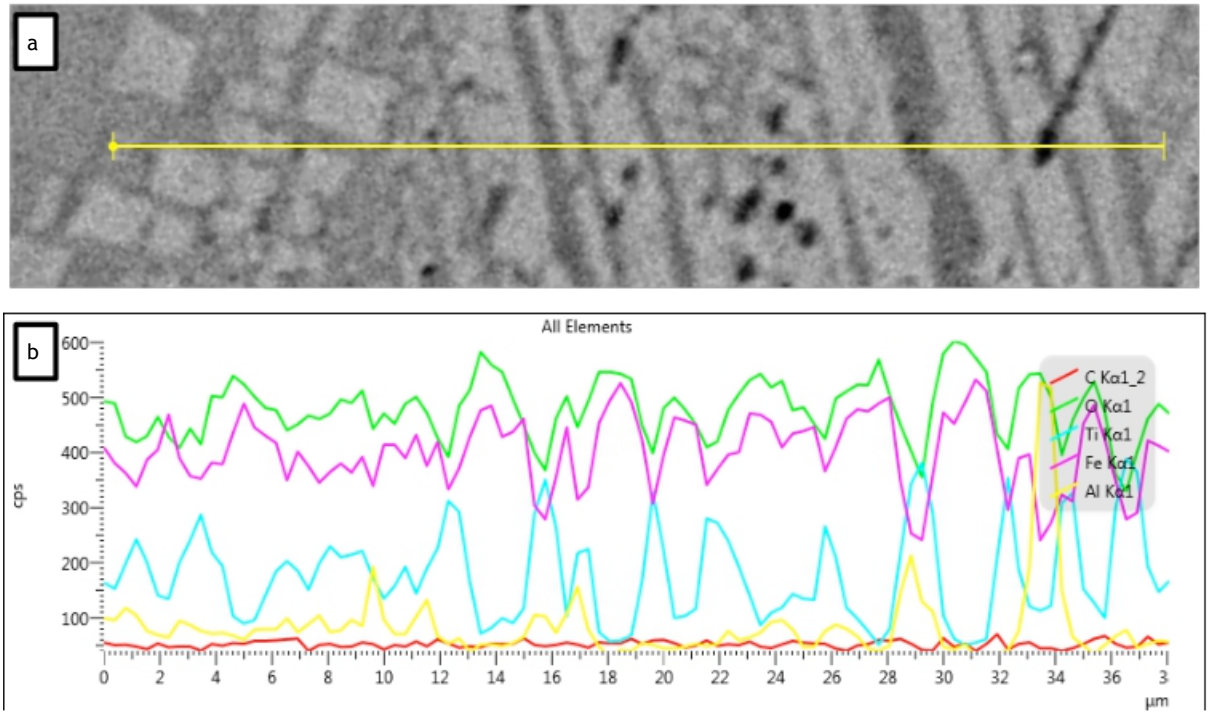

Figure 59. (a): A high magnification SEM image of Figure 57 showing a cloth texture exsolution of a titaniferous-magnetite grain, "trellis" type exsolution in ilmenite, and the extent of Line Data 10. (b): A line scan of Line Data 10.

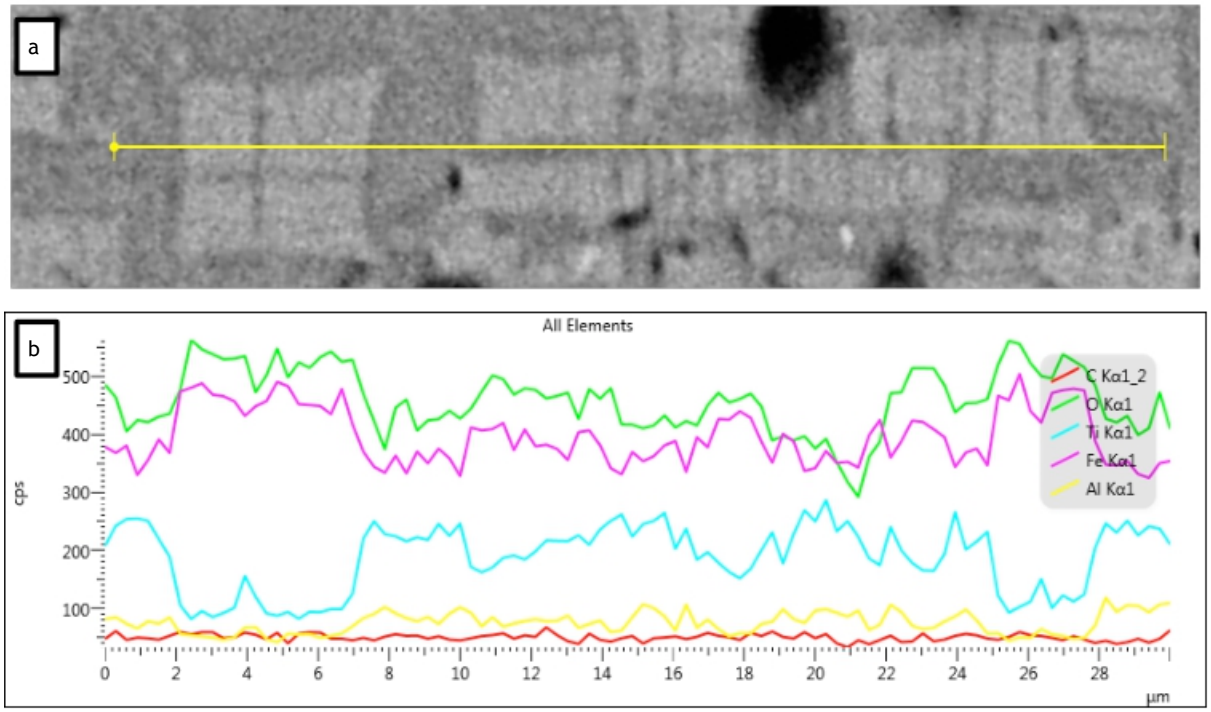

Figure 60. (a): A high magnification SEM image of Figure 57 showing a cloth texture exsolution of a titaniferous-magnetite grain, and the extent of Line Data 11. (b): A line scan of Line Data 11.

Figure 61. A high magnification SEM image of slide 2 MG 2.6 showing various prisms in the cloth texture exsolution of titaniferous-magnetite grains, as well as the area where a line scan of the exsolution pattern was taken. The exsolved phases are magnetite and ulvöspinel.

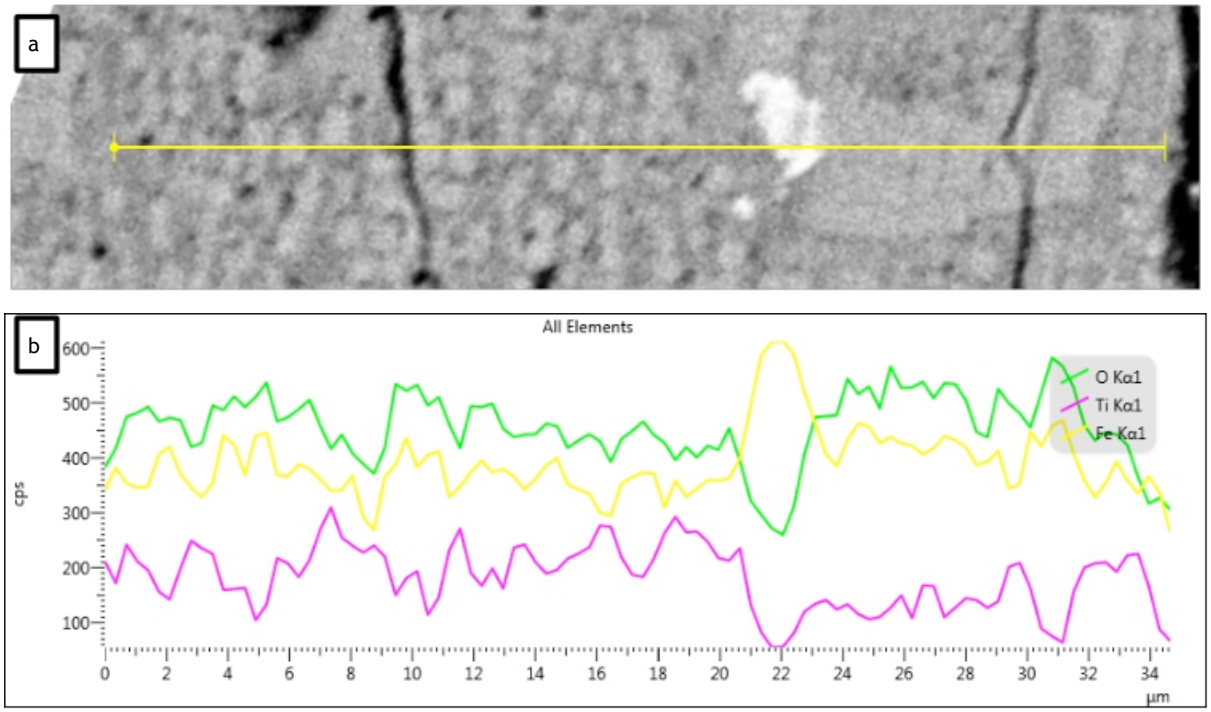

Figure 62. (a): A high magnification SEM image of Figure 60 showing a cloth texture exsolution of a titaniferous-magnetite grain, and the extent of Line Data 15. (b): A line scan of Line Data 15.

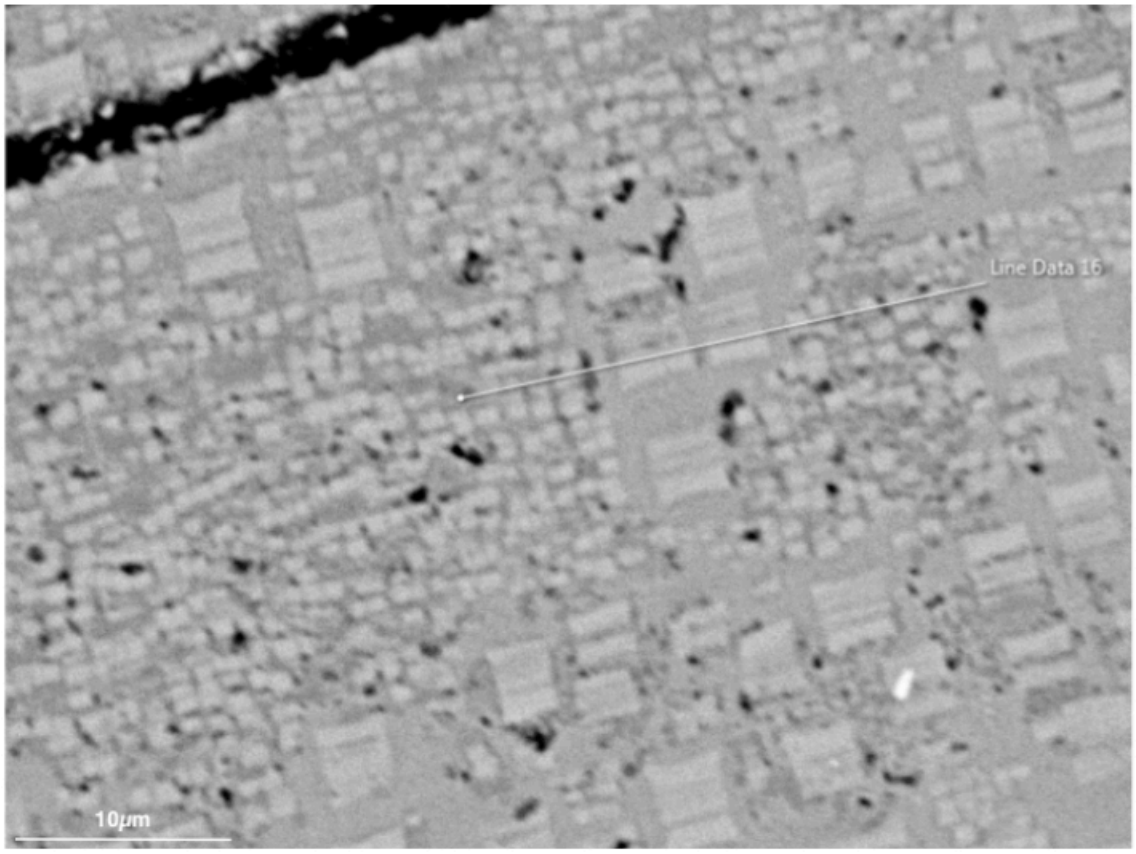

Figure 63. A high magnification SEM image of slide 2 MG 2.6 showing various prisms in the cloth texture exsolution of a titaniferous-magnetite grain, and the area where a line scan of the exsolution pattern was taken. The exsolved phases are magnetite and ulvöspinel.

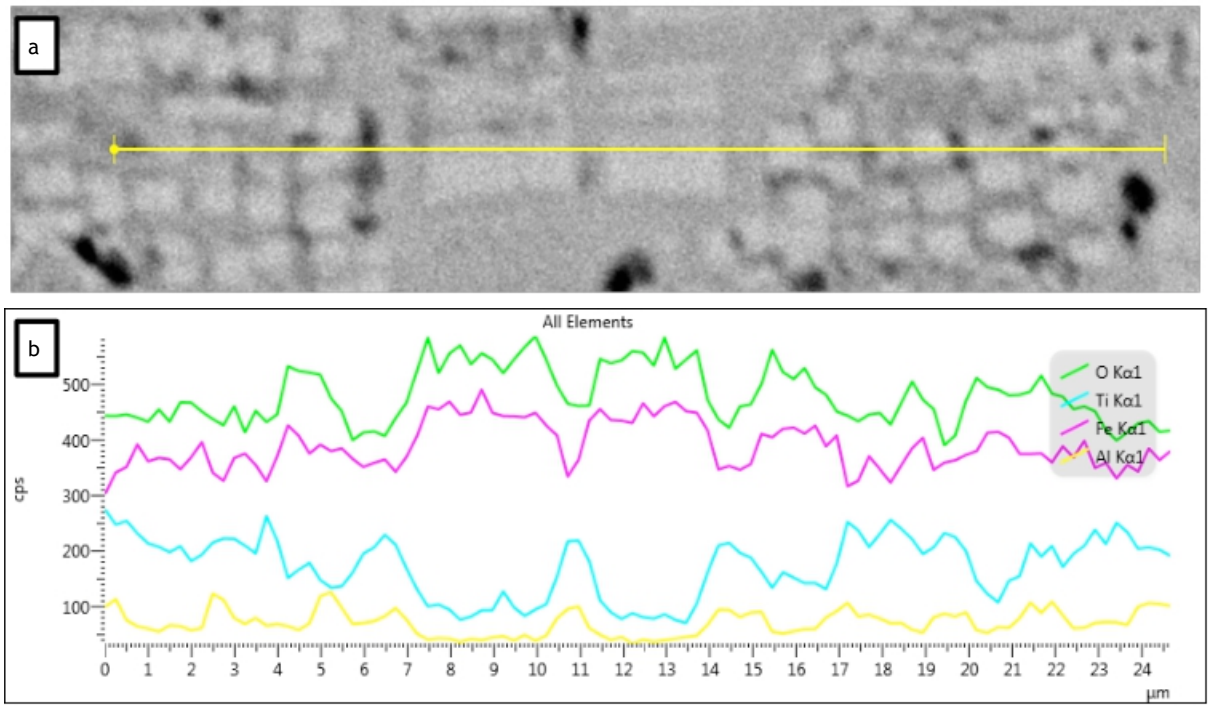

Figure 64. (a): A high magnification SEM image of Figure 62 showing a cloth texture exsolution of a titaniferous-magnetite grain, and the extent of Line Data 16 across various prisms. (b): A line scan of Line Data 16.

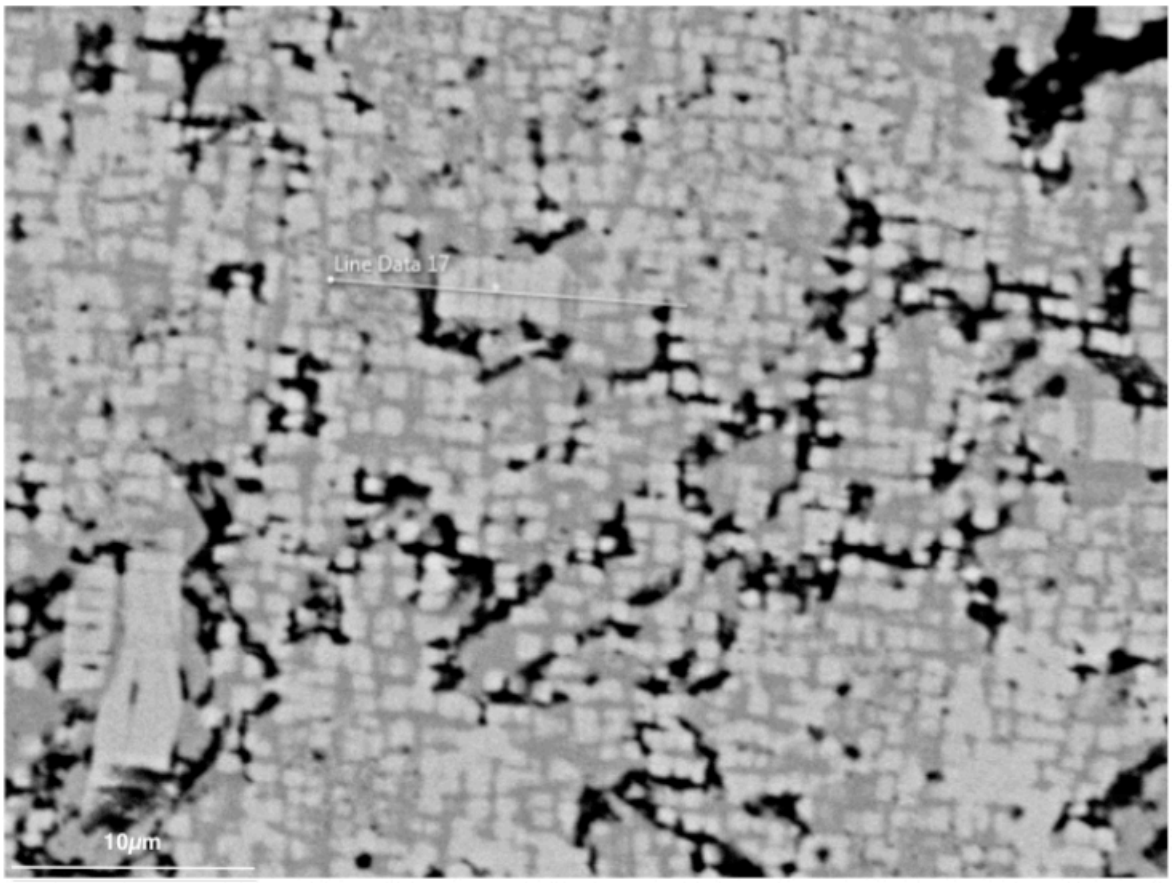

Figure 65. A high magnification SEM image of slide 2 MG 2.6 showing various prisms in the cloth texture exsolution of a titaniferous-magnetite grain, and the area where a line scan of the exsolution pattern was taken. A darker phase is also present.

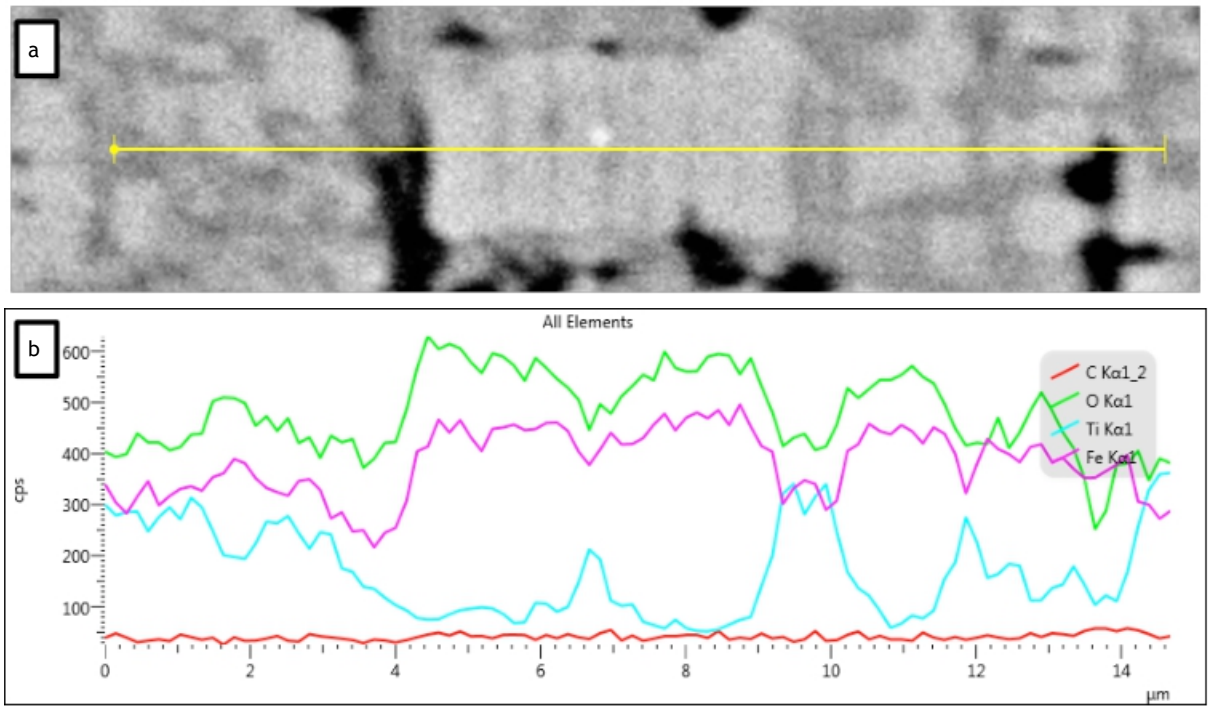

Figure 66. (a): A high magnification SEM image of Figure 64 showing a cloth texture exsolution of a titaniferous-magnetite grain, and the extent of Line Data 17 across various prisms. (b): A line scan of Line Data 17.

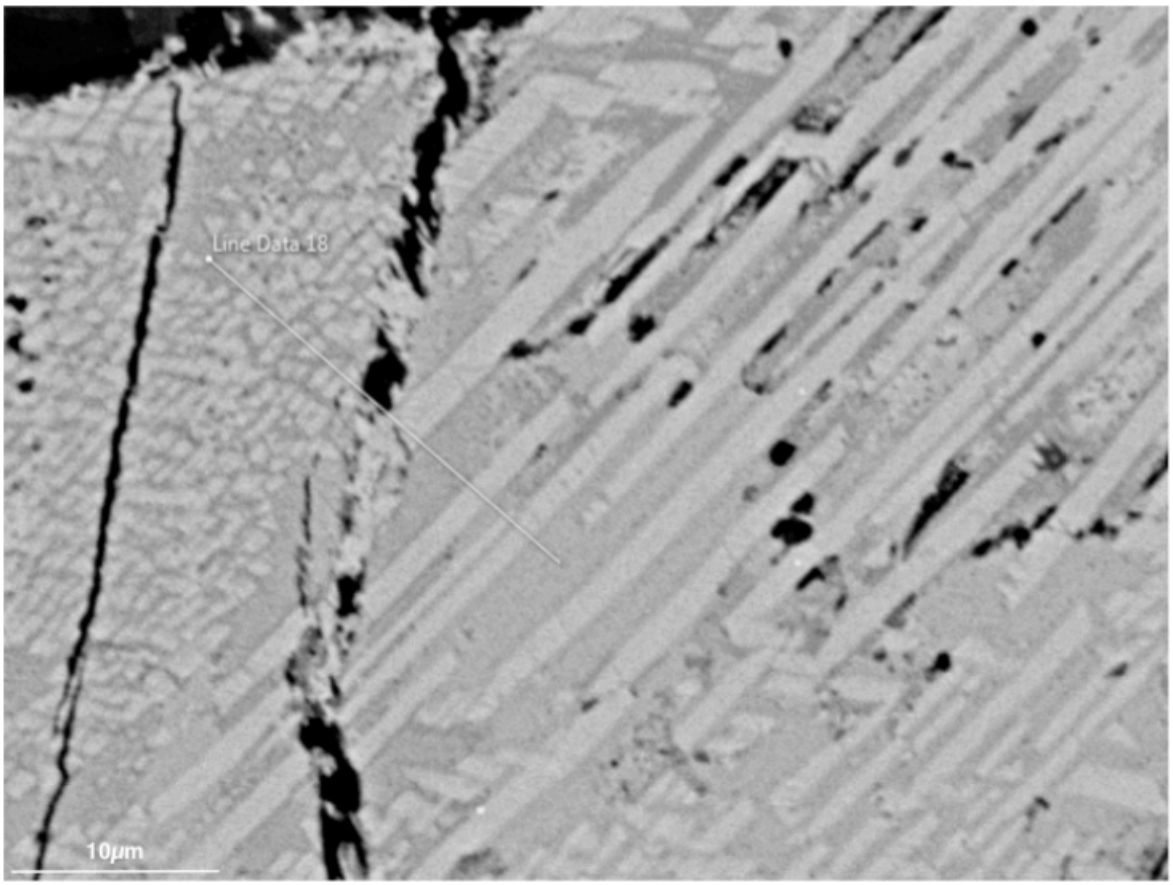

Figure 67. A high magnification SEM image of slide 2 MG 2.6 showing various prisms in the cloth texture exsolution of a titaniferous-magnetite grain, and the area where a line scan of the exsolution pattern was taken. A darker phase is minimally present.

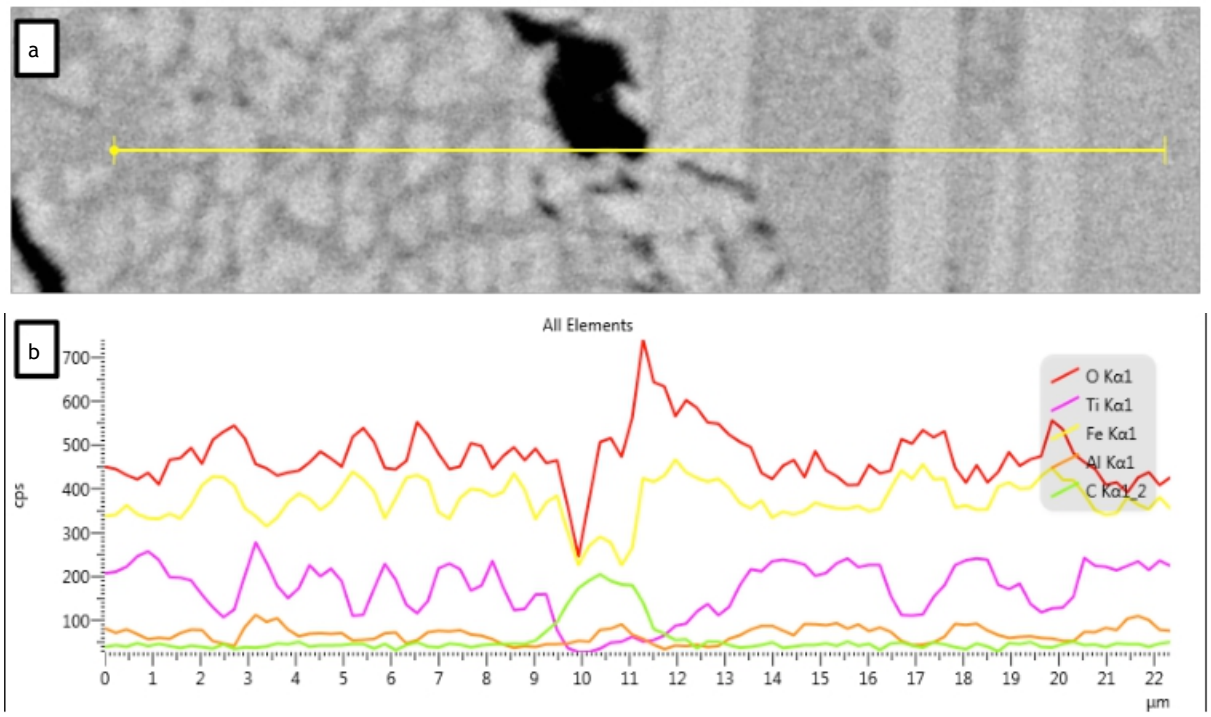

Figure 68. (a): A high magnification SEM image of Figure 64 showing a cloth texture exsolution of a titaniferous-magnetite grain, and the extent of Line Data 18 across various prisms. (b): A line scan of Line Data 18.

Both the iron and titanium elemental weight percentages were sorted into histograms in order to analyse the peaks and dips in terms of elemental weight percent (Figure 69 and Figure 70). Considering Figure 69, the highest peak can be seen between approximately 51 wt-% Fe and 55 wt-% Fe. Considering Figure 70, a peak can be seen between the interval of 0.5 wt-% Ti to 1.0 wt-% Ti, which is indicative of trace values. This peak is not considered in conjunction with the other data. Another peak is seen in Figure 70 from 6.1 wt-% Ti to 6.5 wt-% Ti, with the remainder of the data showing a complex conjunction of peaks and drops. Normal distribution can be seen in Figure 69, but this is not visible in Figure 70.

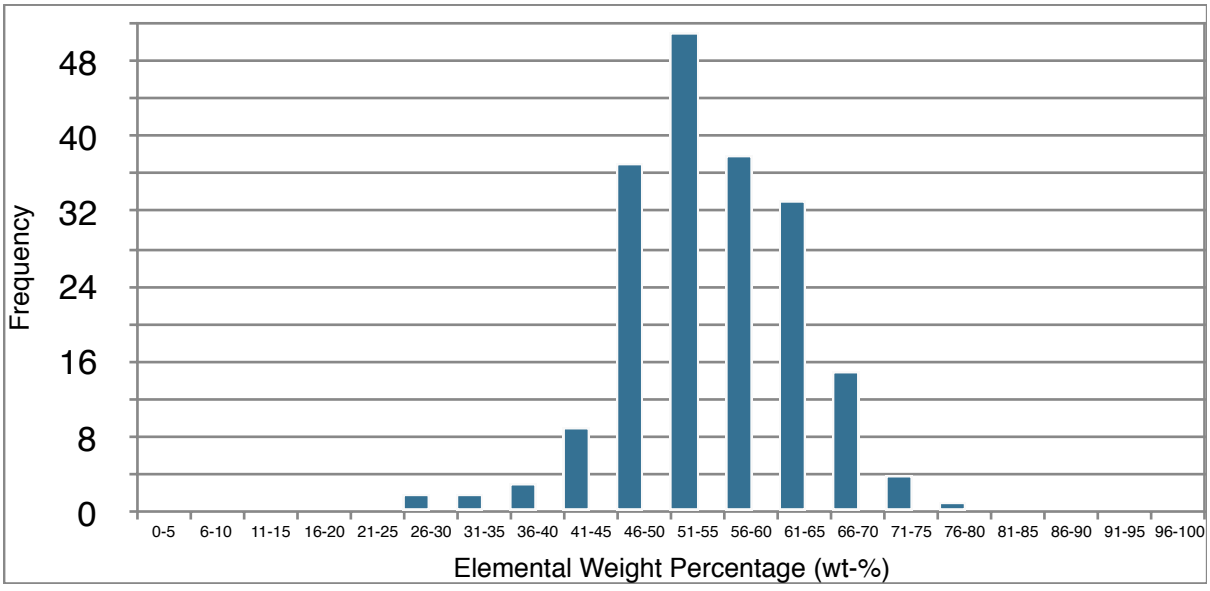

Figure 69. A histogram of the Fe elemental weight percentage (wt-%) data.

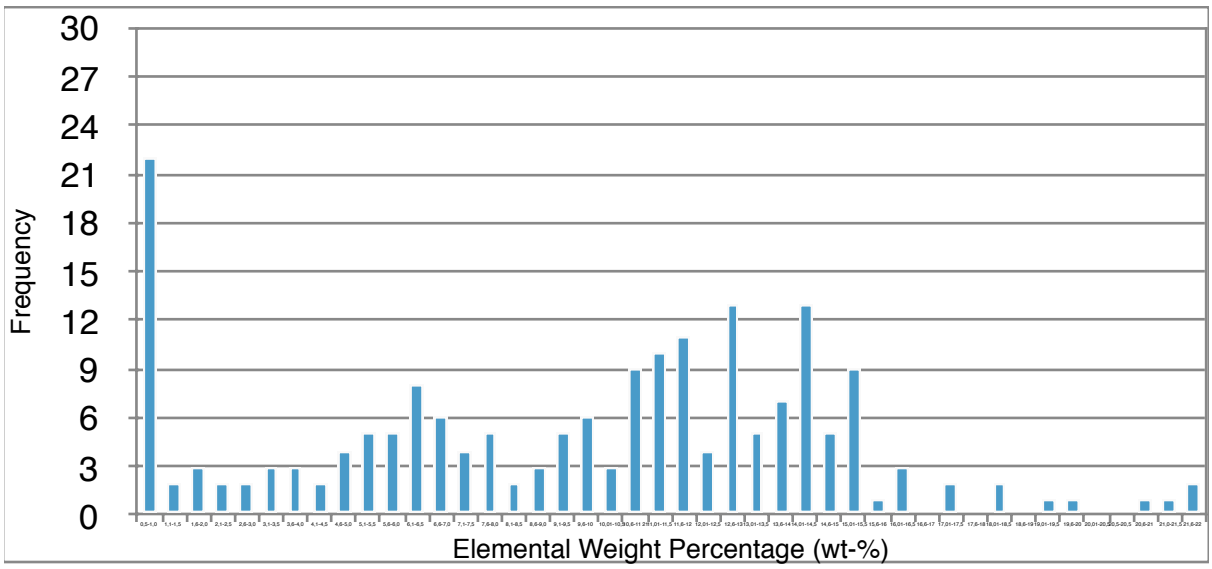

Figure 70. A histogram of the Ti elemental weight percentage (wt-%) data.

Considering pure magnetite, at least 70% Fe is required (Fe2+, Fe3+, or mixed) in order for the magnetite to form. Very small amounts of Fe are above 70%, suggesting small amounts of pure magnetite. Ideal ulvöspinel requires approximately 21.4% Ti for it to be considered ulvöspinel, although only small amounts of Ti are this high in weight percent. Most of the Ti data shows much lower Ti values.

Summary

The 10 slides analysed from Layer 21 in the Upper Zone show titaniferous-magnetite exsolution, as well as ilmenite exsolution. The minerals present in the slides include plagioclase, apatite, various silicates, pyrrhotite, magnetite, titaniferous-magnetite, and ilmenite. Various analyses have been classified under a certain mineral group, but do not meet the exact requirements, and were labeled as “unknown” or “unclassified”.

The exsolution texture of titaniferous-magnetite is not constant, with variation between blocky prisms that are in close proximity, rectangular prisms that are sparsely located, and continuous prisms that are in close proximity. This raises the question as to why there are these types of textural changes in the exsolution. Ilmenite exsolution is only present in certain slides, being very limited. When ilmenite grains are present, they are quite large and range from euhedral to subhedral. Certain images show the presence of ilmenite next to a titaniferous-magnetite grain, but no “trellis” type texture of the ilmenite exsolution is seen in those images.

The silicates tend to form a ring around the titaniferous-magnetite grains, although this is not seen in all the images. Silicates are abundant in the slides, although attention has not been given to determine the exact silicate minerals present. Some silicates also show exsolution textures. Apatite is present in almost every image, with the proportions of the mineral being high. The grain size varies, but the grains are almost always very anhedral and circular. Pyrrhotite grains are present in most images, but the grains are generally small and euhedral to subhedral. Plagioclase is also common and very abundant. No foliation or preferred alignment is shown by the plagioclase. Certain images indicate the infiltration of a mineral, or the inclusion of a mineral, which is usually magnetite or plagioclase.

Line scans performed on slide 2 MG 2.2a and 2 MG 2.6 confirm the presence of magnetite as the lighter areas in the exsolved grains, and ulvöspinel as the grey areas in the exsolved grains. Black and white “holes” are present, with the white spaces considered to be sulphide grains, and the black spaces to be holes caused by the leaching of the small sulphide grains. The line scans do provide some insight into the holes and small sulphide grains, but do not provide insight into the change seen in the cloth texture exsolution between the prisms.

Histograms of the Fe and Ti data indicate a normal distribution for Fe, with the highest peak falling between 51 wt-% Fe and 55 wt-% Fe. Ti shows a very high peak at 0.5 wt-% Ti to 1.0 wt-% Ti, which suggests trace element amounts. The next peak is found at 6.1 wt-% Ti to 6.5 wt-% Ti, with the remainder of the data being rather complex in form.

Although ilmenite exsolution was not present throughout all the investigated slides, its presence indicates changes in conditions that can result in the onset of exsolution. Table 12 compares each polished thin section and whether ilmenite was present or not present.

Table 12. Comparisons of the investigated polished thin sections in terms of ilmenite grains or ilmenite exsolution.

Features	Ilmenite Grains	Ilmenite Exsolution (“trellis” type)	Titaniferous-Magnetite Exsolution (cloth texture)
2 MG 1.3			
	Yes	Yes-Minimal	Yes
2 MG 1.6			
	No	Yes-Minimal	Yes
2 MG 1.8			
	No	Yes	Yes
2 MG 2.0			
	No	No	Yes
2 MG 2.2a			
	No	Yes	Yes
2 MG 2.2b			
	Yes	No	Yes
2 MG 2.4			
	No	Yes	Yes
2 MG 2.6			
	No	No	Yes
2 MG 2.8			
	Yes	No	Yes
2 MG 1.1			
	Yes	Yes	Yes

CHAPTER 5 DISCUSSION

Titaniferous-magnetite exsolution

Paragenetic and palaeomagnetic information is easily obtainable from titaniferous-magnetites. The chemical and physical properties of oxides reflect the conditions that were present during their formation and cooling. Low temperature modification of the oxides, such as oxidation or exsolution, may affect the magnetic properties of titaniferous-magnetite. Magnetite-ulvöspinel exsolution is generally considered less common than oxidation microstructures, but has been investigated more due to the prevalence of these exsolution textures being more widespread than previously thought (Price, 1980).

Mogensen (1946) first noted the existence of the two-phase intergrowth of ulvöspinel-rich and magnetite-rich oxides, and further studies noted that titaniferous-magnetite exsolution is a common feature in rocks occurring in plutonic and hyperbassal environments. The typically described feature is that of a three-dimensional framework (grid pattern) of ulvöspinel-rich lamellae. These lamella usually lie on {100}, with inter-lamellar magnetite-rich blocks (Price, 1980). The exsolution microstructure only develops on a small scale, due to the slow rate of the kinetic processes involved in unmixing at the solvus temperature.

SEM analysis was first used by Nickel (1958) to study the exsolution textures developed in titaniferous-magnetites from Mt. Yamaska, Quebec. Evans and Wayman (1974) experimented using a carbon replica method in order to investigate the exsolution textures. Although other studies have been done on the same topic, no general microstructural survey had been attempted until Price (1980) presented a transmission electron microscope (TEM) survey of the exsolution-derived microstructural types that are developed in titaniferous-magnetites

Not much information is presented in literature regarding the physical formation of the cloth texture exsolution texture of titaniferous-magnetites. As noted earlier in this thesis, changes can be seen in the physical appearance of the cloth texture exsolution throughout the analysed thin sections. These changes in texture are of great interest, as it provides some information regarding the physical formation of the exsolution textures.

The elemental data in this study indicates that no change in the bulk geochemistry can be seen that could be responsible for the change in appearance of the exsolution textures. Similarities seen in the crystal structure, and the chemical bonding between the host and the exsolved phase, particularly the matching between atomic arrangements in specific layers resulting in a shared plane of atoms, dictates that exsolution is crystallographically controlled.

Price (1982) noted major problems in developing more accurate models when it comes to titaniferous-magnetite exsolution. The first problem is modeling three-dimensional diffusion fields, and determining the relative importance of chemical and surface-energy driving forces in cooling systems. The second problem is the assumption that one-dimensional lamellae will grow at similar rates to that of three-dimensional microstructural development. The growth of three, mutually orthogonal planar lamella should be modeled in order to more accurately reproduce the formation of the titaniferous-magnetite microstructures (Price, 1982). This is why a titaniferous-magnetite crystal should not only be considered in 2D, but rather in 3D. Figure 71 indicates a magnetite crystal in its most basic, tetragonal crystal form, not considering constraints that may have been brought about by other minerals. Figure 72 shows the crystal structure of a magnetite grain, with the red spheres representing Fe and the grey spheres representing O.

When the crystal structure is subjected to high temperatures, Ti ions may replace other ions in some crystallographic sites. When the temperature drops and exsolution occurs, the ions that have been kicked out will continue to form part of the crystal structure. These ions will replace ions in other sites, or create space in the structure to move into. This implies that the exsolution texture also forms in 3D throughout the crystal, and is not present as a surface property. The exact positioning of the exsolved ions is not clear, and requires further research.

Figure 71. A 3D model of a magnetite grain in its most basic form.

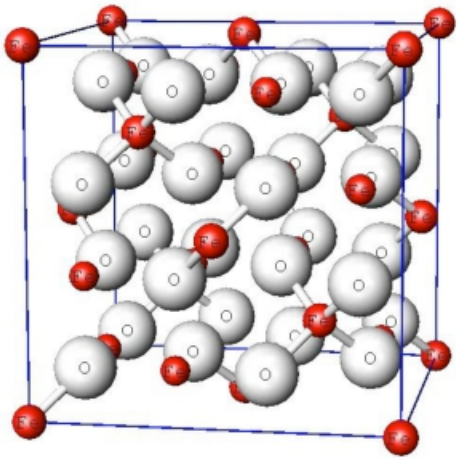

Figure 72. A 3D sketch of the magnetite crystal structure. The red spheres indicate Fe and the grey spheres indicate O. Fe2+ and Fe3+ are mixed and interchangeable in a magnetite crystal (Department of Materials Science, Shimane University).

It is important to consider the 3D appearance of exsolution textures when studying thin sections. If the exsolution texture forms in 3D throughout a crystal, this suggests that the angle at which the crystal and the exsolution texture is cut will result in different physical appearances of the same exsolution texture. Thin sections only allow a very small section of

a grain to be included in the analysis, which similarly results that only a small section of the exsolution texture will be included when investigation occurs.

Figure 73 shows a model with the similar basic structure of a magnetite crystal as in Figure 75, with a cloth texture exsolution on {111}. Figure 73 can be compared directly to Figure 49 in the results section. Figure 74 shows this comparison, also indicating the titaniferous-magnetite crystal seen in Figure 49 has been cut at an angle which allows the exsolution texture to physically present itself as a basic cloth texture.

Figure 75 shows a model with a cloth texture exsolution on {111}, with the rest of the texture extending throughout the crystal, as seen on {1$\bar{1}$1}. Figure 75 can also be compared to Figure 67 in the results section. Figure 76 shows this comparison, also indicating how a titaniferous-magnetite crystal had been cut at an angle to allow a similar physical appearance as the texture seen on {111}. The second crystal shows the texture as it would appear if it were cut along {1$\bar{1}$1}. This model very simply explains how different angles of cut through a 3D crystal and its 3D exsolution textures would yield a change the exsolution texture appearance. This idea is reinforced by the fact that the cloth exsolution texture is not exact in its formation. The areas circled in red in Figure 74 show a lack of a magnetite blocks. Comparing this to Figure 76, which indicates a different angle of the 3D exsolution texture, a termination of a magnetite block can be seen circled in red. This coincides with the model, suggesting that if the magnetite block terminates before hitting the crystal surface or before the area where the crystal is cut, it would not appear in the thin section or during analysis.

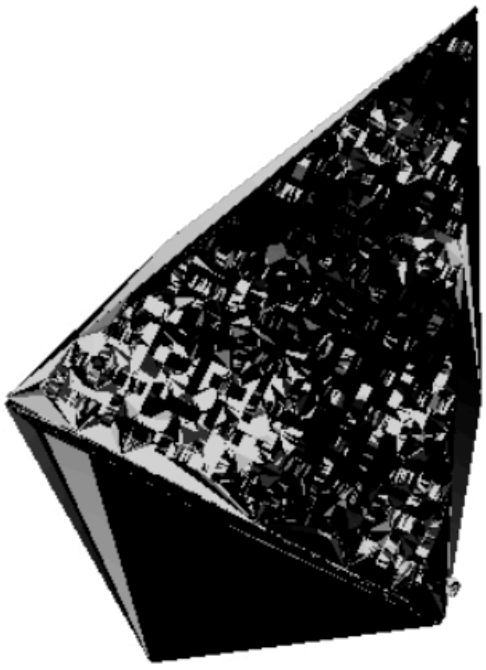

Figure 73. A 3D model of a titaniferous-magnetite grain with a cloth exsolution texture on {111}.

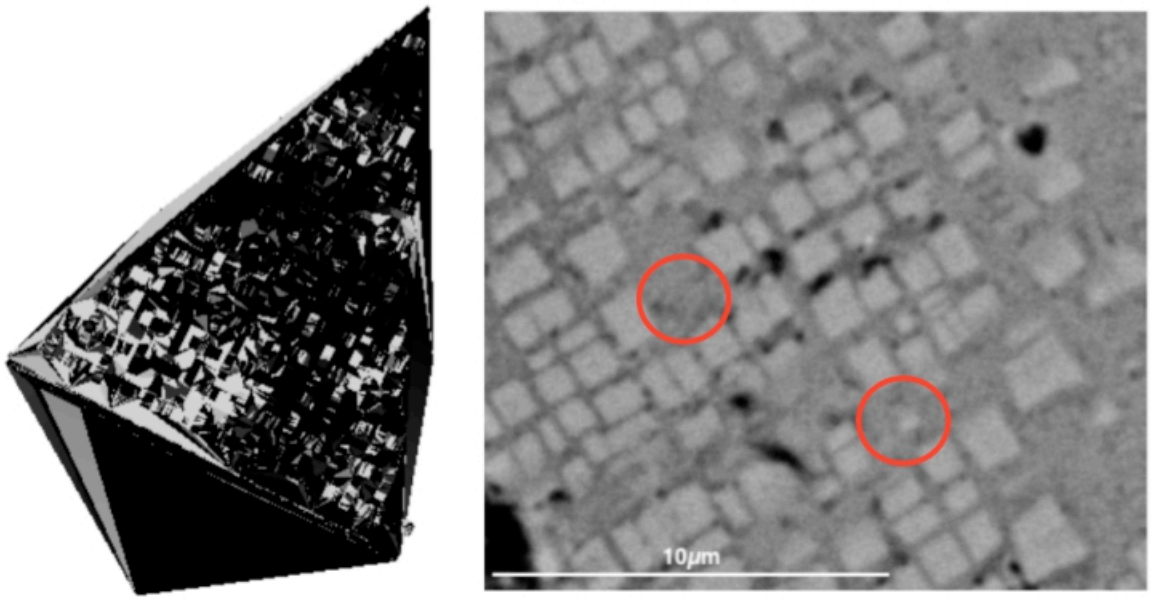

Figure 74. A 3D model of a titaniferous-magnetite grain with a cloth exsolution texture on the surface, compared to a SEM image of a cloth texture exsolution. Areas have been circled in red where the magnetite blocks did not extend to the surface.

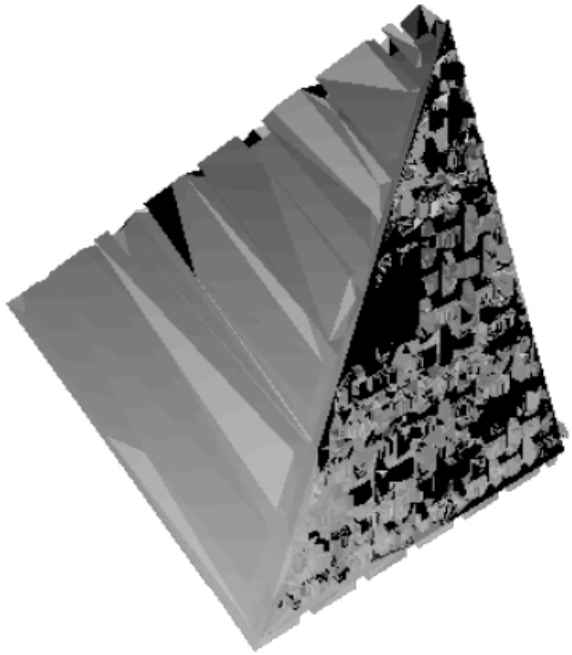

Figure 75. A 3D model of a titaniferous-magnetite grain with a cloth exsolution texture on {111} extending through to {1$\bar{1}$1}.

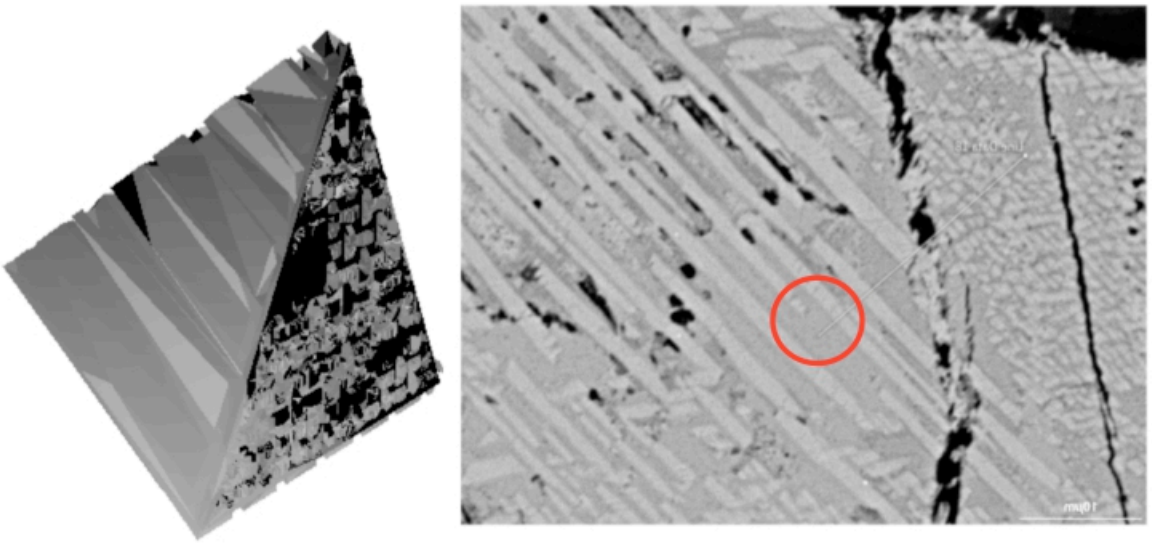

Figure 76. A 3D model of a titaniferous-magnetite grain with a cloth exsolution texture on the surface of {111}, extending into {1$\bar{1}$1}, compared to a SEM image of various cloth texture exsolutions. The area circled in red shows the termination of a magnetite block along the cut surface.

Figure 77 demonstrates how the basic tetragonal magnetite crystal can be cut at various angles. Considering the demonstrated angles as well as the unlimited angles not shown in the figure, the implication is that the crystal can but cut at a large amount of angles which could project the physical appearance of the exsolution texture differently. In the case that the magnetite crystal could not develop into its preferred crystal form, much different angles may be cut which could yield even more variation on the exsolution texture seen during analysis.

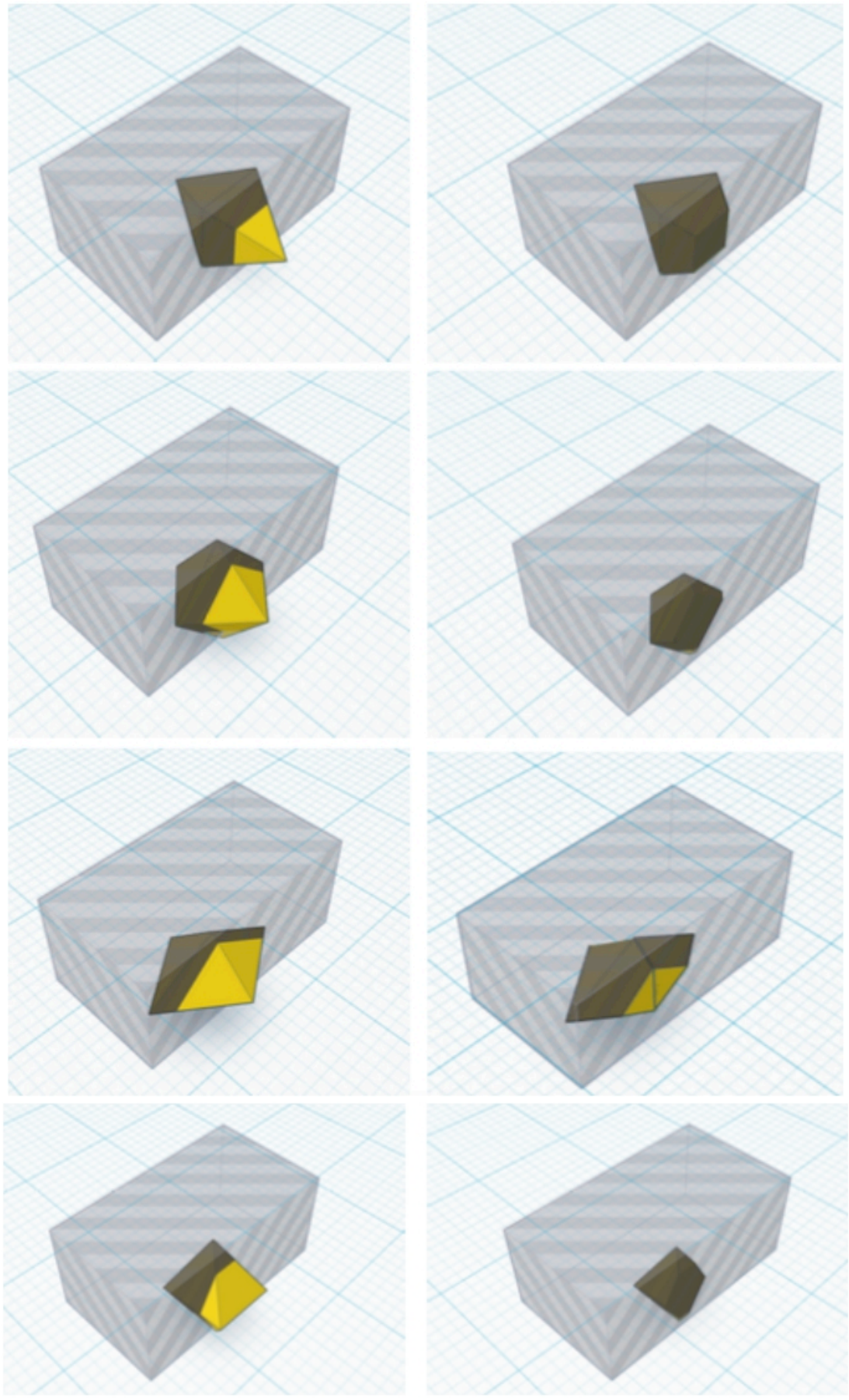

Figure 77. 3D models indicating various angles at which a basic tetragonal prism magnetite crystal can be intersected, and the surface area which would result from such a cut.

In terms of the chemical formation of exsolution textures, exsolution microstructures are considered to develop as a function of the mineral's bulk chemistry and thermal history (McConnell, 1975). The unmixing of titaniferous-magnetites by a nucleation and growth mechanism was suggested by Nickel (1958). Yund and MacCallister (1969) suggested that spinodal decomposition could also occur in the ulvöspinel-magnetite system. The two mechanisms of exsolution are considered to be in competition, with spinodal decomposition being favoured by rapid cooling rates, and nucleation being favoured by systems with slower cooling rates (Price, 1980). Spinodal processes are limited to lower temperatures than that of the nucleation events, and are also limited to oxides where the compositions are near the centre of the ulvöspinel-magnetite join.

Price (1980) noted that the identification of the mechanism of formation of exsolution by only focusing on its textural appearance can be risky, especially when a large degree of coarsening has occurred. Coarsening could result in particular features which may be indicative of a specific mechanism. Price (1980) continued to use this approach in his investigation, using textural applications to interpret titaniferous-magnetite microstructures. The mechanisms were divided by certain characteristics, namely: (a) coarse precipitates found on grain boundaries and other lattice defects that are separated from the rest of the grain by a precipitate-free zone (PFZ), is a texture associated with heterogeneous nucleation (Nicholson, 1968), (b) The random distribution of discrete precipitates found within the body of the grain would be indicative of homogeneous nucleation, and (c) for titaniferous-magnetites, spinodal decomposition produces a periodic distribution of phases on {100}. Initially the interphase boundary will be diffused, but coarsening will lead to a lamellar framework with well defined boundaries (Price, 1980).

Periodic structures can also be produced by the strain-induced alignment of homogeneously nucleated precipitates (Ardell and Nicholson, 1966). The difference between periodic structures produced by a spinodal mechanism and periodic structures produced by a nucleation mechanism will be evident from the relationship of the microstructures to the grain boundary (Price, 1980). Generally, grain boundaries will affect the morphology of nucleation-derived microstructures, but will not affect the morphology of a spinodally-derived microstructure (Nicholson, 1968).

Price (1980) reported both fine-scale microstructures and coarse-scale microstructures. Fine-scale microstructures are periodic lamellar textures and are considered to represent one of the stages in coarsening. Three rock groups from different areas were analysed, and a variety of results were obtained. The first (1) result was a fine-scale, cross hatched micro-texture, characteristic of the spinodal decomposition mechanism. The second (2) result showed a coarser microstructure, with clearly defined boundaries between the exsolved phases. The developed boundaries indicate an increased level of strain. This exsolution texture is considered to be a coarsening of the microstructure seen in (1). The third (3) result showed the coarsest grains, with lamella-rich ulvöspinel and blocks that are magnetite-rich. Block uniformity is reported, but some inconsistencies are present (Price, 1980).

Mt. Yamaska intrusion samples were used for (3) above. The formation of the Mt. Yamaska intrusion is reported as multiple injections of two main phases and two minor phases. The two main intrusions are vertical and pipe-like, and are differentiated by ultramafic rocks at their core that become increasingly felsic towards the outer margin of the phases (Gandhi, 1967). The structure formation of the intrusion is not similar to that of the Upper Zone, but the exsolution textures found in Layer 21 seem to correlate the analytical results of the exsolution. Price (1980) reports that the grain boundary between titaniferous-magnetite and silicate grains do not seem to affect the lamellar texture, which would suggest spinodal decomposition as an origin for the exsolution.

Von Gruenewaldt *et al*., (1985) investigated the changes in the titaniferous-magnetite exsolution features within the Upper Zone of the Eastern Limb of the Bushveld Igneous Complex. Compared to other layered intrusions, the TiO_2 content in the Upper Zone of the Bushveld Igneous Complex is quite low. This indicates that the TiO_2 could have been in solid solution in the titaniferous-magnetites at high temperatures. The result is that the course grained ilmenite found in titaniferous-magnetite layers originated from oxidation of a high temperature titaniferous-magnetite. The observed textural features in titaniferous-magnetites are caused by two processes: (i) the oxidation of the magnetite-ulvöspinel solid solution at temperatures above the magnetite-ulvöspinel solvus resulting in a process similar to exsolution, where most ilmenite is exsolved from the titaniferous-magnetite. (ii) Ulvöspinel exsolution is a true exsolution process that is a result of decreased solubility of one component in the other as the temperature drops (Von Gruenewaldt *et al*., 1985). The changes in the exsolution textures can be described as either exsolution above the magnetite-ulvöspinel solvus, or exsolution below the magnetite-ulvöspinel solvus.

Von Gruenewaldt *et al*., (1985) notes the proportion of ulvöspinel of the titaniferous-magnetite increases higher up in the Upper Zone, which results in a cloth texture exsolution pattern. Exsolved ulvöspinel is very susceptible to oxidation, which would form ilmenite and magnetite. Al_2O_3 and MgO of the titaniferous-magnetites are much higher than in their host rocks, which result in spontaneous crystallisation of layer magnetite layers under conditions of disequilibrium. This results in elements such as Mg and Al, which would usually partition into the silicates, to become enriched in the titaniferous-magnetite layers (Klemm *et al*., 1985). This can be seen in the values reported in Appendix A.

The scale of the lamellar framework developed in titaniferous-magnetites can be used to compliment geothermometric data. As described above, the mechanism of exsolution is affected by the initial temperature and the rate of cooling of the magma. After the investigation of the exsolution textures by Price (1980), Price (1982) developed a mathematical kinetic model with the intent of describing the growth of the titaniferous-magnetite exsolution textures as seen in the Skaergaard intrusion of eastern Greenland, the Mt. Yamaska intrusion of Quebec, and the Taberg intrusion of southern Sweden (Figure 78).

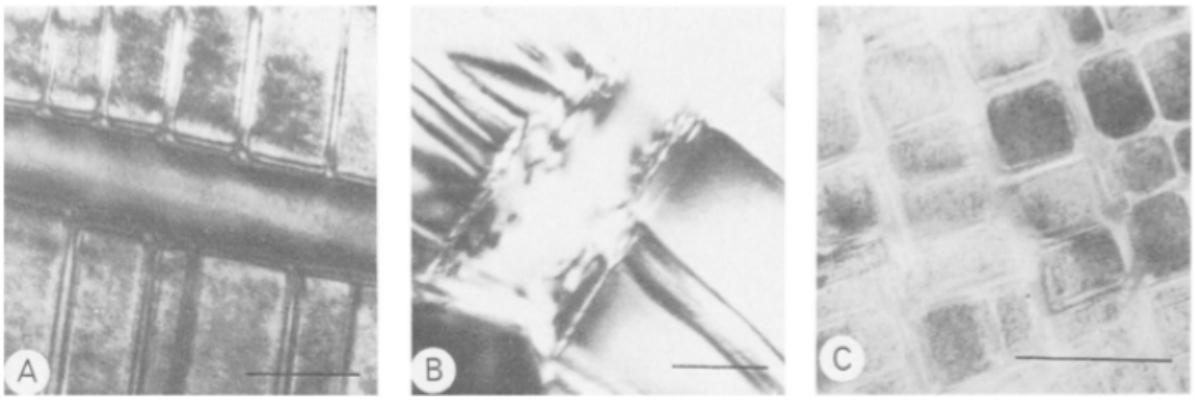

Figure 78. Electron micrographs of exsolution textures developed in some titaniferous-magnetites (scale bar = 200 nm). (a) Ulvöspinel-rich lamella in titaniferous-magnetites from the Taberg intrusion. (b) An ulvöspinel-rich lamella developed in a titaniferous-magnetite from the Skaergaard intrusion. (c) Blocks of magnetite are separated from each other by lamellae of ulvöspinel in this titaniferous-magnetite from Mt. Yamaska. From Price (1982).

The mathematical kinetic model is used to explain that course microstructures and their development is a complex process which involves variations in the growth rates of particles. Some particles impinge on each other and some are resorbed. The rate of development of microstructures in cooling systems is considered a complicated function of both surface and chemical-free energy changes, although it is generally assumed that the

chemical-free energy changes play the dominant role (Price, 1982). At first, an ulvöspinel lamella should have a small finite width, and can be found in a homogeneous matrix. As time passes, the concentration gradients within the lamella and matrix will change as the lamella grows.

The evolution of the concentration gradients within the lamella is a function of the changing equilibrium composition of the lamella-matrix interface and the increasing diffusion distance as the system cools. When the temperature is low, the gradients within the lamella and the matrix cannot equilibrate, because of the slow diffusion at these temperatures. The growth of ulvöspinel lamellae can be described in terms of composition (C) and transmission electron microscopy (TEM), and the diffusion coefficient (D) (Price, 1982). The cooling rates of the Taberg, Skaergaard, and Mt Yamaska intrusions were calculated to be 135ºC per 1000 years, 10.7ºC per 1000 years, and 487ºC per 1000 years respectively.

Bowles *et al*., (2009) conducted exsolution experiments which tested whether the consolute temperature of a pure titaniferous-magnetite solvus is lower than non-pure titaniferous-magnetite. The results of the study showed micrometer scale exsolution textures in oxide phases. Using samples similar to that of Bowles *et al*., (2009) and other samples, new time-series experiments were conducted by Petrochilos (2010), and were used to infer exsolution mechanisms. The experiments also investigated the time-dependent changes with a growth of the exsolution texture. Two sets of experiments where temperature is the primary variable were also conducted in order to evaluate changes brought about by variation in temperature.

The experiments conducted by Petrochilos (2010) set out to determine new constraints on the position of the solvus in multicomponent Fe-Ti-Al-Mg spinel-structured oxide. Magnetite, ulvöspinel, magnesioferrite (MgFe2O4), hercynite (FeAl2O4), and chromite (FeCr2O4) were selected for the experiment as end-members of spinel-structured oxide phases. The key aspects of the results were grouped into two categories. These categories were pertaining to the experimental variables of bulk composition, time, and temperature, as well as non-pure titaniferous-magnetite exsolution. Different oxide assemblages between crystalline starting materials were observed; although Petrochilos (2010) reports that the experimental variables do not seem to be responsible for this change. Time and temperature also shows a progressive oxide composition change.

Petrochilos (2010) labeled the experiments as Group 1, Group 2, and Group 3. Two compositional starting phases were used, namely Meteorite-Type (M-Type) and Terrestrial-Type (T-Type). Figure 79 shows the experimental conditions each group was subjected to for the study. Two exsolution types were observed in Group 1. In the first (I) type, exsolved phases contained magnetite and Al-bearing titaniferous-magnetite as end-members. The exsolution showed a cation partitioning pattern of Ti-Al and Mg-Fe with positive correlations, and a negative correlation between these two pairs. The Fe and Ti present major partitioning. The second (II) type of exsolution, Fe-Mg spinel oxide and Fe-Mg-Al spinel oxide exsolution had a precursor oxide phase of Fe-Mg-Al spinel oxide. The partitioning pattern shows Al-Ti and Fe-Mg positive correlations, and a negative correlation between these pairs. Mg and Al present major partitioning. Figure 80 shows backscattered images of Group 1 M-Type exsolution. The compositional characteristics shown by the oxide phases suggest if the starting material contains hematite, Type (I) exsolution is present. On the other hand, the presence of Fe-Mg-Al spinel oxide in the starting material is most likely parental to Type (II) exsolution (Petrochilos, 2010).

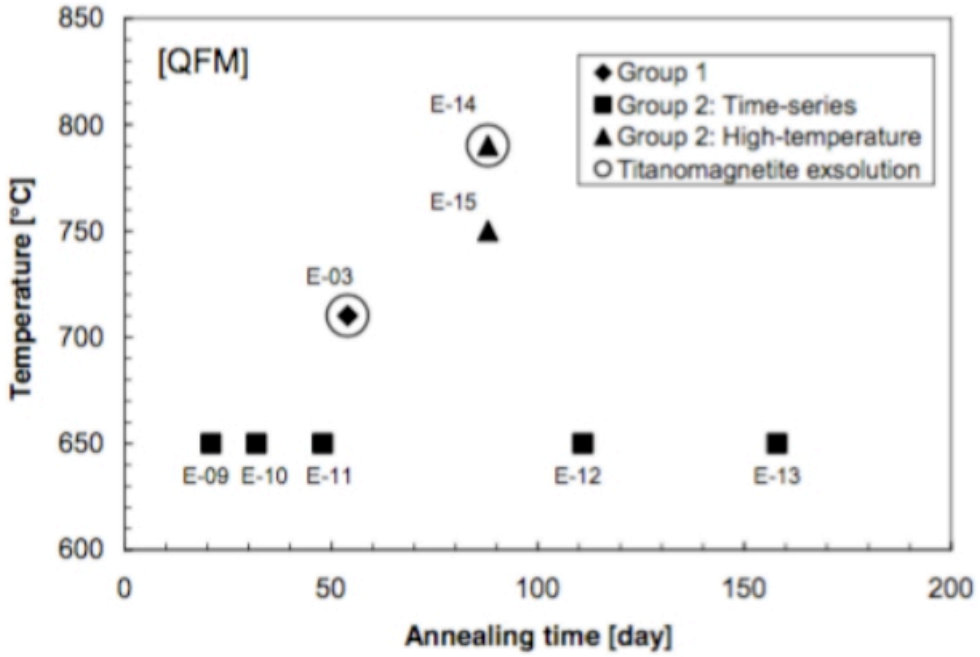

Figure 79. A temperature vs. time plot of the experimental conditions in the study by Petrochilos (2010). Bulk compositions varied, described as either M-Types or T-types. All experiments are at the quartz-fayalite-magnetite (QFM) buffer curve. From Petrochilos (2010).

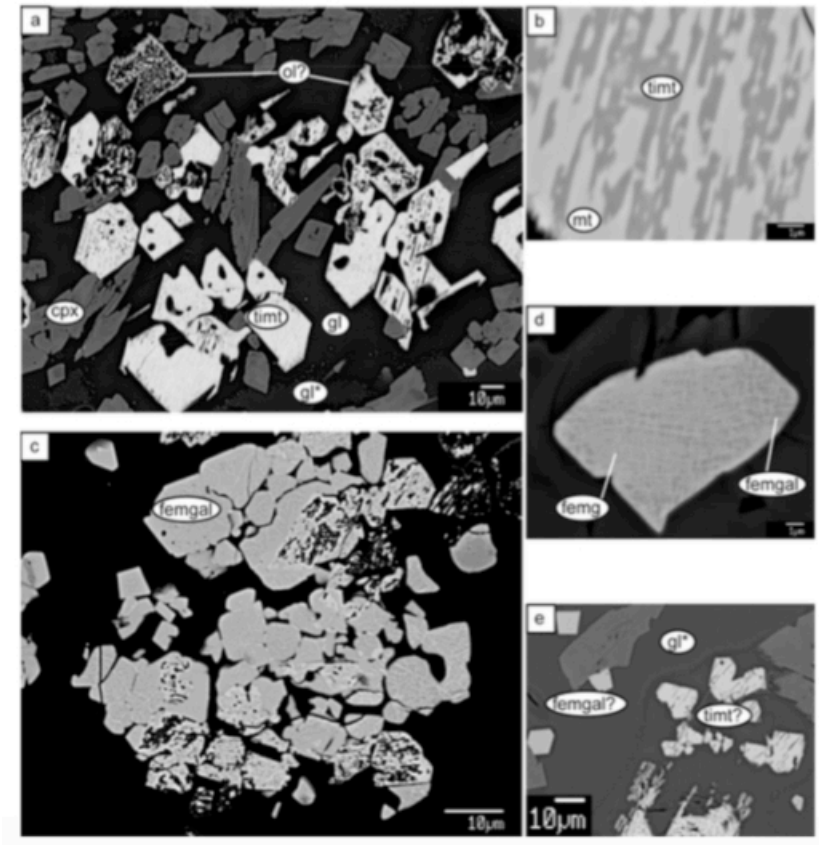

Figure 80. Back-scattered electron images of the Group 1 M-type annealed sample. (a-b): Type (1) exsolution, magnetite (light) and Al- bearing titaniferous-magnetite (dark). Some grains have an olivine reaction rim. (c-d): Type (2) exsolution, Fe-Mg spinel oxide (light) and Fe-Mg-Al spinel oxide (dark). (e): Non-exsolved oxide phases. cpx=clinopyroxene, gl=glass, gl*=devitrified glass, timt=titaniferous-magnetite, ol=olivine, mt=magnetite, femgal=Fe-Mg-Al spinel oxide,femg=Fe-Mg spinel oxide. From Petrochilos (2010).

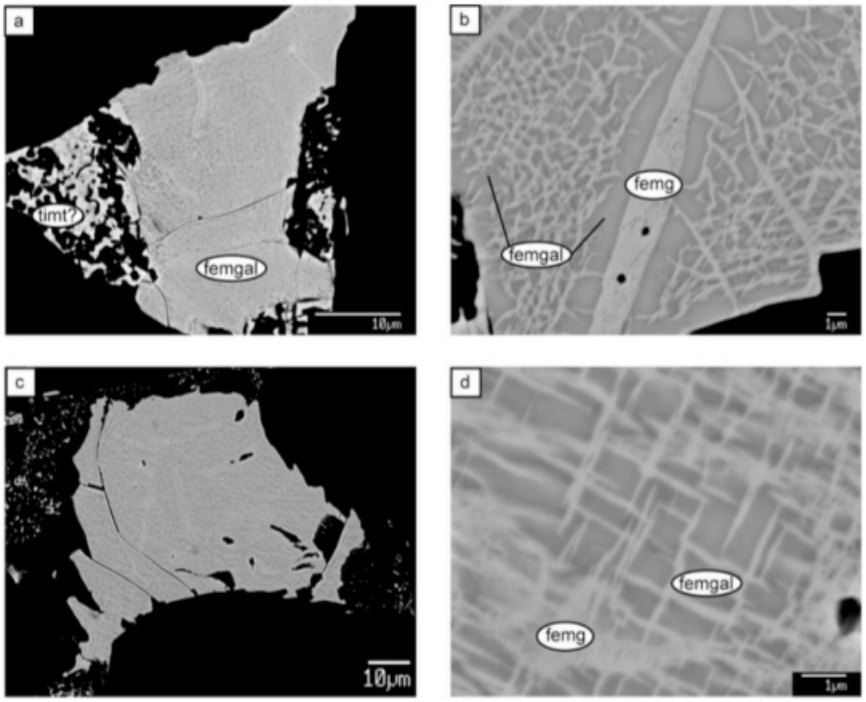

Figure 81. Back-scattered electron images of the Group 1 T-type annealed sample. (a-d): Type (2) exsolution is present, Fe-Mg spinel oxide (light) and Fe-Mg-Al spinel oxide (dark). (a) a relatively rare highly porous and compositionally heterogeneous oxide phase is present. timt=titaniferous-magnetite, femgal=Fe-Mg-Al spinel oxide, femg=Fe-Mg spinel oxide. From Petrochilos (2010).

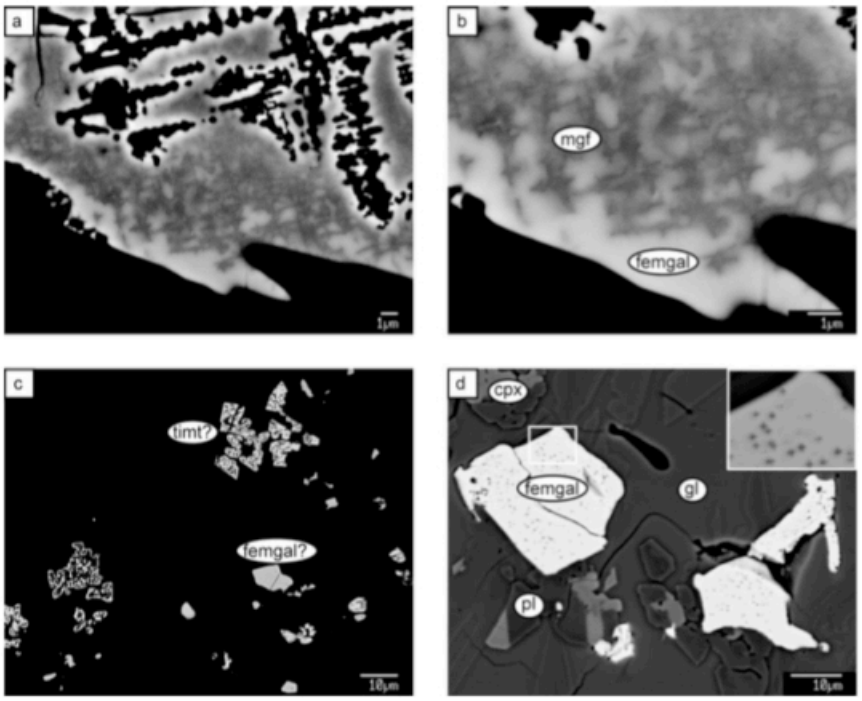

Figure 82. Back-scattered electron images of the Group 1 T-type annealed sample (Continued). (a-b): Type (3) exsolution is visible, Fe-Mg-Al spinel oxide (light) and Al-bearing magnesioferrite (dark). (c) Porous grains resembling titaniferous-magnetite exsolution in the M-type sample. (d) Non- exsolved oxide grains with pores texturally similar to that of grains with Type (3) exsolution. The small inset in (d) shows a magnified region in (d) to show pore morphology of these grains. femgal=Fe-Mg-Al spinel oxide, mgf=magnesioferrite, timt=titanomagnetite, gl=glass, pl=plagioclase, cpx=clinopyroxene.

In Type (I) exsolution, the Ti and Al partition into a titaniferous-magnetite phase, but Fe partitions into magnetite phase. A slight co-variation of Fe and Mg is spotted, although Mg is considered a trace element in this system. In Type (II) exsolution only a small number of the investigated oxide grains in the annealed run product do not texturally exhibit exsolution compositionally similar to the Fe-Mg-Al spinel oxide phase from its starting material (Petrochilos, 2010).

When experimenting with T-Type material, plagioclase is the most abundant phase. Three texturally distinct oxide exsolution phases were spotted. One oxide exsolution phase is Type (II) exsolution discussed above, with the end-members Fe-Mg spinel oxide and Fe-Mg-Al spinel oxide. An additional exsolution, Type (III), has Al-bearing magnesioferrite and Fe-Mg-Al spinel oxide as end-members. The exsolution had a precursor oxide phase of Fe-Mg-Al spinel oxide. The partitioning pattern is an Al-Ti-Fe positive correlation, and a negative correlation between these elements and Mg, where Mg and Al present major partitioning. The remainder of the oxide exsolution phases texturally resembles Type (I) exsolution of titaniferous-magnetite as identified in the M- type product. Figure 81 and Figure 82 show backscattered electron images indicating the types of exsolution that were observed in the samples. Petrochilos (2010) conducted further experiments on Group 2 and Groups 3, but these studies were omitted from this discussion as no correlation can be seen in the results.

None of the backscattered images provide an outcome that is exactly similar to that of Layer 21, with T-Type annealed samples being the closest in terms of the exsolution texture. It is important to consider that the experiments were not carried out on natural grains, and this could result in different outcomes. In terms of the physical model proposed above, this could indicate that the small changes in the chemical characteristics of the titaniferous-magnetites result in different ions being present in the crystal lattice. These ions will once again affect the portioning of all the ions kicked out during exsolution, which in turn will affect how the exsolution texture forms and is expressed physically.

In the work by Feinberg *et al.*, (2005), where the magnetic remanence behaviour of inclusions is the main focus, titaniferous-magnetite inclusions of mafic intrusive rocks were studied in order to analyse magnetic properties of the minerals. Exsolution textures in magnetic material can increase its coercivity. Analysed grains showed a cloth texture exsolution pattern that was divided evenly between black and white magnetic domains, and in this way created a checkerboard pattern. The low-relief lamellae which separate the prisms in the AFM (Atomic Force Microscopy) images appear grey in the MFM (Magnetic Force Microscopy) images, which indicates a mineral phase within the oxide inclusion that is nonmagnetic (Figure 83). This non-magnetic phase is ulvöspinel (Feinberg *et al.*, 2005).

Feinberg *et al.*, (2005) notes that an important parameter of the oxide cloth texture is the formation temperature. Similar to Petrochilos (2010), subsolidus exsolution is attributed to the arrays of needle-shaped titaniferous magnetite lamellae. Feinberg *et al.*, (2005) reports precipitation of the titaniferous-magnetite grains from their host silicate at approximately 865ºC, based on cation exchange geothermometry, which is well above the 580ºC Curie temperature for pure magnetite. Thermodynamic models have proposed that magnetic ordering at the paramagnetic-ferromagnetic transition in titaniferous-magnetite results in the unmixing of ulvöspinel (Feinberg *et al.*, 2005). This would suggest that as a titaniferous-magnetite solid solution cools and approaches its Curie temperature, it begins to acquire a thermo-remanence, and this early stage magnetic ordering triggers the oxide unmixing, forming ulvöspinel lamellae and magnetite prisms.

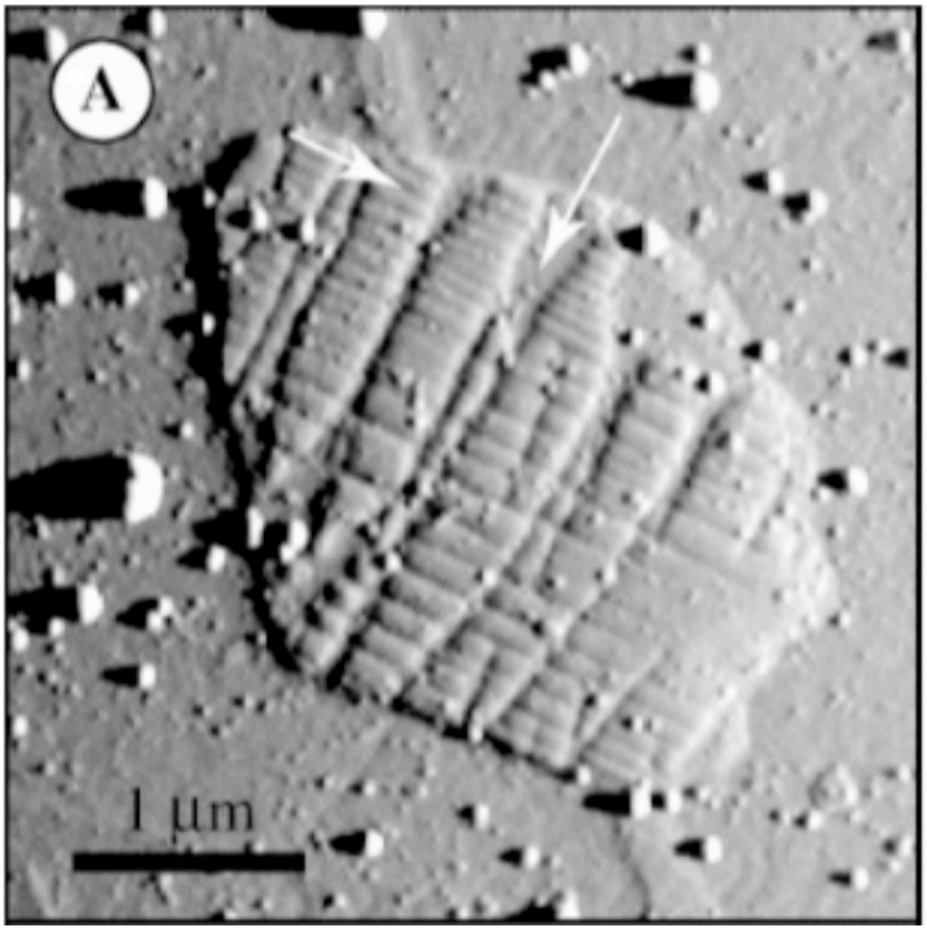

Figure 83. AFM and MFM images of a magnetite inclusion in clinopyroxene. (A): Topographic image that shows a boxwork texture where magnetite is segmented by ulvöspinel lamellae (arrows). From Feinberg *et al*., (2005).

The Presence of Ilmenite

Research has shown that the solubility of ilmenite in magnetite between 600ºC and 1300ºC is too low to account for the amount of ilmenite present in magnetite (Taylor, 1961; Lindsley,1962). It was therefore considered that Ti was present as an ulvöspinel component at high temperatures, rather than an ilmenite component. Differing degrees of oxidation and diffusion can lead to a variety of exsolution textures (Von Gruenewaldt *et al*., 1985). External granule diffusion would result in the diffusion of ilmenite constituents to the grain boundaries of the host magnetite. With decreased rates of ilmenite diffusion in the magnetite-ulvöspinel solid solution, ilmenite cannot leave its host and presents as internal granule exsolutions. The type and quantity of the ilmenite exsolution is thus dependent on the ulvöspinel content, which in turn will depend on the rate of cooling, the *fo2* of the magma at the time of crystallisation, and the remaining *fo2* during cooling (Von Gruenewaldt *et al*., 1985).

Exsolved ulvöspinel is very susceptible to oxidation, which would form ilmenite and magnetite. This is termed second degree protoilmenite, and causes a patchy anisotropy in titaniferous-magnetite (Figure 84). The proportion of exsolved ilmenite versus exsolved ulvöspinel in titaniferous-magnetites can vary, especially at the top of the Upper Zone. This is said to be dependent on the oxidation state during cooling (Von Gruenewaldt *et al*., 1985). Only “trellis” type exsolution is visible in the SEM images of the polished thin sections that were investigated in this dissertation.

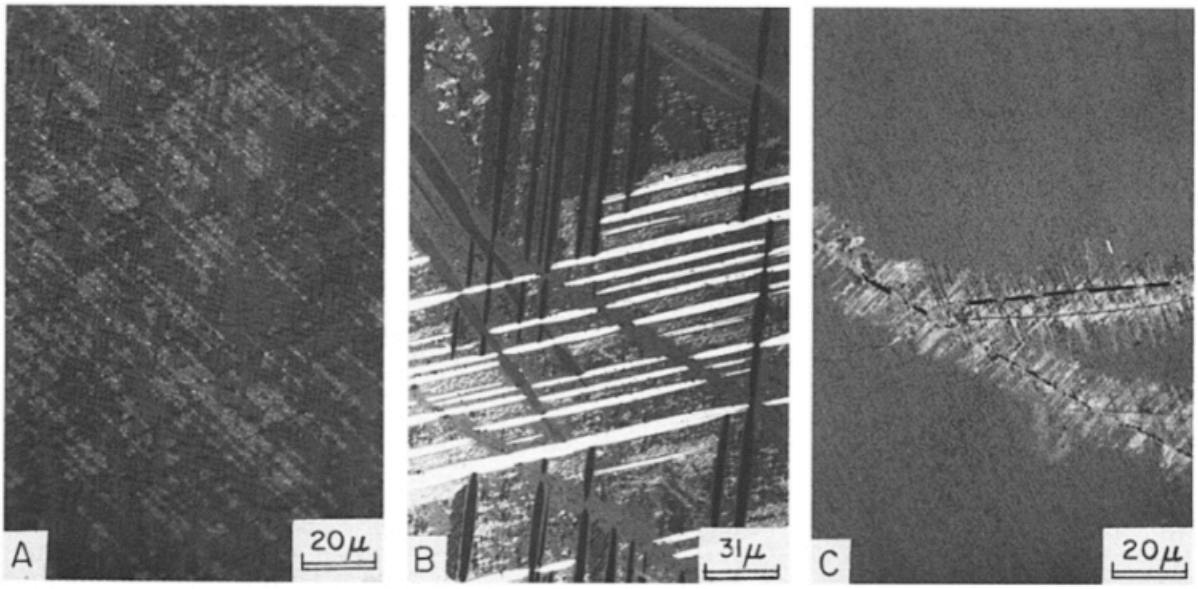

Figure 84. Protoilmenite textures. (A) Patchy anisotropism in a titaniferous-magnetite grain caused by oxidation of the ulvöspinel in the cloth texture to ilmenite. (B) "Trellis" type exsolution of ilmenite from Layer 21. (C) A titaniferous-magnetite grain from Layer 19. Oxidation of ulvöspinel to magnetite advances along fractures. From Von Gruenewaldt *et al.*, (1985).

Von Gruenewaldt *et al*., (1985) reported that in the grains where both "trellis" type and cloth texture exsolution is present, the lamella show either blunt terminations, or have pointed terminations. The terminations seen in the polished thin sections of Layer 21 show both of these terminations. In both cases, the cloth texture will not extend into the ilmenite lamella if they are closely spaced, which is clearly visible in Figure 57 in the results section.

Formation of the cloth texture exsolution

Although a number of studies have been done on the exsolution textures of titaniferous-magnetite, not much progress has been made with regards to an explanation for the formation conditions of these textures. The phenomenon of solid solution are a common feature of many rock-forming minerals. High temperatures allow the accommodation of ions with sizes between 15%-30% larger than the lattice would generally allow. As the physical conditions change, the ions can no longer fit into the space they occupy, creating internal lattice strain. As a reaction to the present strain, the composition of the mineral adjusts in order to relieve the strain. The system can respond in various ways, with one possible response resulting in the elements in a crystal moving from one chemical site to another via intracrystalline diffusion. This would result in segregated domains, with each domain being enriched in one element or another.

The next focus is on the physical mechanisms of exsolution, which follows the adjustment and movement of ions.The model suggested above emphasises that the exsolution texture also forms in 3D along with the 3D crystal. This indicates that as the titaniferous-magnetite crystal is cut at different angles, the exsolution texture is also cut, resulting in changes in the physical appearance of the texture, although no chemical change has occurred.

Chemically, titaniferous-magnetite exsolution is attributed to spinodal decomposition, although other possibilities include nucleation, continuous decomposition, or cellular decomposition (Yund and Mcallister, 1970). After the spinodal decomposition mechanism results in exsolution, the microstructures coarsen, and the volume of the magnetite-rich

regions increase, with their shape changing from cubic to plate-like (Price, 1980). The mechanism of exsolution for ilmenite is reported as external granular diffusion of the ilmenite to the titaniferous-magnetite grain. When the rate of diffusion decreases, the ilmenite can no longer leave the titaniferous-magnetite grain, and presents as an internal granular exsolution.

The Curie temperature of magnetite is another important concept to consider when discussing titaniferous-magnetite exsolution. Homogenization experiments show that naturally exsolved titaniferous-magnetite grains are annealed at a range of temperatures and various amounts of time, to drive homogenization of the two phases. Not much is known about the exact conditions present during formation, except that oxygen fugacity is also important.

The histograms presented in the results section considers what the implications of the peaks of both the Fe and Ti. Limited amounts of 70 wt-% Fe and higher are present for pure magnetite to form. Similarly, limited amounts of the 21.4 wt-% Ti are present for ideal ulvöspinel. This suggests that magnetite retains small amounts of Ti, with the limited large amounts partitioning directly into the ulvöspinel. This makes sense when considering that titaniferous-magnetite is the addition of Ti into the lattice. When exsolution occurs and Ti is kicked out and forced to arrange, the large values of Ti will immediately partition into ulvöspinel. The magnetite will retain smaller Ti values that have not partitioned into the ulvöspinel.

The available information on the topic of titaniferous-magnetite exsolution is limited, and a theory of formation can only be described as an outline rather than a complete model. Cawthorn and Walraven (1998) reported that the Bushveld Igneous Complex emplacement was due to a series of magma pulses, but that the last pulse occurred right after the Pyroxenite Marker, at a temperature of 1150ºC. This would suggest an initially high temperature, with a drop in temperature as no more magma pulses would enter the system to increase the temperature. Considering the formation of titaniferous-magnetite, the best model of formation was proposed by Reynolds (1985), as discussed earlier in this thesis. Fractional crystallisation was suggested as the mechanism which would result in magnetite layers forming between silicate layers.

Titaniferous-magnetite forms a solid solution between ulvöspinel and magnetite (Figure 78), but this is only present at high temperatures. Also, long periods of Fe-Ti enrichment is needed in the system before precipitation can occur. This is affected by pressure, temperature, and a decrease in oxygen fugacity during crystallisation. Although the Upper Zone in the Bushveld Igneous Complex shows a drop in bulk TiO_2, an increase in TiO_2 is seen with the fayalitic olivine present higher up in the Upper Zone. This TiO_2 increase also requires oxygen fugacity to decrease, which coincides with the oxygen fugacity drop needed for precipitation of Fe-Ti.

Exsolution textures are generally less common than oxidation microstructures, as the textures are considered to be uncommon in the Earth's crust. Cloth texture exsolution of titaniferous-magnetite forms a 3D framework of ulvöspinel lamella separating prisms of magnetite. This happens as a result of the unmixing of the solid-solution of titaniferous-magnetite to compositions close to the two end-members. The bulk mineral chemistry and the bulk thermal chemistry thus affect the unmixing of the solid-solution.

Unmixing occurs by either nucleation or by spinodal decomposition as a mechanism of exsolution. These two mechanisms are in competition with each other, and depend on various factors such as temperature as well as the cooling date of the magma. Spinodal decomposition occurs over a rapid loss of temperature, although the initial temperature

would not be very high. A nucleation mechanism can occur anywhere within the chemical solvus, but a spinodal decomposition mechanism is limited to the field within the chemical spinodal. Spinodal decomposition is thus limited to oxides where the compositions are near the centre of the ulvöspinel-magnetite join.

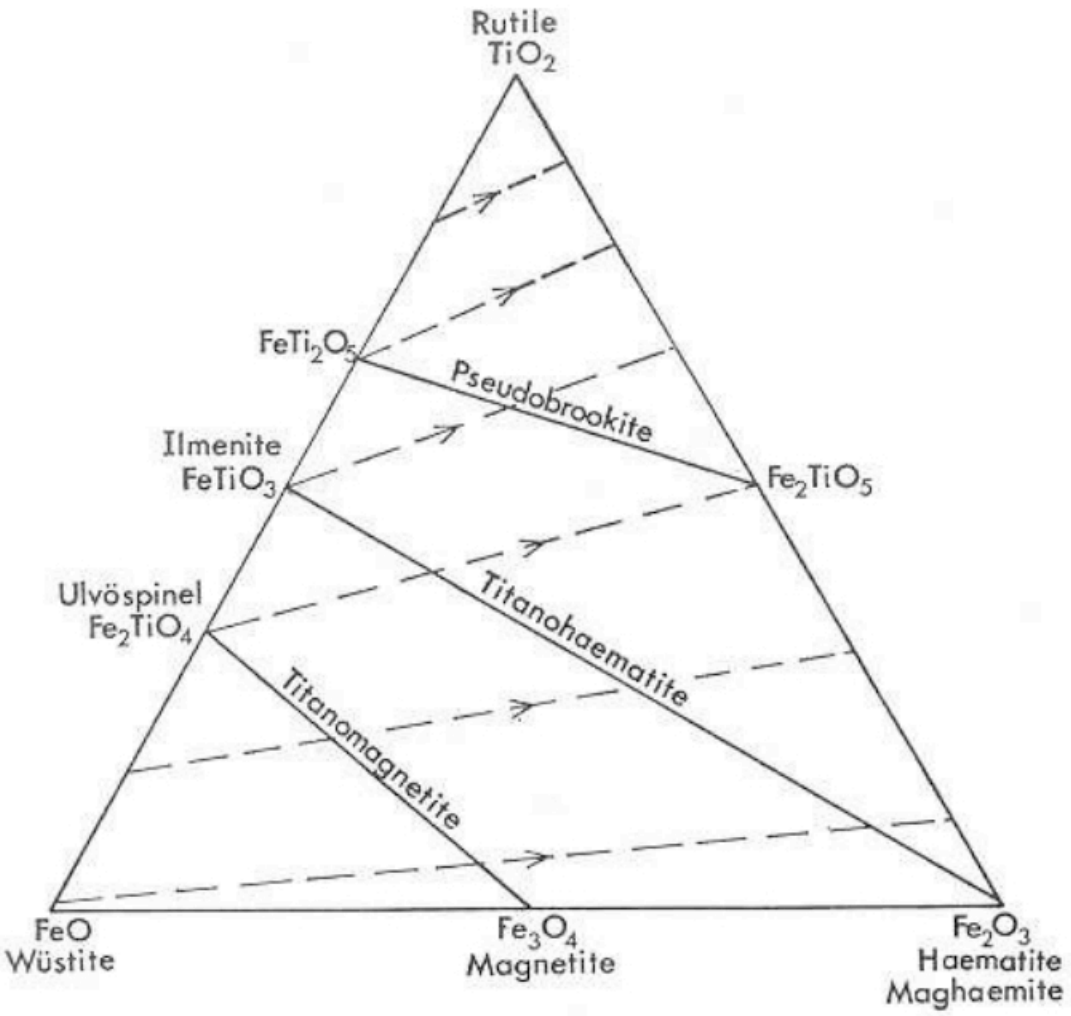

Figure 85. FeO-TiO2-Fe2O3 ternary system, where the principle solid solution series are shown in order to understand the process between ulvöspinel and magnetite.

For titaniferous-magnetites, spinodal decomposition produces a periodic distribution of phases on {100}. Initially, the interphase boundary will be diffused, but coarsening will lead to a lamellar framework with well defined boundaries as seen in Layer 21. The rate of development of microstructures in cooling systems is considered a complicated function of both surface and chemical-free energy changes. Initially, the ulvöspinel lamella should have a small finite width, and as time passes the concentration gradients within the lamella and matrix will change as the lamella grows. The evolution of the concentration gradients within the lamella is considered a function of the changing equilibrium composition of the lamella-matrix interface and the increasing diffusion distance as the system cools (Price, 1982). When the temperature is low, the gradients within the lamella and the matrix cannot equilibrate.

The ulvöspinel lamellae which separate the magnetite prisms from one another do not allow multi-domain behaviour in inclusions with intraoxide exsolution. The magnetostatic field that is generated by each magnetite prism will influence the magnetic direction of its neighbouring prisms. This results in the three-dimensional checkerboard pattern. Precipitation of the titaniferous-magnetite grains from their host silicate was reported by

Feinberg *et al.*, (2005) to be at approximately 865ºC, which is above the Curie temperature of magnetite. As a titaniferous-magnetite solid solution cools and approaches its Curie temperature, it begins to acquire a thermo-remanence, which triggers oxide unmixing.

The solubility of ilmenite in magnetite in a certain temperature range is too low to account for the amount of ilmenite present in magnetite. It was therefore considered that Ti was present as an ulvöspinel component at high temperatures, and not as an ilmenite component. External granule diffusion would result in the diffusion of ilmenite constituents to the grain boundaries of the host magnetite, and as the rates of ilmenite diffusion decreases, the ilmenite cannot leave its host and presents as internal granule exsolutions.

Considering the above, this would suggest the following for the formation of Layer 21:

(1) Titaniferous-magnetite precipitation occurs at around 865ºC, with low oxygen fugacity. Ilmenite is not abundant, due to the fact that Ti would be present as ulvöspinel at high temperatures, rather than ilmenite.

(2) At some point during the cooling of the solid-solution, spinodal decomposition is triggered as the exsolution mechanism. This starts to produce the periodic distribution of phases on {100}, forming ulvöspinel lamellae and magnetite prisms.

(3) As the titaniferous-magnetite solid solution continues to cool, it approaches the Curie temperature of the system and acquires a thermo-remanence. The ulvöspinel lamellae which separate the magnetite prisms from one another do not allow multi-domain behaviour. The magnetostatic field that is generated by each magnetite prism will influence the magnetic direction of its neighbouring prisms. This continues to ensure the formation of the three-dimensional checkerboard pattern.

(4) The lamella will continue to grow during equilibrium, but as time passes, the concentration gradients within the lamella and matrix will change. This change in the concentration gradients within the lamella is a function of the changing equilibrium composition of the lamella-matrix interface. When the system cools, equilibration between the lamella and the matrix can no longer occur and the final cloth texture is formed. This may be coarsened and lead to a lamellar framework with well defined boundaries.

(5) External granular diffusion results in ilmenite constituents diffusing across the grain boundary. When the rates of diffusion decrease, the ilmenite cannot leave the titaniferous-magnetite grain and exsolves. Ilmenite is dependent on the ulvöspinel content, which in turn is dependent on the temperature and oxygen fugacity during cooling. This would indicate why some slides show ilmenite exsolution whilst others do not.

(6) Coarsening of the exsolution texture and the addition of other oxides result in similar cloth texture patterns in titaniferous-magnetites from different locations, although the patterns will not be identical. These different physical appearances of exsolved titaniferous-magnetites may seem to indicate a change in chemistry. Although this may be true, the chemical change results in a change in the 3D ionic arrangement in the crystal structure. This in turn changes the 3D formation of the exsolution texture.

(7) The angle of cut of the formed texture will affect the physical appearance of the texture, as various angles of the 3D cut exsolution texture would yield varying results.

The suggested outline of a model points out that titaniferous-magnetite needs to be viewed in 3 components: physical properties, chemical properties, and factors influencing the chemical properties. Physically, a crystal will always retain its structure. Although some

change is allowable, the ideal structure will be returned to as soon as the factors present no longer allow this change. This is, at its core, the base of exsolution. The ions present in the crystal lattice that are kicked out and forced into other sites or to create space will control the exact physical formation of the exsolution texture in terms of its 3D appearance. How the exsolution continues to form chemically will then be controlled by the factors present, such as temperature, pressure, and oxygen fugacity, and how these factors affect the system as a whole. When crystallization occurs and no more change occurs, the 3D formation of the exsolution texture is dependent on the angle it has been cut in, the conditions present, and how these conditions affected the ionic structure and exsolution texture that forms.

CHAPTER 6 SUMMARY AND CONCLUSIONS

The purpose of this investigation was to gain more insight in into the conditions present during the formation of Layer 21 in the Upper Zone of the Bushveld Igneous Complex. The collected elemental data, SEM images, and SEM line scans have been presented and discussed throughout this dissertation. Comparison of the investigated results to previous studies have shown the relevance of investigating exsolution textures, especially exsolution textures in titaniferous-magnetites. Comparison and examination of the SEM data have provided some insights into the factors influencing the formation of the layer, although it is still not possible to suggest a complete model.

The formation of the Upper Zone of the Bushveld Igneous Complex has been suggested by various models, with the most popular model being that of a single magma pulse, or multiple magma injections. The mineralogy of the Upper Zone was shown to be cyclic, with the precipitation of magnetite layers following the cyclic pattern.

Upon investigation of thin sections from Layer 21 in the Western Limb of the Bushveld Igneous Complex, interesting exsolution textures were observed in the titaniferous-magnetite grains. As the Eastern Limb of the Bushveld Igneous Complex is better exposed and studied, most investigations revolve around data collected from the east. Limited information exists surrounding formation in the Western Limb, but the resulting information from the Eastern Limb can be assumed to apply similarly to the Western Limb.

Titaniferous-magnetite formation was discussed by Reynolds (1985), with the model suggesting that large-scale *in situ* plagioclase crystallisation led to an increase in the total iron content. This resulted in a density increase of the surrounding melt, which formed as a thick layer on the bottom of the magma chamber. The overlying magma did not interact with the enriched liquid, forming an inactive layer from which great amounts of titaniferous-magnetite crystallised. Interaction of factors such as temperature, the Fe_2O_3/FeO ratio of the liquid, *fo2*, and the *fh2o/fh2* ratio also resulted in large amounts of titaniferous-magnetite crystallising. Magnetite precipitation lowered the density of the inactive layer until it equaled the density of the overlying magma. Mixing of the magmas occurred which ended that specific cycle of magnetite layer formation. Fractionation once again became silica dominated.

The formation of the exsolution texture seen in titaniferous-magnetite is debatable, as not much information exists on the exact conditions. SEM analysis allowed for elemental data collection as well as images of the exsolution textures. Line scan data of the exsolution textures were also collected in order to further analyse the chemistry of the titaniferous-magnetite grains. Mineral calculation allowed for the determination of mineral species, with initial confusion regarding the titaniferous-magnetite. This led to the conclusion of the following minerals being present in the samples: titaniferous-magnetite, magnetite, plagioclase, silicates, pyrrhotite, ilmenite, and apatite.

SEM image analysis showed titaniferous-magnetite exsolution in all titaniferous-magnetite grains. Some slides did not indicate ilmenite exsolution in the titaniferous-magnetite, although ilmenite may be present as separate grains. The titaniferous-magnetite grains indicated black spots and lighter spots, with the lighter spaces considered to be small sulphides, and the black spaces indicating holes where the sulphides may have been leached out. These holes and grains always appeared to be localized and weren't uniform across a titaniferous-magnetite grain. Exsolution textures of the titaniferous-magnetite grains seem to change, although it was suggested that this may due to the angle at which a titaniferous-magnetite grain was cut and is not attributed to elemental changes.

Some silicates also show exsolution textures, and on many slides the silicates form a ring around the titaniferous-magnetite grains. Apatite is quite abundant, but does not show any interaction with titaniferous-magnetite if the grains are adjacent. Pyrrhotite is the main sulphide present, but was not found in all images. Most of the pyrrhotite grains were small, but some large grains were found in slides from a lower depth. Magnetite appears on its own sporadically, usually as a vein or inclusion.

Line scan data confirms the presence of magnetite and ulvöspinel, with the Fe increasing across the lighter areas and decreasing across the grey areas. The opposite is true for Ti, which increases across the grey areas and decreasing across the lighter areas. Line scan results did not show any changes in the line shape when analysed across two different textures. Line scan data was not the same for all grains, with some grains having an overall lower average for the elements than others. Line scans over the darker spaces and lighter spaces as seen in the titaniferous-magnetite grains confirmed the assumption that the light spaces are possibly small sulphide grains, and the dark spaces are holes formed due to the leaching of the small sulphides.

Histograms of the Fe and Ti elemental data suggests that when exsolution occurs, large amounts of Ti will partition into the ulvöspinel. When these amounts are no longer available, the magnetite will retain small amounts of Ti. The various peaks at different percentages confirms this in terms of chemical balance in a crystal structure.

The cloth exsolution texture is considered to have formed as a result of spinodal decomposition. Mogensen (1946) first noted the existence of the two-phase intergrowth of ulvöspinel-rich and magnetite-rich oxides. The typically described feature is that of a three-dimensional framework (grid pattern) of ulvöspinel-rich lamellae. This lamella usually lies on {100}, with inter-lamellar magnetite-rich blocks (Price, 1980). The exsolution microstructure only develops on small scale, due to the slow rate of the kinetic processes involved in unmixing at the solvus temperature.

Exsolution microstructures are considered to develop as a function of the mineral bulk chemistry and thermal history (McConnell, 1975). The two mechanisms of exsolution are considered to be in competition, the “winner” being dependent on the conditions at play. Spinodal decomposition favours rapid cooling rates, and nucleation favours systems with slower cooling rates (Price, 1980). Spinodal processes are limited to lower temperatures the nucleation events, and also to oxides where the compositions are near the centre of the ulvöspinel-magnetite join.

Price identified the mechanisms of exsolution in his study by considering certain characteristics, namely: (a) coarse precipitates found on grain boundaries and other lattice defects that are separated from the rest of the grain by a precipitate-free zone (PFZ), is a texture associated with heterogeneous nucleation (Nicholson, 1968), (b) The random distribution of discrete precipitates found within the body of the grain would be indicative of homogeneous nucleation, and (c) for titaniferous-magnetites, spinodal decomposition produces a periodic distribution of phases on {100}.

The scale of the lamellar framework developed in titaniferous-magnetites can be used to compliment geothermometric data. The mechanism of exsolution is affected by the initial temperature and the rate of cooling of the magma. After the investigation of the exsolution textures by Price (1980), Price (1982) developed a mathematical model to describe the growth of the exsolution patterns in titaniferous magnetite. The model explains that course microstructures and their development is a complex process which involves variations in the growth rates of particles. The rate of development of microstructures in cooling systems is considered a complicated function of both surface and chemical-free

energy changes, although it is generally assumed that the chemical-free energy changes play the dominant role.

Von Gruenewaldt *et al*., (1985) investigated the changes in the titaniferous-magnetite exsolution features within the Upper Zone of the Eastern Limb of the Bushveld Igneous Complex. The observed textural features in titaniferous-magnetites was suggested to be caused by two processes: (1) the oxidation of the magnetite-ulvöspinel solid solution at temperatures above the magnetite-ulvöspinel solvus results in a process similar to exsolution, where most ilmenite is exsolved from the titaniferous-magnetite. (2) Ulvöspinel exsolution is a true exsolution process that is a result of decreased solubility of one component in the other as the temperature drops. The changes in the evolution textures can be described as either exsolution above the magnetite-ulvöspinel solvus, or exsolution below the magnetite-ulvöspinel solvus.

Bowles *et al*., (2009) conducted exsolution experiments which tested whether the consolute temperature of pure titaniferous-magnetite solvus is lower than non-pure titaniferous-magnetite. Using samples similar to that of Bowles *et al*., (2009) and other samples, new time-series experiments were conducted by Petrochilos (2010), and were used to infer exsolution mechanisms. The experiments also investigated the time-dependent changes with a growth of the exsolution texture. Two sets of experiments in which temperature is the primary variable was also conducted to evaluate changes brought about by temperature changes.

In the work by Feinberg *et al.*, (2005), where the magnetic remanence behaviour of inclusions are the main focus, titaniferous-magnetite inclusions of mafic intrusive rocks were studied in order to analyse magnetic properties of the minerals. Exsolution textures in magnetic material can increase its coercivity. Analysed grains showed a cloth texture exsolution pattern that was divided evenly between black and white magnetic domains, and in this way created a checkerboard pattern.

A rough model was described using all of the data presented by pervious investigations of specific conditions or properties of the exsolution of titaniferous-magnetites. The model suggests that during the cooling of the solid-solution, spinodal decomposition is triggered which starts to produce the periodic distribution of phases on {100}, forming ulvöspinel lamellae and magnetite prisms. During cooling the solid-solution approaches the Curie temperature of the system and acquires a thermo-remanence, which continues to ensure the formation of the three-dimensional checkerboard pattern. The lamella continue to grow during equilibrium, but as time passes, the concentration gradients within the lamella and matrix will change. When the system cools, equilibration between the lamella and the matrix can no longer occur and the final cloth texture is formed. External granular diffusion results in ilmenite constituents diffusing across the grain boundary. When the rates of diffusion decrease, the ilmenite cannot leave the titaniferous-magnetite grain and exsolves. Coarsening of the exsolution texture and additional oxides could be the result of titaniferous-magnetites from different locations exhibiting similar but not identical textures. Various chemical differences will result in the original chemical formation varying. When this is presented in 3D, textures may vary but this would not an occurrence of chemical changes between crystals, but rather angles at which the 3D exsolution texture is hit, which presents the exsolution differently in appearance.

In conclusion, the data collected and investigated throughout this study has prompted the discussion of the formation of exsolution textures in titaniferous-magnetites. Although a rough chemical model has been suggested, an outline of the physical formation has been presented in an attempt to roughly explain what may have happened. The collected data included elemental data collected from a SEM, SEM images, and SEM line scans. Most

research indicates that although specific properties or conditions have been investigated, no proper model has been proposed and would be important to consider for future investigations. The suggested way forward is that titaniferous-magnetite needs to be viewed in 3 components: physical properties, chemical properties, and factors influencing the chemical properties. The combination of these three components will yield the best result when suggesting a formal model of formation.

Future Research

The data presented in this project indicates that there is a lack of more in-depth investigations of the exsolution of titaniferous-magnetites. Many authors investigated specific properties and conditions surrounding the microtexture formation, but not much attention has been given to propose an overall model that explains formation.

The magnetic remanence of titaniferous-magnetite appears to play a larger role in the microtexture formation than one would assume, but has also not been given much attention. Unfortunately it was outside the scope of this project and was not investigated during the data collection for this thesis.

Future research would include analysing samples over a larger area, and focusing more on the interaction of the titaniferous-magnetite with the surrounding grains, especially sulphides. Microprobe analysis will be used to confirm mineral species more accurately and to discover any minerals that may have been missed. A similar study to that of Petrochilos (2010) would be beneficial, especially when trying to recreate the conditions present at the time of formation in order to analyse the exsolution textures.

It would also be beneficial to try and analyse the exsolution textures by modeling three-dimensional diffusion fields. This allows the investigation to determine the relative importance of chemical and surface-energy driving forces in cooling systems. Price (1982) suggested that the growth of three, mutually orthogonal planar lamella should be modeled in order more accurately reproduce the formation of the titaniferous-magnetite microstructures.

REFERENCES

Ardell, A.J. Nicholson, R.B. 1966. On the modulated structure of aged Ni-Al alloys. Acta Metallurgica 14, pp 1295-1309.

Ashwal, L.D., Webb, S.J., Knoper, M.W. 2005. Magmatic stratigraphy in the Bushveld Northern Lobe: continuous geophysical and mineralogical data from the 2950 m Bellevue drillcore. South African Journal of Geology 108, pp 199-232.

Britt, T. 2015. A mineralogical and geochemical review of Cycles V and VI of the Upper Zone of the Bushveld Complex. Pretoria, Kitskopie.

Bowles, J. A., Hammer, J. E., and Brachfeld, S. A. 2009. Magnetic and petrologic characterization of synthetic Martian basalts and implications for the surface magnetization of Mars. Journal of Geophysical Research 114. E10003, doi:10.1029/2009JE003378.

Cawthorn, R.G., Ashwal, L.D. 2009. Origin of Anorthosite and Magnetitite Layers in the Bushveld Complex, Constrained by Major Element Compositions of Plagioclase. Journal of Petrology 50, pp 1607-1637.

Cawthorn, R.G., Walraven, F. 1998. Emplacement and Crystallization Time for the Bushveld Complex. Journal of Petrology 39, pp 1669-1687.

Cawthorn, R.G., Webb, S.J. 2001. Connectivity between the western and eastern limbs of the Bushveld Complex. Tectonophysics 330, pp 195-209.

Clarke, B., Uken, R., Reinhardt, J. 2009. Structural and compositional constraints on the emplacement of the Bushveld Complex, South Africa. Lithos 111, pp. 21–36.

Deer, W. A., Howie, R. A., and Zussmann, J. 1962. Rock-Forming Minerals, vol. 5, Non Silicates. Wiley, New York.

Du Toit, A. L.1918. Plumasite (corundum-aplite) and titaniferous magnetite rocks rom Natal. Geological Society of South Africa 21, pp 53-73.

Eales, H.V. and Cawthorn, R.G. 1996. The Bushveld Complex. Developments in Petrology 15, pp 181-229.

Eriksson, P.G. and Reczko, B.F.F. 1995a. The sedimentary and tectonic setting of the Transvaal super group floor rocks to the Bushveld Complex. Journal of African earth Sciences 21, pp 487-504.

Evans, M.E., Wayman, M.L. 1974. An investigation of the role of ultra-fine titanomagnetite intergrowths in palaeomagnetism. Geophysical Journal of the Royal Astronomical Society 36, pp 1-10.

Feinberg, J.M., Scott, G.R., Renne, P.R., Wenk, H. 2005. Exsolved magnetite inclusions in silicates: Features determining their remanence behavior. Geological Society of America 3, pp 513-516

Fischer, R.P. 1975. Vanadium Resources in Titanifeorus Magnetite Deposits. Geologcial Survey Professional Paper 926-B,

Frost, B. R. and Lindsley, D. H. 1991. Occurrence of iron-titanium oxides in igneous rocks. Reviews in Mineralogy and Geochemistry 25, pp 433-468.

Gandhi, S.S. 1967. Igneous Petrology Of Mount Yamaska. Doctorate Thesis. McGill, Canada.

Gibbs, J. W. 1961. The Scientific papers of J. Willard Gibbs, 1. Dover Publications, New York, N.Y. pp 434.

Haggerty, S. E. 1991. Oxide textures; a mini-atlas. Reviews in Mineralogy and Geochemistry, Mineralogical Society of America 25, pp 129-219.

Hartzer, F.J. 1995. Transvaal super group inliers: geology, tectonic development and relationship with the Bushveld complex, South Africa. Journal of African Earth Sciences 21, pp 521-547.

Hatton, C.J. and Schweitzer, J.K. 1995. Mantle plume origin for the Bushveld and Ventersdorp magmatic provinces. Journal of African Earth Sciences 21, pp 571-577.

Hunt, J.P. 2006. Geological Characteristics of Iron Oxide-Copper-Gold (IOCG) Type Mineralisation in the Western Bushveld Complex. MSc dissertation, School of Geosciences, Faculty of Science.

Irvine, T.N. 1975. Crystallization sequences in the Muskox intrusion and other layered intrusions II. Origin of chromitite layers and similar deposits of other magmatic ores. Geochimica et Cosmochimica Acta 39. pp 991-1020.

Kawai, N. 1956. Exsolution of titanomagnetites and its effect on rock-magnetism III. Proceedings of the Japanese Academy 32, pp 464-468.

Klemm, D. D., Snethlage, R., Dehm, R. M., Henckel, J., Schmidt-Thome, R., 1982. The formation of chromite and titanomahgnetite deposits within the Bushveld Igneous Complex. Ore genesis--the State of the Art: Berlin. pp 351-370.

Klemm, D. D., Von Gruenewaldt, G,. Henckel, J., and Dehm, R. 1985. The geochemistry of titanomahgnetite in magnetite layers and their host rocks. Economic Geology 80, pp 1075-1088.

Lee, C.A. 1996. A Review of Mineralization in the Bushveld Complex and some other Layered Intrusions. Geology Department, Anglo American Platinum Corporation Limited.

Lindsley, D. H. 1962. Investigation on the system FeO-Fe203-TiO2. Carnegie Institution Washington Year Book 61, pp 100-106.

Lindsley, D. H. 1981.Some experiments pertaining to the magnetite-ulvöspinel miscibility gap. American Mineralogist 66, pp 759-762.

McConnell, J.D.C., 1975. Microstructures of minerals as petrogenetic indicators. Annual Review of Earth and Planetary Sciences 3, pp 125-155.

Mitchell, A.A. 1990. The stratigraphy, petrography and mineralogy of the Main Zone of the Northwestern Bushveld Complex. South African Journal of Geology 93, pp 818-831.

Mogensen, F. 1946. A ferro-orthotitanate ore from Sodra Ulvon. Geologiska Foreningens Stockholm Foerhandlingar 68, pp 578-588.

Molyneux, T.G. 1970a. The geology of the area in the vicinity of Magnet Heights, eastern Transvaal, with specific reference to the magnetic iron ore. The Geological Society of South Africa Special Publication 1, pp 228-241.

Molyneux, T.G. 1970b. A geological investigation of the Bushveld Complex in Sekhukhuneland and part of the Steelpoort valley, eastern Transvaal, with particular reference to the oxide minerals. Unpublished D.Sc. dissertation, University of Pretoria, South Africa.

Molyneux, T.G. 1974. A geological investigation of the Bushveld Complex in Sekhukhuneland and part of the Steelpoort valley. Transactions of the Geological Society of South Africa 77, pp 329-338.

Nickel, E.H. 1958. The composition and microstructure of an ulvospinel-magnetite intergrowth. The Canadian Mineralogist 6, pp 191-200.

Nicholson, R.B. 1968. Nucleation at imperfections. In: Phase Transformations. American Society of Metallurgists, Metal Parks, OH, pp 632.

Petrochilos, L. 2010. Experimental and Analytical Studies of Titanomagnetite in Synthetic and Natural Samples. University of Hawaii, Master thesis.

Price, G. D. 1980. Exsolution microstructures in titanomagnetites, and their magnetic significance. Physics of the Earth Planetary Interiors 23, pp 2-12.

Price, G. D. 1981. Subsolidus phase relations in the titanomagnetite solid solution series. American Mineralogist 66, pp 751-758.

Price, G. D. 1982. Exsolution in titanomagnetites as an indicator of cooling rates. Mineralogical Magazine 46, pp 19-25.

Reynolds, I.M. 1985. Contrasted Mineralogy and Textural Realtonships in the Uppermost Titaneferous Magnetite Layers of the Bushveld Complex in the Bierkraal Area North of Rustenburg. Economic Geology 80, pp 1027-1048.

Samanta, S., Mukherjee, S., Dey, R. 2014. Oxidation behaviour and phase characterization of titaniferous magnetite ore of eastern India. Trans. Nonferrous Met. Soc. China 24, pp 2976−2985.

Singewald, J.T. 1913. The Titaniferous Iron Ores in the United States. Their composition and economic value. Department of the Interior Bureau of Mines 64.

Scoon, R.N., and Mitchell, A.A. 2012. The Upper Zoe of the Bushveld Complex at Roossenekal, South Africa:Geocgemical Stratigraphy and Evidence of multiple episodes of magma replenishment. South African Journal of Geology 115, pp 515-534.

Taylor, R.W. 1961. An experimental study of the system FeO-Fe2O3-TiO2 and its bearing on mineralogical problems. Unpublished Ph.D. dissertation. Pennsylvania State University.

Tegner, C., Cawthorn, R., Kruger, F., 2006. Cyclicity in the Main and Upper Zones of the Bushveld Complex, South Africa: Crystalization from a Zoned Magma Sheet. Journal of Petrology 47, pp 2257-2279.

Turnock, A. C. and Eugster, H. P. 1962. Fe-Al oxides: phase relations below 1000 °C. Journal of Petrology 3, PP 533-565.

Ulmer, G. C. 1969 Experimental investigation of chromite spinels. Economic Geology Monograph 4. pp 114-131.

Vantongeren, J.A., Mathez, E.A. 2013. Incoming magma Composition and Style of Recharge Below the Pyroxenite Marker, Eastern Bushevld Complex, South Africa. Journal of Petrology 54, pp 1585-1605.

Vincent, E. A., Phillips, R. 1954. Iron-titanium oxide minerals in layered gabbros of the Skaergaard intrusion, East Greenland. Geochimica et Cosmochimica Acta, 6, I-26.

Von Gruenewaldt, G. 1971. A petrological and mineralogical investigation of the rocks of the Bushveld Igneous Complex in the Tauteshoogte-Roossenekal area of the Eastern Transvaal. Pretoria, Zendubind

Von Gruenewaldt, G. 1976. Sufides in the Upper Zone of the Eastern Bushveld Complex. Economic Geology 71, pp 1324-1336

Von Gruenewaldt, G., Klemm, D.D., Henckel, J., Dehm, R.M. 1985. Exsolution Features in Titanomagnetites from Massive Magnetite Layers and Their Host Rocks of the Upper Zone, Eastern Bushveld Complex. Economic Geology 80, pp 1049-1061

Webb, S., Ashwal, L., Cawthorn, R. 2010. Continuity between eastern and western Bushveld Complex, Sotuh Africa, confirmed by xbnolths from kimberlite. contributions to Mineralogy and Petrology 162, pp101-107.

Yund, R. A. and McCallister, R. H. 1970. Kinetics and mechanisms of exsolution. Chemical Geology 6, pp 5-30 .

Zeh, A., Ovchtarova, M., Wilson, A.H., Shaltegger, U. 2015. The Bushveld Complex was emplaced and cooled in less than one million years – results of zirconology, and geotectonic implications. Earth and Planetary Science Letters 418, pp 103–114.

APPENDICES

APPENDIX A

Elemental weight percentages of the analysed minerals in Figures 8-48 have been included in this disc. Only elements of importance have been listed.